Performance of the Compact Turbo and the Alicoco spiral separators in the recovery of Zircon at the Wet Circuit of the Grande Côte Opérations

by

ELLIOT MANDLAKAYISE DONDA

submitted in accordance with the requirements for

the degree of

MASTER OF ENGINEERING

in the subject

ENGINEERING: CHEMICAL

at the

UNIVERSITY OF SOUTH AFRICA

SUPERVISOR: Professor Francois Mulenga

22 August 2026

Declaration

Name: Elliot Mandlakayise Donda

Student number: 33880808

Degree: Master of Engineering

I declare that:

Performance of the Compact Turbo and the Alicoco spiral separators in the recovery of Zircon at the Wet Circuit of the Grande Côte Opérations

I declare that the dissertation is my own work and that all the sources that I have used or quoted have been indicated and acknowledged by means of complete references, and that any use of Artificial Intelligence (AI) has been fully disclosed.

I further declare that I submitted the dissertation to the appropriate originality detection system which is endorsed by Unisa and that it falls within the accepted requirements for originality.

I further declare that I have not previously submitted this work, or part of it, for examination at Unisa for another qualification or at any other higher education institution.

I further declare that where Artificial Intelligence (AI) tools have been used in the preparation of this thesis/dissertation, their use has been limited to ethical permissible support, has been fully disclosed, and does not replace my own original research, my independent critical thinking and analysis, or authorship responsibilities.

I understand that failure to disclose AI use, plagiarism and/or lack of academic integrity may constitute academic misconduct under Unisa's policies.

(The dissertation will not be examined unless this statement has been included.)

EMDonda. 22 August 2025

SIGNATURE DATE

UNIVERSITY OF SOUTH AFRICA

KEY TERMS DESCRIBING THE TOPIC OF A DISSERTATION/THESIS

This dissertation investigates the performances of a Compact Turbo spiral and of an Alicoco spiral and compares them to MG12 and HG10 spirals. The performances are about their abilities to separate zircon from aluminium silicates in a classifier underflow stream. A test work was conducted in a closed-loop pilot plant or spiral rig at different pulp densities and splitter settings, and the performance was assessed at difference operating conditions. The Compact Turbo spiral could not handle all the feed types, but it produced the best concentrate with the highest ZrO_2 and lowest Al_2O_3 while the Alicoco spiral was unable to handle the feed streams. The MG12 spiral handled all types of feed, but the quality was not good. The HG10 spiral handled the feed better that the Compact Turbo but could not separate the stream any better. Particle size was key for the Compact Turbo to achieve good separation.

Title of thesis/dissertation:

Performance of the Compact Turbo and the Alicoco spiral separators in the recovery of Zircon at the Wet Circuit of the Grande Côte Opérations in Senegal

KEY TERMS:

Compact Turbo spiral, Alicoco spiral, MG12 spiral, HG10 spiral, zircon recovery, Kyanite rejection, Staurolite rejection, Spiral separator, Gravity separation, Senegal mineral processing

Dedication

To my young family, my wife Nomalanga and our little Sijabule, thank you for supporting me in achieving this goal of many years.

Acknowledgement

My boss Davin Beukes thank you very much for your genial leadership and for all your support. The Metallurgy team: Nene, Diarra, Malick, Cisse, Malou, Massaer and everyone thank you for the support throughout the exercise.

Sanelisiwe Sibisi-Gumede thank you very much for never tiring to encourage me along the way.

Thank you, Professor Mulenga, for your guidance, teachings and patience. It really could not happen without you.

May God bless you all.

Abstract

Mineral beneficiation is a process of separation valuable minerals from gangue minerals for economic purposes. Grande Côte Opérations mines and beneficiates mineral sands to produce ilmenite, zircon, rutile and leucoxene through its Wet Concentrator Plant and Mineral Separation Plant. The Mineral Separation Plant has a wet gravity circuit which is unable to reach its zircon recoveries due to the presence of the silicates. The aim of this research was to test the ability of the new spirals by Mineral Technologies and Alicoco to separate zircon and alumina silicate.

A pilot plant or spiral rig was used to treat a sample taken from a classifier underflow stream at the Wet Circuit. The sample was treated through the Compact Turbo and Alicoco spirals respectively. They were compared to the performance of the MG12 and HG10 spirals already installed in the Wet Circuit. A slurry with 30% (1.30 g/cm^3 pulp density), 35% (1.36 g/cm^3 pulp density) and 40% (1.44 g/cm^3 pulp density) solids content was separated with splits to the concentrate varying from 80%, 85 and 90% at each solids content in the feed.

The Compact Turbo spiral was found to perform the best, producing a concentrate with 30.5% ZrO_2 at 86.3% recovery with low Al_2O_3 content of 4.3% at 40% solids content in the feed and 68% split to the concentrate. There was clear separation between zircon and the silicate gangue. QEMSCAN shows that particle size was key to separation. The MG12 and the HG10 spirals, on the other hand, showed lower separation under intended conditions. The Alicoco spiral could not handle any of the feed samples tested. Comparing its performance to the HG10 spiral in a separate historical test at low pulp densities in the feed, separation was noted but with 90% of Al_2O_3 recovery to the concentrate and less than 70% ZrO_2 recovery. It is therefore recommended that the Compact Turbo spiral be further tested online for its ability to separate the zircon from the alumina.

Keywords: Compact Turbo spiral, Alicoco spiral, Zircon recovery

Table of contents

Declaration ii
Dedication iv
Acknowledgement v
Abstract vi
List of figures xi
List of tables xvi
List of symbols and abbreviations xix
Chapter 1 Introduction 1
1.1 Background 1
1.2 Problem statement and purpose of the study 2
1.3 Research objectives 7
1.4 Scope of the research 8
1.4.1 Research questions 8
1.4.2 Selection of operational variables 9
1.4.3 Limitation of the research 9
1.5 Layout of the dissertation 10
1.6 Summary 11
Chapter 2 Literature review 12
2.1 Introduction 12
2.2 Mineral sands in West Africa 13
2.3 Spiral concentrators 14
2.3.1 Gravity separation: Principles 14
2.3.2 Design of the commonly used spirals 17
2.3.3 Effects of feed rate on spiral recovery 19
2.3.4 Effects of splitter position on spiral recovery 20
2.3.5 Effects of pulp density on spiral separation 23
2.3.6 Effects of feed properties on spiral separation 24
2.4 Beneficiation of mineral sands 26
2.4.1 Production of heavy mineral concentrates 27
2.4.2 Common heavy sand minerals 29
2.5 Relationship between mineral recovery and concentrate grade 34
2.6 Detailed analysis by QEMSCAN 37

2.6.1 Briefly about geometallurgy 37
2.6.2 Components of the QEMSCAN instrument 38
2.6.3 Analysis of samples by QEMSCAN 39
2.6.4 QEMSCAN on gravity separation 40
2.6.5 Gravity separation tests at pilot plant scale 43
2.7 Developments in spiral concentration 45
2.7.1 Performance of the Humphrey spiral concentrator 45
2.7.2 Special spirals: Compact Turbo and Alicoco spirals 46
2.8 Concluding remarks 53
Chapter 3 Experimental procedures, pilot testing and data collection methodology 55
3.1 Introduction 55
3.2 The Wet Circuit of Grande Côte Opérations 56
3.3 Collection of the bulk sample from the Wet Circuit 57
3.3.1 Description of the tertiary concentrate stream 57
3.3.2 Preparing the plant conditions for adequate bulk sampling 58
3.3.1 Sampling point of the underflow stream from the tertiary classifier 59
3.3.2 Collection of a bulk sample from the Wet Circuit 61
3.4 Pilot testing programme 63
3.4.1 Presentation of the spiral rig fitted with the spirals 64
3.4.2 Equipment and tools used for the rig test work 65
3.4.3 Experiments in closed-circuit configuration 67
3.4.4 Preparation of the slurry feeds for pilot testing 68
3.4.5 Experimental procedure used for the closed-circuit configuration 69
3.5 Laboratory characterisation of pilot test samples 72
3.5.1 Sample drying 72
3.5.2 Chemical and mineralogical analysis of product samples 73
3.5.3 Particle size analysis 77
3.6 Problems experienced during the experimental work 78
Chapter 4 Performance of the Alicoco, the Compact Turbo, the MG12, and the HG10 spiral separators 80
4.1 Introduction 80
4.2 Recovery performance of the spirals 82
4.2.1 Separation recoveries at 30% solid content in the slurry feed 83
4.2.2 Separation recoveries at 35% solid content in the slurry feed 86

4.2.3 Recovery performance at 40% solids level in the feed 88
4.3 Quality performance of the spirals 91
4.3.1 Quality performance at 30% solids level in the feed 91
4.3.2 Quality performance at 35% solids level in the feed 94
4.3.3 Quality performance at 40% solids level in the feed 95
4.4 Spirals operational feed rate variation 97
4.4.1 Compact Turbo spiral operational feed rate 98
4.4.2 MG12 spiral operational feed rate 99
4.4.3 HG10 Spiral operational feed rate 100
4.5 Problems observed with the Alicoco spiral 101
4.6 Particle size distributions of various streams 106
4.7 QEMSCAN quality analysis for the feed and Compact Turbo concentrates samples 108
4.8 QEMSCAN particle size distribution for the feed and Compact Turbo concentrates samples 113
4.9 Summarised conclusion 118
Chapter 5 Influence of operating conditions on the recovery of zircon and aluminium 120
5.1 Introduction 120
5.2 Recovery of zircon and aluminium to the concentrate 120
5.3 Quality of concentrates with changing operating feed conditions and split 122
5.4 Alicoco and HG10 spirals performance at low density feed 127
5.5 Understanding the effects of particle size 129
5.6 QEMSCAN for the concentrates from the Compact Turbo spiral 130
5.6.1 Mineralogy analysis 130
5.6.2 Analysis of particle size distribution results 131
5.6.3 Analysis of particle density results 134
5.7 Design features of the Compact Turbo spiral 136
5.8 Zircon balance and recovery at Wet Circuit without and with Compact Turbo spiral 136
5.9 Concluding remarks 139
Chapter 6 Conclusion and recommendations 142
6.1 Introduction 142
6.2 Summary of the research findings 143
6.3 Recommendations for future work 147

References **149**
Appendices **157**
Appendix A: Spirals Performance at 30% Solids in the Feed (1.30 g/cm^3 pulp density) 158
Appendix B: Spirals Performance at 35% Solids in the Feed (1.36 g/cm3 pulp density) 161
Appendix C: Spirals Performance at 40% Solids in the Feed (1.44 g/cm3 pulp density) 164
Appendix D: Mineral Assemblage 166
Appendix E: Particle Size Distributions 169
Appendix F: Comparison of Alicoco and HG10 spirals in 2022 173
Appendix G: QEMSCAN Results 175
Appendix H: Recovery and grade curves 177
Appendix I: Splitter Positions 180

List of figures

Figure 1.1: Schematic diagram of the wet and dry circuits at the MSP 4

Figure 1.2: The Wet Circuit that treats the heavy mineral concentrate (HMC) to produce concentrates Con 1, Con 2, Con 3, magnetics, and tails (GCO, 2022) ... 6

Figure 2.1: (a) Plant A and (c) the five-stage circuit of Plants B and C in 1990 at Richards Bay Minerals with (b) a Reichert cone (Walklate and Fourie, 2006; Wills and Napier-Munn, 2006) 15

Figure 2.2: Illustration of a typical modern WCP process (after Jones, 2006) ... 16

Figure 2.3: Original design of a spiral concentration (Wills and Napier-Munn, 2006) 17

Figure 2.4: Spiral splitters (a) outside, (b) from the top to the bottom (c) some at the bottom (GCO, 2022) 18

Figure 2.5: Effects of feed rate on Cr_2O_3 recovery (Tripathy and Murthy, 2012) 19

Figure 2.6: Effects of feed rate on zircon recovery for various slimes content in the feed (Ramsaywork et al., 2010) 20

Figure 2.7: Effects of splitter position on Cr2O3 recovery (Tripathy and Murthy, 2012) 21

Figure 2.8: A spiral prototype showing some splitter positions (Alaee et al. 2025) 21

Figure 2.9: Visual bands appearing on the spiral surface due to stratification on the spiral trough (Wills and Finch, 2016) 22

Figure 2.10: Bottom splitters of a spiral separator (Dixit et al. 2015) 23

Figure 2.11: Effects of pulp density on Cr_2O_3 recovery (Tripathy and Murthy, 2012) 24

Figure 2.12: Typical mining and production of heavy mineral concentrate (adapted from Perks and Mudd, 2019) 28

Figure 2.13: A typical HMC separation process (adapted from Perks and Mudd, 2019) 29

Figure 2.14: Zirconium silicate (source: Abduriyim et al., 2012) 30

Figure 2.15: (a) Kyanite and (b) Staurolite (Alderton, 2021) 30

Figure 2.16: Tourmaline (source: Alderton, 2021) 31

Figure 2.17: Quartz (Source: Pan et al., 2022) 31

Figure 2.18: Typical recovery-grade curve (Wills and Napier-Munn, 2006) 35

Figure 2.19: Grade-recovery for copper froth flotation (Neethling and Cilliers, 2012) 36

Figure 2.20: Spiral performance at different solid contents and feed rates (Sivamohan and Forssberg, 1985) 36

Figure 2.21: Examples of a QEMSCAN image for zircon characterisation (Ramsaywork et al., 2010; Wallmach et al., 2012) 37

Figure 2.22: A QEMSCAN instrument (Tonzetic et al., 2006) 39

Figure 2.23: The process of analysing a sample using QEMSCAN (Amao et al. 2016) 40

Figure 2.24: Comparing particle size from QEMSCAN and conventional dry screening (Grobler and Bosman, 2009). 41

Figure 2.25: Gravity separator model (Pascoe 2007) 42

Figure 2.26: Model predictions of Cr_2O_3 recovery using QEMSCAN (Pascoe et al., 2007) 42

Figure 2.27: Theoretical representation of a pilot plant (Dehaine and Filippov, 2016) 44

Figure 2.28: (a) A Compact Turbo spiral by Mineral Technologies (Pty) Ltd and (b) Alicoco spirals by Alicoco Mineral Technology Co. Ltd 49

Figure 2.29: A Type H Alicoco spiral installed in the Spiral Rig at GCO 50

Figure 2.30: The MG12 spiral separator installed at the Spiral Rig at GCO..... 51

Figure 2.31: The theoretical performance of an MG6.3 type spiral as determined by feed rate and pulp density (GCO, 2013) 52

Figure 2.32: Comparing the MG12 and the MG6.3 spiral separators (Mineral Technologies, 2021) 52

Figure 2.33: Operating windows for (Left) the HC33 spiral separator and (Right) the HC1RS (Mineral Technologies, 2021) 53

Figure 3.1: The Wet Circuit of the Mineral Separation Plant at Grande Côte Opérations 56

Figure 3.2: Production trends of the Wet Circuit displaying steady-state conditions before and during bulk sampling 60

Figure 3.3: (a) Underflow of the tertiary classifier as it enters the dedicated sump and (b) sampling point where the slurry discharges into the sump 61

Figure 3.4: A labelled calico bag used to collect small samples from the classifier CL003 underflow stream 62

Figure 3.5: Sample collected in 70 calico bags making about 350 kg of bulk sample 62

Figure 3.6: The two spiral rigs used for spiral test work at GCO – (a) Spiral rig fitted with the Alicoco spiral, the Compact Turbo spiral, and the HG10 Spiral; and (b) Spiral rig fitted with the MG12 spiral and the HG10 spiral 64

Figure 3.7: Tools used to collect timed fraction samples (a) stopwatch, (b) calico bag and (c) hand-held scale 66

Figure 3.8: The closed circuit used for spiral pilot testing at GCO 68

Figure 3.9: Splitter positions for the MG12 spiral separator at GCO 71

Figure 3.10: A Marc Technologies drying oven (2 m^3, 415 V, 50 Hz) at GCO laboratory 73

Figure 3.11: A 15-kg Kern weighing scale at GCO Laboratory 73

Figure 3.12: A Quantachrome Instruments sieving riffler splitter (220 V, 50/60 Hz) at GCO Laboratory 74

Figure 3.13: The manual splitter that can split a 100-g sample at the GCO Laboratory 75

Figure 3.14: One of the two X-Ray Fluorescent (XRF) machines stationed at the GCO Laboratory 76

Figure 3.15: A QEMSCAN machine at Eramet Ideas, France 76

Figure 3.16: A stack of screens on the shaking machine at the GCO Laboratory 77

Figure 4.1: A screenshot of the Laboratory Information Management System (LIMS) at GCO 81

Figure 4.2: Recovery of ZrO_2 to the concentrate at 30% solid concentration in the slurry feed 84

Figure 4.3: Recovery of Al_2O_3 to the concentrate at 30% solid concentration in the slurry feed 85

Figure 4.4: Recovery of ZrO_2 to the concentrate at 35% solid concentration in the slurry feed 86

Figure 4.5: Recovery of Al_2O_3 to the concentrate at 35% solid concentration in the slurry feed 87

Figure 4.6: Recovery of ZrO_2 to the concentrate at 40% solid concentration in the slurry feed 89

Figure 4.7: Recovery of Al_2O_3 to the concentrate at 40% solid concentration in the slurry feed 89

Figure 4.8: Effects of slurry feed rate on the recovery of ZrO_2 and Al_2O_3 to the concentrate by the Compact Turbo spiral 98

Figure 4.9: Effects of slurry feed rate on the recovery of ZrO_2 and Al_2O_3 to the concentrate by the MG12 spiral 100

Figure 4.10: Effects of slurry feed rate on the recovery of ZrO_2 and Al_2O_3 to the concentrate by the HG10 spiral 101

Figure 4.11: Alicoco spiral unable to separate slurry even when water was added at the top of the spiral to reduce beaching 102

Figure 4.12: The particle size distribution of the feed to and the concentrates from the spirals 106

Figure 4.13: The QEMSCAN image of the classifier 3 underflow (spirals feed)109

Figure 4.14: The QEMSCAN image of the 30% solids (1.30 g/cm^3 pulp density) and 85% split concentrate..... 110

Figure 4.15: The QEMSCAN image of the 35% solids (1.36 g/cm^3 pulp density) and 78% split concentrate..... 110

Figure 4.16: The QEMSCAN image of the 40% solids (1.36 g/cm^3 pulp density) and 68% split concentrate..... 111

Figure 4.17: QEMSCAN sizing of the tertiary classifier underflow and the Compact Turbo spiral concentrates at 30%, 35% and 40% solids in the spiral feed 113

Figure 4.18: The density of (a) the zircon particles in the samples and (b) aluminium bearing particles 115

Figure 5.1: The recovery and grade chart for the operating regimes separation of the classifier underflow through the Compact Turbo (CTS), MG12 and HG10 spiral..... 121

Figure 5.2: The MG12 operating regimes performance as the feed rate increased 123

Figure 5.3: Operating regimes performance of the Compact Turbo as feed rate increased..... 124

Figure 5.4: Design performance of Compact Turbo and MG12 spirals (Source: Mineral Technologies) 125

Figure 5.5: The HG10 operating regimes performance as the feed rate increased 126

Figure 5.6: The operating window for the HG10 spiral (Source: Mineral Technologies)..... 126

Figure 5.7: The Alicoco performance from historical data 128

Figure 5.8: The HG10 performance from historical data..... 129

Figure 5.9: QEMSCAN images of (a) tertiary classifier underflow, (b) 30% solid concentrate, (c) 35% solid concentrate, (d) 40% solid concentrate and (e) minerals identification 131

Figure 5.10: QEMSCAN particle size analysis of staurolite for the classifier underflow, 30% solids concentrate, 35% concentrate, and the 40% solids concentrate (C is for cumulative, NC is for non-cumulative)..... 134

Figure E1: PSD for the Compact Turbo Spiral 168

Figure E2: PSD for the MG12 Spiral 169

Figure E3: PSD for the HG10 Spiral 170

Figure E4: PSD for the UCC3 Underflow …….……171

Figure G1: The QEMSCAN mineralogy analysis, showing the quality of the Compact Turbo spiral feed and the concentrates……...……..175

Figure H1: The MG12 recovery and grade curves for the ZrO_2 ……..……..176

Figure H2: The Compact Turbo recovery and grade curve for the ZrO_2…….……..……176

Figure H3: The HG10 recovery and grade curve for the ZrO_2 ……177

Figure H4: The MG12 recovery and grade curve for the Al_2O_3……...177

Figure H5: The Compact Turbo recovery and grade curve for the Al_2O_3 ……...……..……..178

Figure H6: The HG10 recovery and grade curve for the Al_2O_3 ……..…...178

List of tables

Table 2.1: Example of chemical analysis showing Cr_2O_3 at different particle sizes (after Tripathy and Murthy, 2012)..... 25

Table 2.2: Average specific gravities of common sand minerals or associated silicates (after Wills and Napier-Munn, 2006; Perry et al., 1997; Krynine, 1946; Jones, 2006)..... 32

Table 2.3: Theoretical separation ratios from Equation (2.1) 33

Table 2.4: Some Mineral Technologies and Multotec spirals in the market (Mineral Technologies, 2026; Multotec, 2026) 47

Table 3.1: Indicative properties and assays of the stream to be sampled (GCO, 2022) 58

Table 3.2: List of equipment used for the experimental test work programme 66

Table 4.1: The quality performance of the spirals at 30% solids and 80%, 85% and 90% split to the concentrate..... 92

Table 4.2: Quality performance of the spirals at 35% solids or 1.36 g/cm^3 pulp density and 80%, 85% and 90% split to the concentrate..... 94

Table 4.3: The quality performance of the spirals at 40% solids or 1.44 g/cm^3 pulp density in the feed and 80%, 85% and 90% split to the concentrate 96

Table 4.4: Test 1 results for Alicoco and HG10 spirals separating Classifier 3 Underflow in 2022..... 103

Table 4.5: Test 2 results for Alicoco and HG10 spirals separating Classifier 3 Underflow in 2022..... 104

Table 4.6: Test 3 results for Alicoco and HG10 spirals separating Classifier 3 Underflow in 2022..... 105

Table 4.7: The d_{50} sizes for the Compact Turbo spiral concentrates 107

Table 4.8: The d_{50} sizes for the MG12 spiral concentrates 108

Table 4.9: The d_{50} sizes for the HG10 spiral concentrates..... 108

Table 4.10: The QEMSCAN mineralogy analysis, showing the quality of the Compact Turbo spiral feed and the concentrates..... 112

Table 4.11: The d_{50} and the d_{80} of the classifier underflow and the Compact Turbo spiral concentrates 114

Table 4.12: Summary of the density of the zircon particles of the classifier underflow and the Compact Turbo spiral concentrates 116

Table 4.13: Summary of the density of the aluminium-bearing particles of the classifier underflow and the Compact Turbo spiral concentrates 117

Table 5.1: QEMSCAN elementary results 133

Table 5.2: The Gill (1991) separation ratio of the zircon and aluminium-bearing particles in the classifier underflow 135

Table 5.3: Mass balance around the Wet Circuit 138

Table 5.4: Recovery of ZrO_2 at the Wet Circuit without and with the Compact Turbo spiral..... 138

Table 5.5: Recovery of Al_2O_3 at the Wet Circuit without and with the Compact Turbo spiral..... 139

Table A1: Flow rates, at 80% split to concentrate, chemical analysis and recovery at 30% solids in the feed (1.30 g/cm^3 pulp density) ……157

Table A2: Flow rates, at 85% split to concentrate, chemical analysis and recovery at 30% solids in the feed (1.30 g/cm^3 pulp density) ……..……..158

Table A3: Flow rates, at 90% split to concentrate, chemical analysis and recovery at 30% solids in the feed (1.30 g/cm^3 pulp density) …..……..159

Table B1: Flow rates, at 80% split to concentrate, chemical analysis and recovery at 35% solids in the feed (1.36 g/cm^3 pulp density) …..……..160

Table B2: Flow rates, at 85% split to concentrate, chemical analysis and recovery at 35% solids in the feed (1.36 g/cm^3 pulp density) ……..……..161

Table B3: Flow rates, at 90% split to concentrate, chemical analysis and recovery at 35% solids in the feed (1.36 g/cm^3 pulp density) ……...……162

Table C1: Flow rates, at 80% split to concentrate, chemical analysis and recovery at 40% solids in the feed (1.44 g/cm^3 pulp density) ……...……163

Table C2: Flow rates, at 85% split to concentrate, chemical analysis and recovery at 40% solids in the feed (1.44 g/cm^3 pulp density) ……...……164

Table C3: Flow rates, at 90% split to concentrate, chemical analysis and recovery at 40% solids in the feed (1.44 g/cm^3 pulp density) ……...……164

Table D1: Compact Turbo spiral mineral assemblage for the concentrate (by GCO Laboratory) ……165

Table D2: MG12 spiral mineral assemblage for the concentrate (by GCO Laboratory ……...……...166

Table D3: HG10 spiral mineral assemblage for the concentrate (by GCO Laboratory) ……..……...167

Table E1: d_{50} for the Compact Turbo Spiral……..……168

Table E2: d_{50} for MG12 Spiral ……..……169

Table E3: d_{50} for HG10 Spiral ….……170

Table F1: Alicoco spiral treating UCC3 underflow in 2022 ….……..……172

Table F2: HG10 spiral treating UCC3 underflow in 2022..…….....……..173

Table G1: QEMSCAN mineralogy results ….……...……174

Table I1: Splitter positions for the MG12, HG10 and the Compact Turbo spirals at 30%, 35% and 40% feed pulp densities ….…….……..……179

Table I2: Splitter positions for the Alicoco and the HG10spirals at low feed pulp densities ……..…….……..…180

List of symbols and abbreviations

%	Percentage
°C	Degrees Celsius
Al	Aluminium
Al_2O_3	Alumina or aluminium oxide
Al_2SiO_5	Kyanite
C	Concentrate
c	Concentrate grade
CL002	Classifier 2
CL003	Classifier 3
Con 1	Primary concentrate
Con 2	Secondary concentrate
Con 3	Tertiary concentrate
Con	Concentrate
Cr_2O_3	Chrome or chromium oxide
CTS	Compact Turbo spiral
CV054	Conveyor belt 54
F	Feed
f	Feed grade

Fe''', Al, Li, Mn, and Cr	Tourmaline
$Fe^{+2}Al_4[Si_4O_{11}]_2O_2(OH)_2$	Staurolite
g	gram
g/cm^3	grams per cubic centimetre
GCO	Grande Côte Opérations
h	Hour
$H_5NaFe_2Fe_2Al_8B_4Si_8O_{4l}$	Iron tourmaline
$H_5NaLi_2Al_2Al_8B_4Si_80_{4l}$	Elbaite or lithium tourmaline
$H_5NaMg_2Mg_2Al_8B_4Si_{4l}$	Magnesium tourmaline
HC	High capacity
HC1RS	High-capacity spiral type
HC33	High-capacity spiral type
HG10	Spiral type
HM	Heavy Mineral
HMC	Heavy Mineral Concentrate
Hz	Hertz
kg	Kilogram
km	Kilometre
kW	Kilowatts
LIMS	Laboratory Information Management System

m	Meter
m^3	cubic metre
m^3/h	cubic metre per hour
MG12	Spiral type
MG4	Spiral type
MG6.3	Spiral type
ml	millilitre
MSP	Mineral Separation Plant
O/F	Overflow
QEMSCAN	Quantitative evaluation of minerals by scanning electro-microscopy
R	Recovery
rpm	Revolutions per minute
s	Solids specific gravity
SiO_2	Quartz or silica
T	Tails
t	Tails grade
TBE	Tetrabromoethane
TiO_2	Rutile or titanium dioxide
$TiO_2.FeO$	Ilmenite
tph	Metric tons per hour

U/F	Underflow
VHM	Valuable Heavy Mineral
WCP	Wet Concentrator Plant
WHIMS	Wet High Intensity Magnetic Separator
XRF	X-Ray Fluorescence
Zr	Zirconium
$ZrO_2.SiO_2$	Zircon or zirconium silicate
ρ	Slurry specific gravity

Chapter 1 Introduction

1.1 Background

Haldar (2020) defines mineral beneficiation as the science and art of separating valuable metallic and non-metallic minerals from unusable gangue minerals. The separation occurs through a well-researched and designed process that treats the run-of-mine ore through various stages to produce saleable products. These stages generally entail comminution, screening and size classification, physical separation (i.e., gravity, magnetic and electrostatic separation), and froth flotation.

In mineral sands, the beneficiation process is mainly centred on physical separation and mainly solids-solids separation. Spiral concentrators are the most used unit for solids-solids separation and mineral sands beneficiation in the industry (Sinott, 2005).

Van Gosen et al. (2013) identified countries per continent with economic mineral deposits. Senegal is one such a country in West Africa currently mining and producing mineral sands. It achieves this through the Eramet-owned Grande Côte Opérations (GCO) that has an open-pit dredge mine, a Wet Concentrator Plant (WCP) and a Mineral Separation Plant (MSP). The WCP produces a heavy mineral concentrate (HMC) rich in heavy minerals (HM). These heavy minerals include ilmenite, zircon, rutile, leucoxene, kyanite, staurolite, chromite, monazite and other silicates. The heavy minerals are classified into valuable heavy minerals (VHM) and gangue minerals or trash. The VHM consists of zircon, ilmenite, rutile and leucoxene. The trash minerals consist of kyanite, staurolite, chromite, monazite and other heavy silicates. The Mineral Separation Plant (MSP), on the other hand, consists of wet and dry circuits that process the heavy mineral concentrate (HMC) into four final mineral products of zircon, ilmenite, rutile and leucoxene. Zircon and ilmenite are the principal products.

This means that the valuable heavy minerals in the HMC are what the minerals sands miners are after in beneficiation.

Zircon silicate ($ZrO_2.SiO_2$) or zircon is widely used in ceramics, foundries, abrasives and refractory for its thermal stability, high light reflectivity, and opacifying qualities. Ilmenite ($TiO_2.FeO$), rutile, and leucoxene (TiO_2) are used as the primary feed material for the pigment industry (Van Gosen et al., 2013). At GCO, the qualities of some of the final products can be highly dependent on the performance of the spiral concentrators in both WCP and in the Wet Circuit of the MSP.

Spirals find a wide range of applications in the physical concentration of minerals such as chrome, coal, beach sand and iron ore (Ramsaywork et al., 2010). They are used in roughing, middlings, scavenging, cleaning and finishing separation stages (Sadeghi and Bazin, 2020). They are preferred for gravity separation because they are robust, easy to operate, and cheaper than other concentration units. However, their ability to maintain high recoveries is affected by the concentration of the gangue material and by various geometallurgical properties of mineral particles (Grobler and Zietsman, 2017). It is in this light that two new spiral technologies were tested at GCO to establish their ability to separate the valuable zircon and the unwanted silicates in zircon-rich process streams. The performance of the Compact Turbo, the Alicoco, and a currently used spiral separator were compared through systematic experimental work at pilot scale. This was to enable GCO to make an informed decision on the adoption or not of either technology, i.e., Compact Turbo or Alicoco.

1.2 Problem statement and purpose of the study

At GCO, the MSP consists of two sections: a Wet Circuit and a dry circuit (see Figure 1.1 below). The Wet Circuit receives the HMC from WCP, slurries it and uses wet-high-intensity-magnetic separators (WHIMS) to split the HMC into two

fractions: magnetic and non-magnetic. The magnetic fraction is full of ilmenite. It goes to one part of the dry circuit where it is processed further to produce final ilmenite products. The non-magnetic fraction from the WHIMS contains zircon, rutile and leucoxene. It remains in the Wet Circuit where it goes through a series of spirals, wet tables and classifiers. This processing chain produces primary, secondary, and tertiary intermediate concentrates which are indicated as non-magnetic concentrates in Figure 1.1. The concentrates are fed to another part of the dry circuit to produce final zircon, rutile and leucoxene products.

The problem that GCO has is that the Wet Circuit has been unable to reach the desired feasibility study recovery of zircon to primary and secondary concentrates since production began in 2014. The situation is exacerbated by the fact that more zircon than planned reports to the tertiary concentrate. This zircon ends up in a low-grade zircon product instead of going to the premium product via the primary concentrate at the Wet Circuit.

Reconciliation reports (GCO, 2024) and circuit balances (GCO, 2022) show that past attempts to adjust the circuit to produce more zircon in the primary and secondary concentrates have resulted in more trash minerals contaminating the zircon concentrates. As these contaminated concentrates are treated in the dry circuit, they cause the final zircon products in the dry circuit to fail to comply with customer's specifications. This ultimately affects the viability of the plant since the primary and secondary concentrates are the main sources of zircon products.

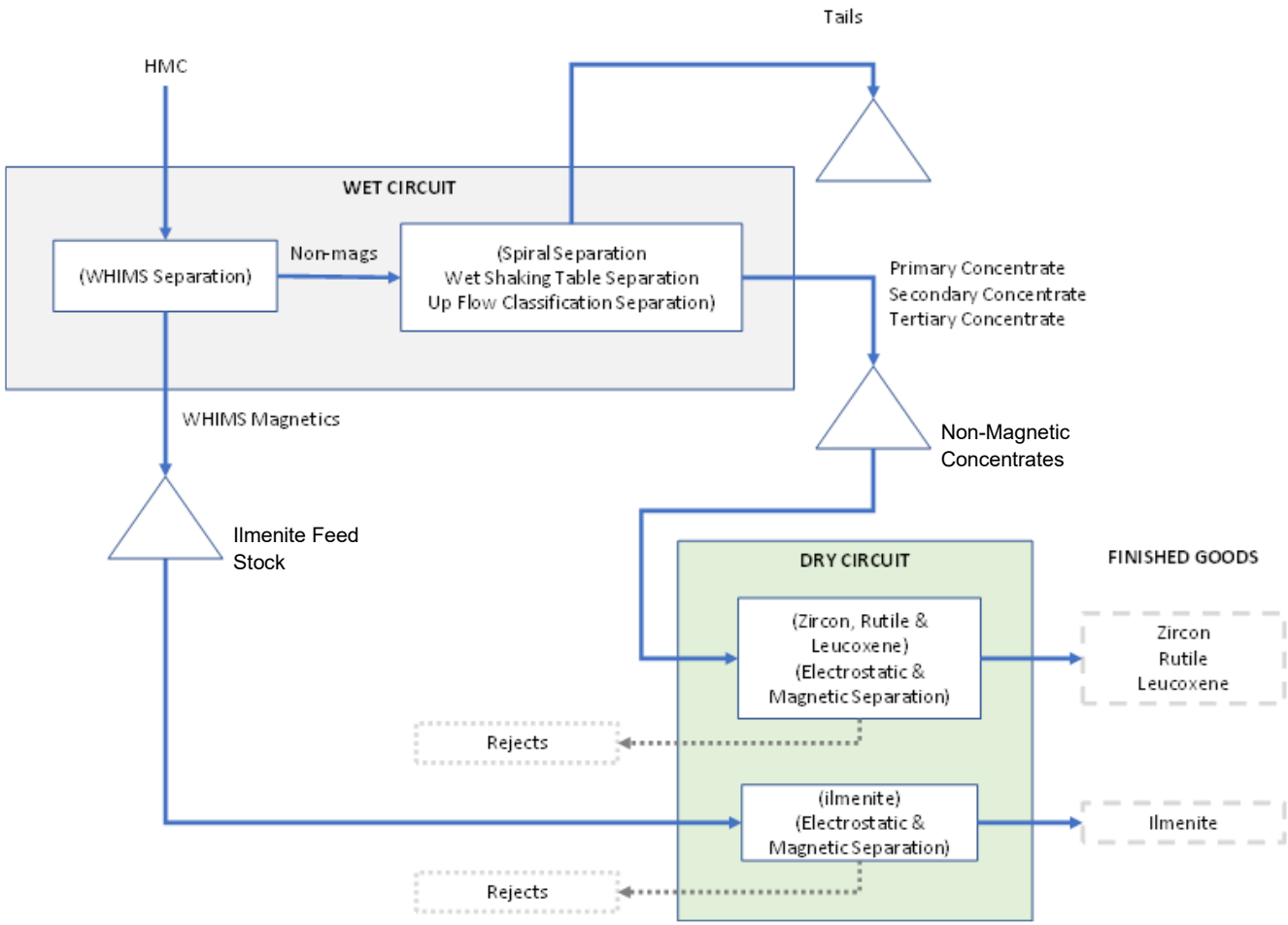

Figure 1.1: Schematic diagram of the wet and dry circuits at the MSP

Figure 1.2 below shows a detailed section of the Wet Circuit treating the non-magnetic fraction from the WHIMS separation stage. Three main steps are involved in the Wet Circuit: spiral separation, wet shaking tables separation and up-flow classification separation. The main contaminants in the concentrates which are produced by the Wet Circuit are aluminium silicates including mainly kyanite, staurolite and tourmaline. These contaminants are represented generically by Al_2O_3 in routine chemical analyses. The Wet Circuit removes Al_2O_3 and other silicates. The zircon content is represented by ZrO_2 in chemical analyses done at GCO.

Efforts to maximise the yield of the concentrates from the primary and middlings wet tables as in Figure 1.2 come with increased Al_2O_3 content. This negatively affects the quality of the primary concentrate which is referred to as Con 1. Similarly, attempts to maximise the yield from the scavenger wet tables worsens the quality of the secondary concentrate which is called Con 2. The adjustments eventually result into the tertiary concentrate or Con 3 becoming zircon-rich while at the same time being contaminated with the silicates. Trying to produce all the three concentrates which are clean of Al_2O_3 leads to zircon losses to tails.

It can therefore be argued that the current separation technology employed in the Wet Circuit has limited efficiency. Indeed, the combination of spirals, wet shaking tables and up-flow classifiers is unsuccessful at separating zircon from the silicates even though their specific densities, a physical property which plays a role in the separation process, are different theoretically. This impasse has called for the exploration of the two new separation technologies: the Compact Turbo spiral and the Alicoco spiral.

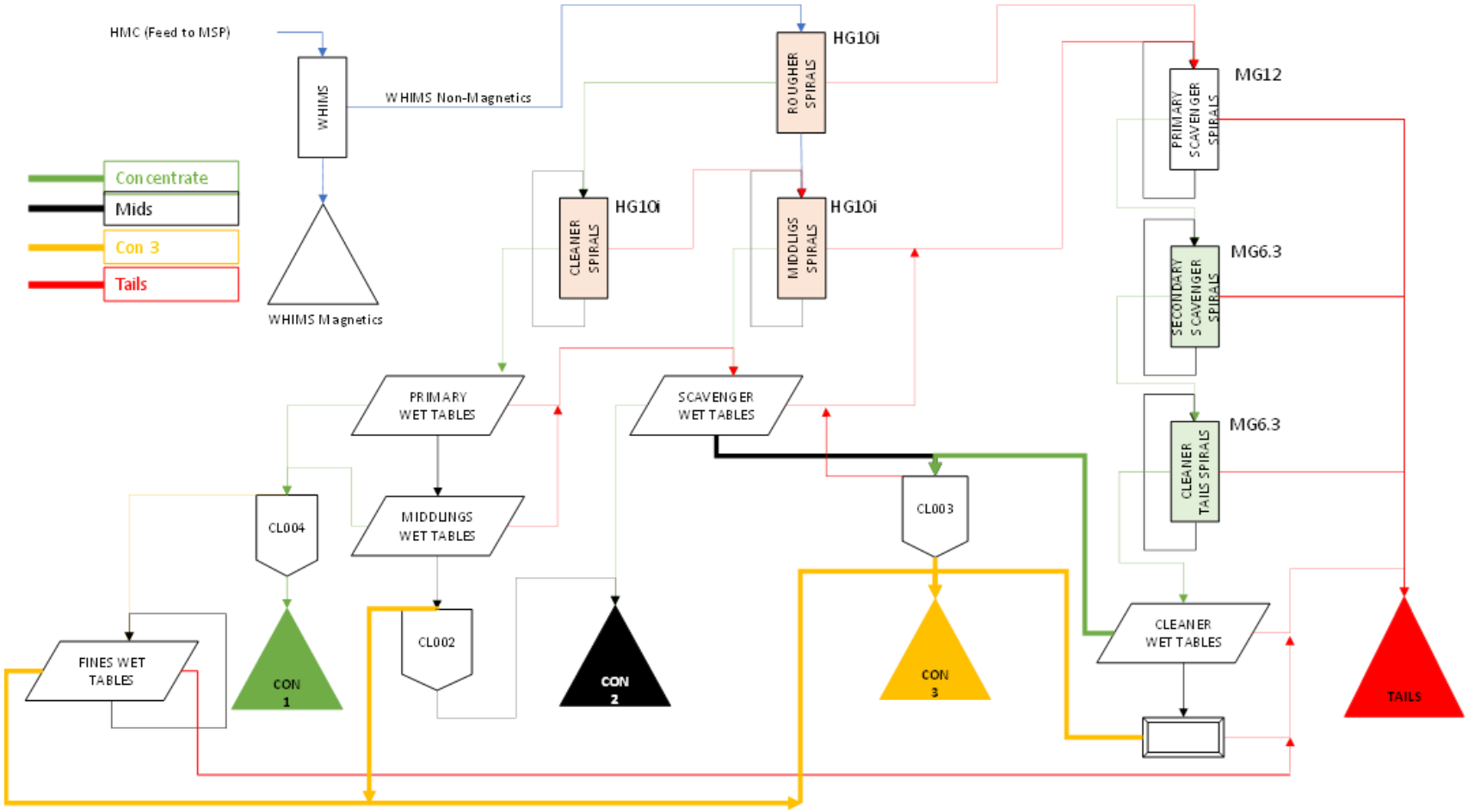

Figure 1.2: The Wet Circuit that treats the heavy mineral concentrate (HMC) to produce concentrates Con 1, Con 2, Con 3, magnetics, and tails (GCO, 2022)

The Compact Turbo is produced and commercialised by Mineral Technologies (Pty) Ltd, Australia. The Australian company has purported that the Compact Turbo would yield superior performance compared to the spirals currently used at the Wet Circuit. On the other hand, Alicoco Mineral Technology Co. Ltd (Alicoco) is a Chinese company that manufactures the Alicoco spirals. The spiral is said to be efficient in separating Al_2O_3 from zircon at good recovery. The objective of this research study is to conduct pilot tests with the two spiral technologies to ascertain their performance in separating zircon from the silicates in the Wet Circuit of GCO.

1.3 Research objectives

The primary aim of this research project was to test the ability of the Compact Turbo and the Alicoco technologies to improve the recovery of zircon while rejecting aluminium. Zircon is more valuable than other minerals such as ilmenite while aluminium is a contaminant in a mineral sands process (Jones and O'Brien, 2014); hence, the motivation for this research study. The associated objectives of the research can therefore be formulated as follows:

- To test the performance of the Compact Turbo and of the Alicoco spirals in rejecting Al_2O_3 while recovering zircon from a stream that makes up the tertiary concentrate.
- To compare the performance of the two new types of spirals to that of the old spirals currently installed in the Wet Circuit, which are the MG12 and the HG10 spirals.

The ability of the Compact Turbo and Alicoco spirals to separate zircon from aluminium could lie in the properties of the particles of the two minerals. The differentiator could be particle size, particle density or any other property (Grobler and Zietsman, 2017). Be that as it may, a better understanding of the performance of the two technologies would be valuable for GCO and could lead to innovative solutions to the problem. In addition to this, should any of the two

spirals be able to reject aluminium without losing the valuable zircon to tails or to low-grade products, GCO will pursue a continuous improvement initiative for the Wet Circuit. To support these future efforts, the following secondary objectives were also explored:

- To establish why it could be difficult or possible to separate zircon from aluminium in the streams that make up Con 3.
- To model zircon recovery resulting from scavenging zircon to the tertiary concentrate using the best performing spiral and the plant data.

Modelling the zircon recovery was however not as critical as establishing the good separation performance and the principles through which it could occur. This is because irrespective of the results of the modelling endeavour, the best performing spiral would have to be proved by conducting further tests in the field beyond the scope of this research.

1.4 Scope of the research

1.4.1 Research questions

Previous work has shown that the splitter positions, the feed rate and the pulp density affect the performance of the spiral concentrator (Tripathy and Murthy, 2012; Ramsaywork et al., 2010). By varying these three factors, the following questions associated with the primary objectives of this research study could be addressed:

(1) Can the Compact Turbo and Alicoco spirals improve the quality of a stream that makes up the tertiary concentrate by rejecting aluminium silicates and retain zircon?
(2) Why is it currently difficult to separate the zircon and aluminium particles in the tertiary concentrate?

To answer the first research question, a sample from the major stream that makes up the tertiary concentrate (Con 3), which was the classifier 3 (CL003)

underflow (refer to Figure 1.2 above), was collected. The sample was run through the Compact Turbo spiral, the Alicoco spiral, and the MG12 and HG10 spirals which were each installed in a test rig that is later presented in Chapter 3. So, all experimental test work was done on the pilot plant (or test rig) available at GCO.

To explore the second research question, samples from the best performing spiral were sent to the Eramet Ideas Laboratory in Paris (France) for QEMSCAN (quantitative evaluation of minerals by scanning electro-microscopy) analysis. This was to characterise the density, the sizes, the possible inclusions, and the associated mineralogy of particles present. This information may ultimately assist in understanding the challenges inherent with physical separation at GCO.

1.4.2 Selection of operational variables

Tripathy and Murthy (2012) demonstrated that the feed rate, feed pulp density and splitter position of a spiral are the main parameters that affect the recovery of chrome (Cr_2O_3). For this research study, the three operational variables are also considered: the splitter position, the pulp density and the operational conditions feed rate to the Turbo Compact and Alicoco spirals. The variables are adjusted one at a time to test their individual effects on the performance of the two new spirals while the other variables are kept constant. And while the focus of the work by Tripathy and Murthy (2012) was on the recovery of Cr_2O_3, this study specifically looks at the recovery of ZrO_2 and the rejection of Al_2O_3.

1.4.3 Limitation of the research

The effects of feed grade were not investigated as part of this research project. Indeed, Grobler and Zietsman (2017) already reported that an increase in trash minerals in the feed displaced the valuable content which in turn adversely affected the performance of a spiral.

Secondly, this research study did not look at the design of the two new spirals. The motivation was not to identify the design features of the two spirals that govern performance. It was rather to see how the two spiral units would perform in terms of recovery of the target mineral and separation of the unwanted mineral fraction.

Lastly, the pilot plant was used for the test work programme. Testing the two spirals as part of the actual Wet Circuit was outside the scope of this work. However, results obtained from this pilot test work and the research study as a whole would serve to consider full-scale testing of the Wet Circuit.

1.5 Layout of the dissertation

This research is organised in six chapters.

Chapter 1 introduces the basic concept of mineral beneficiation, the spiral as a gravity separator in mineral sands, the problem facing GCO, the research objectives, and the research questions.

The second chapter is a literature review where the history of innovation in mineral processing leading to the arrival of spiral separators in the market is presented. Factors affecting gravity separation such as feed rate, particle size and density are discussed in detail.

Chapter 3 details the rig test work which was conducted. The planning and collection of adequate samples from the Wet Circuit as well as the handling before the test work are also presented. The preparation of all experimental tests carried out at the spiral rig and the associated performance are then covered. Lastly, the problems that were experienced before, during and after the test work are highlighted.

Chapter 4 presents the results emanating from the chemical, particle size, mineralogy and QEMSCAN analysis of the various products obtained from the

test work. A qualitative interpretation of the results obtained around the Alicoco spiral, the Compact Turbo spiral, the MG12 spiral and the HG10 spiral is done.

The quantitative meaning of these results is then presented in Chapter 5 with the view to rank the performance of individual spirals in line with the objectives of this research study.

Finally, Chapter 6 provides some answers to the research questions based on the findings from Chapter 5. Recommendations are also made for further testing on the high-performing spiral.

1.6 Summary

The Wet Circuit part of the mineral separation plant of the Grande Côte Opérations (GCO) in Senegal makes use of spirals for gravity concentration. It has not been successfully separating zircon and aluminium in some streams, which has resulted in the lower-than-expected recovery of zircon. The introduction of two new spiral technologies to the market with promising efficient separation of zircon and aluminium has prompted this research study. The two separation technologies are the Compact Turbo spiral from Mineral Technologies (Pty) Ltd, Australia and the Alicoco spiral from Alicoco Mineral Technology Co. Ltd (Alicoco), China. They are tested using a feed from one stream which is rich in both zircon and aluminium in the Wet Circuit of the GCO. This is to establish their separation efficiency. The pulp density, splitter position and the feed rates of the two spirals are systematically tested in a pilot rig to provide some answers to the research questions presented in Section 1.4.

The next chapter discusses the theory underpinning the working principle of spiral concentration, the factors affecting spiral recoveries, the pilot plant testing and the types of mineralogical analysis used in gravity separation. This is to pave the way for the experimental work for this research.

Chapter 2 Literature review

2.1 Introduction

Gravity separation refers to any process that exploits differences in physical properties of mineral particles to separate them. Spiral separators, also known as spiral concentrators or spirals for short, are one versatile type of equipment manufactured to perform gravity separation at roughing, middling, cleaning, or finishing stages.

Tests are conducted continuously on various types and designs of spirals to determine whether they are still performing their duty well. These tests also assist in finding a suitable replacement or in the design of a new circuit. The pulp density and flow rate a spiral as well as the position of the splitter are the three most important parameters (Ramsaywork et al., 2010; Sivamohan and Forssberg, 1985). Each parameter can be manipulated to alter the concentrate grade-recovery relationship which is a good indicator of spiral performance. The properties of the ore to be treated have equally been found to affect recovery. Indeed, Grobler and Zietsman (2017) demonstrate that particle size distribution, agglomeration, near-density particles, and trash contents affect the spiral performance. Lishchuk et al. (2020) add that, as a result of the challenges associated with these ore properties, geometallurgy has become a risk mitigator for mining companies. Geometallurgy enables various sections or departments of the mine such as geology, metallurgy, engineering, and environment to come together and identify in advance difficulties that will be brought by ore body variations (Lund and Lamberg, 2014). These problems extend through several stages of the mine value chain including comminution, magnetic separation, electrostatic separation and gravity separation.

The literature review covers four main themes. It looks at the concept of gravity separation and spiral separators as main role players in the field.

Factors affecting the efficiency of spiral performance are explored. It reviews mineral beneficiation and recovery theory. And finally, it contextualises how a geometallurgy tool such as QEMSCAN enhances understanding of equipment performance and business viability through ore body knowledge.

2.2 Mineral sands in West Africa

Killian et al. (2016) list South Africa, Senegal, Sierra Leone, Mozambique and Kenya as African countries which operate heavy mineral sands mines. Egypt and Madagascar are two other African countries with heavy minerals mining operations. In Egypt black sands deposits in the Nile Delta contain heavy minerals (Hedrick and Waked, 1989). Egyptian Black Sand Company was inaugurated in 2023 to extract heavy metals from the black sand deposits (Hattab et al, 2023). Ranobe deposit near Toliara and deposits between Manombo River and Monombo in Madagascar are rich in heavy minerals (Reyneke and Wallmach, 2007). Senegal and Sierra Leone are the two countries that have mining operations in heavy minerals in West Africa.

Grande Côte Opérations (GCO) mines a 100 km long and 5 km wide mineral deposits that belong to the Senegal-Mauritanian basin. The basin includes western Mauritania, Senegal, Gambia, Guinea-Conakry and Guinea-Bissau (Dieye et al. 2020). In their study, Dieye et al. (2020) used QEMSCAN to characterise the heavy mineral concentrate (HMC) of GCO which contained in average 11.27% zircon, 21.72% ilmenite, 52.81% pseudorutile, 1.16% anatase, and 2.56% rutile.

Gbangbama, Sembehun, Rotifunk and Kambia deposits in Sierra Leone make up the largest natural rutile reserve in the world. Discovered in 1954, the rutile grade in the reserve is estimated to be between 1.5% and 2% with a Rotifunk deposit estimating 235 million tons at 0.62% (Jalloh et al. 2013). Sierra Rutile Limited produce the natural rutile from the Sierra Leone deposits.

2.3 Spiral concentrators

Spiral concentrators or spirals are gravity separation processing units which exploit physical properties in a mixture of solids particles. The mixture of particles or feed is presented to the top of a spiral, normally in a slurry form at certain solids content by weight with fluid medium. As the slurry finds its way down the spiral separation occurs between the particles influenced by gravitational and centrifugal forces that act on them (Sudikondala et al., 2022).

2.3.1 Gravity separation: Principles

Gravity separation or gravity concentration refers to a class of physical separating methods which take advantage of the difference in density among mineral particles (Gulsoy and Gulcan, 2019). To put it another way, gravity separation entails all methods that "separate minerals of different specific gravity by their relative movement in response to gravity and one or more other forces, the latter often being the resistance to motion offered by a viscous fluid, such as water or air" (Wills and Napier-Munn, 2006).

Because gravity concentration was practiced over 3000 years ago, Burt and Mills (1985) consider it to be a process that was developed in the dark ages. Be that as it may, its advantage over flotation at the time was due to its low costs of installation per ton of throughput and low installed power requirements. It also does not use reagents, making it environmentally friendly (Richards et al., 1999). For a long time, gravity concentration was erroneously considered to be a coal and iron ore application. However, Burt and Mills (1985) later reported its widespread applications in processing tantalum/columbium, tungsten, chromite, uranium, gold, silver, diamond, fluorspar, mineral sands and barite.

The history of gravity separation provides insights into the current challenges of various operations. Gulsoy and Gulcan (2019) list six methods that have been employed for gravity separation: jigs, pinched sluices (trays and cones),

spirals, shaking tables (wet and dry), fine particle separators (Falcon concentrator and multi-gravity separators), and gravity sizing (hydrosizers and cyclones). Walklate and Fourie (2006) provide an example of the process flow sheet of the primary concentrator at Richards Bay Minerals (RMB) in South Africa in 1990. As can be seen in Figure 2.1, the concentrator consisted of Reichert cones (Figure 2.1b) throughout the production process of the heavy mineral concentrator (Figure 2.1c).

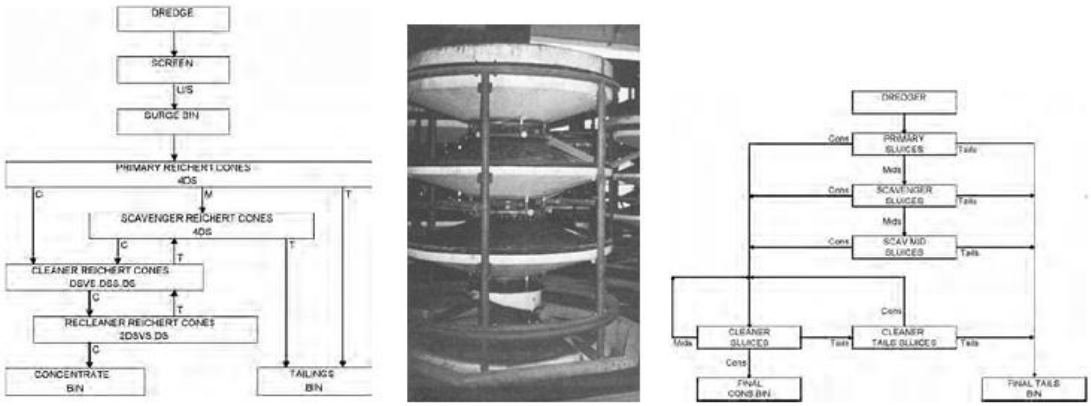

(a) (b) (c)

Figure 2.1: (a) Plant A and (c) the five-stage circuit of Plants B and C in 1990 at Richards Bay Minerals with (b) a Reichert cone (Walklate and Fourie, 2006; Wills and Napier-Munn, 2006)

Gravity separation technologies have been evolving over the years. There is not even a single Reichert cone in use in processing circuits today. Modern technologies exemplified in the wet concentrator plant (WCP) in Figure 2.2 below have taken over the scene. Thickeners, hydrocyclones, and spirals have hence become ubiquitous.

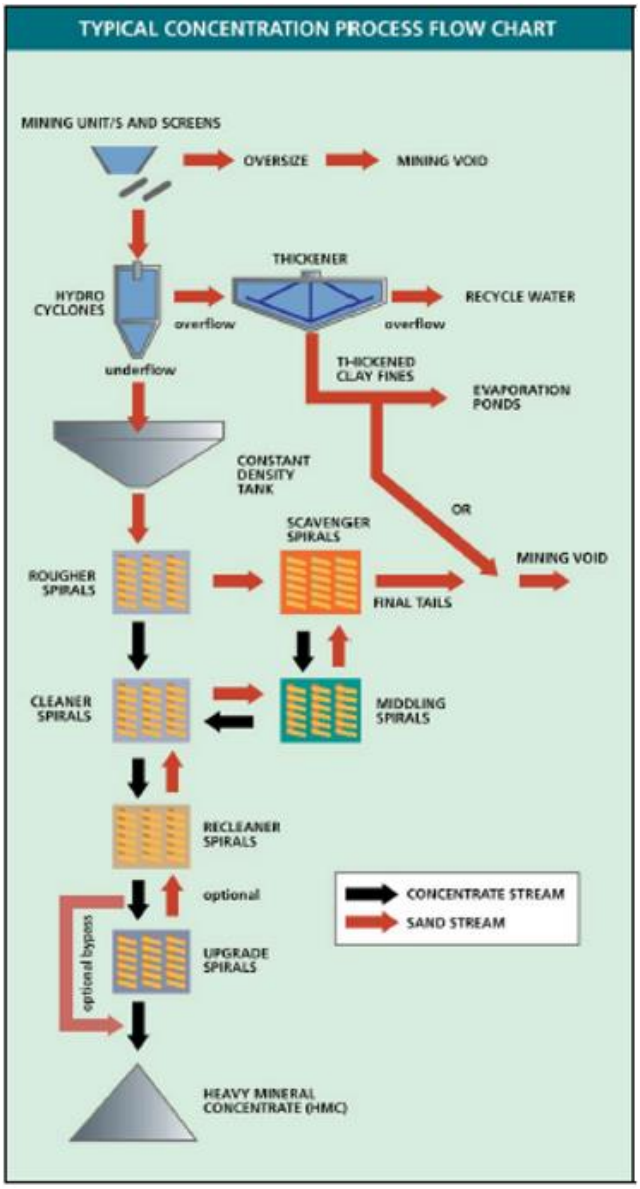

Figure 2.2: Illustration of a typical modern WCP process (after Jones, 2006)

Progress in gravity concentration has been based on commercial objectives and on solving problems that faced the industry at the time (Burt and Mills, 1985; Gulsoy and Gulcan, 2019; Walkate and Fourie, 2006; Jones, 2006). When Reichert cones could not further improve the quality of separation, spirals then came into the market to bridge the gap. The most common type of spiral concentrating unit is covered in the next section.

2.3.2 Design of the commonly used spirals

According to Wills and Napier-Munn (2006), the Humphrey spirals are the most widespread design of spiral concentrators. They have been in commercial applications treating chrome-bearing sands since 1943. They treat pulps of density between 15% and 45% of solid content by mass through their helical conduit of modified semi-circular cross-section with the feed spiralling down from the top to the bottom (see Figure 2.3 below). They are available in columns of different heights and different number of starts. Note that “start” here refers to the number of feed pipes going to the number of helical conduits around a column. It can be a one start for a single spiral, two starts for double spiral, a triple start for three spirals or a four-start for four spirals around one column.

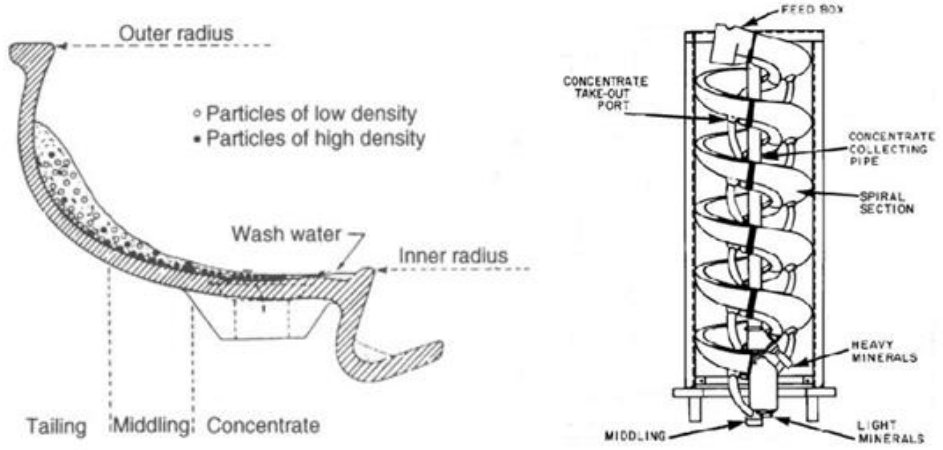

(a) (b)

Figure 2.3: Original design of a spiral concentration (Wills and Napier-Munn, 2006)

Sivamohan and Forssberg (1985) explain that a centrifugal force acts on particles along the helical conduit of the spiral as the slurry gravitates from the top to the bottom. As a result of this spiral motion, the heavier particles concentrate to the centre column while the lighter particles are pushed to the edge of the conduit as shown in Figure 2.3(a). Some particles however stay in the middle and never get to migrate fully outwards.

Characteristics of the pulp such as feed grade, percent solids, flow rate and particle size distribution affect the effectiveness of a spiral concentrator (Sivamonah and Forssbeg, 1985). Perry et al. (1997) recommend feeding at high pulp density if the valuable heavy mineral (VHM) content is contained in coarse and heavy mineral particles while low pulp density is preferred when valuables are contained in finely sized heavy minerals.

The angle of the slopes of the helical (see Figure 2.3b for reference) affects the cut-off density of the separation, with steeper angles being favourable for heavy mineral-silica separation. Splitters located along the spiral height to the bottom (Figure 2.4) are also used to draw out a concentrate towards the centre of the spiral column as the slurry gravitates to the bottom (Wills and Napier-Munn, 2006).

(a) (b) (c)

Figure 2.4: Spiral splitters (a) outside, (b) from the top to the bottom (c) some at the bottom (GCO, 2022)

In a simulation of a particulate flow in a spiral concentrator, Mahran (2015) considered the following design parameters: the pitch, the profile shape length, and the inner and outer trough radii. Note here that the pitch of a spiral refers to the vertical distance between similar points on successive turns on the helix (Davies et al., 1991). A profile, on the other hand, is the section of the spiral that provides separation and migration of heavy minerals through relative density.

The spiral length or the number of helix turns is determined relative to the pitch and the profile. In terms of the simulation, the researcher observed that the number of turns of the spirals is critical in determining the stability of the distribution of particulate solids toward the end of the trough. As for the pitch, a steeper pitch was noted to yield good loading for heavy minerals in the spiral feed.

2.3.3 Effects of feed rate on spiral recovery

High throughput (or high feed rate) is generally favoured for spirals as this translate into more concentrate products for the operations and therefore higher revenue. However, increasing feed rates are known to negatively affect the recovery of valuable mineral. Figure 2.5 illustrates the relationship between feed rate and recovery for Cr_2O_3 in a chrome processing plant. As the feed rate increases, the recovery decreases and reaches a minimum before it starts to slowly increase. This is observed at the two different concentrations of solids in the feed tested (Tripathy and Murthy, 2012).

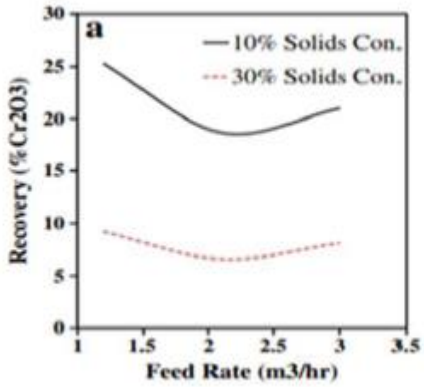

Figure 2.5: Effects of feed rate on Cr_2O_3 recovery (Tripathy and Murthy, 2012)

In another mineral sands study, Kari et al. (2006) observed that when treating the heavy mineral concentrate (HMC) optimum conditions are established when the feed rate increases, which equally leads to an increase in the

concentrate grade. This implies that there would be a point where the concentrate grade would start to decrease as the feed rate further increases.

Lastly, Ramsaywork et al. (2010) investigated the recovery of zircon as a function of feed rate and content of fine particles (or slimes) in the feed. And as summarised in Figure 2.6, the group of researchers was able to show that zircon recovery consistently decreased when feed rate increased irrespective of the slimes content in the feed.

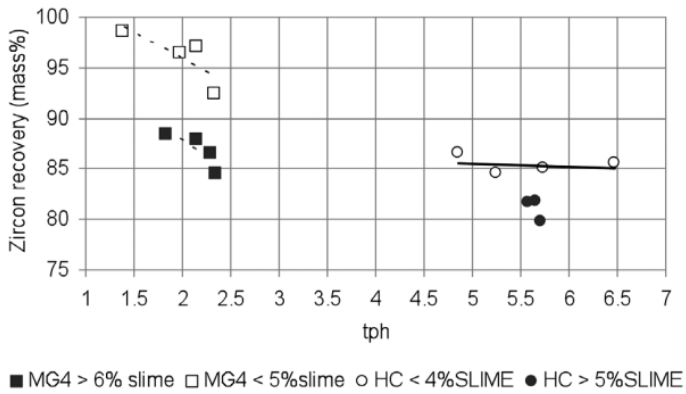

Figure 2.6: Effects of feed rate on zircon recovery for various slimes content in the feed (Ramsaywork et al., 2010)

2.3.4 Effects of splitter position on spiral recovery

A splitter is a feature placed along the length of the active surface of the spiral to channel heavy particles (or concentrate) towards the collection launder. The splitter is adjusted once the separation has been established on a spiral surface and the thickness of the separated concentrate has grown (Holland-Batt, 1995).

While the positions of splitters on the active surface of a spiral are well known for their limited effects on the yield and quality of the product streams, they are critical for the control of spiral performance as they directly impact the recovery. Indeed, as illustrated in Figure 2.7 below, at low feed rate (1.2 m^3/h) and diluted slurry feed (10% solid content), Cr_2O_3 recovery is seen to increase from 25%

to more than 45%. Such an increase in recovery is noted as the position of splitters changes from 12 cm to 14 cm measured from calibrated marks on the split cutter or designated positions on spiral surface (refer to Figure 2.4b and Figure 2.10).

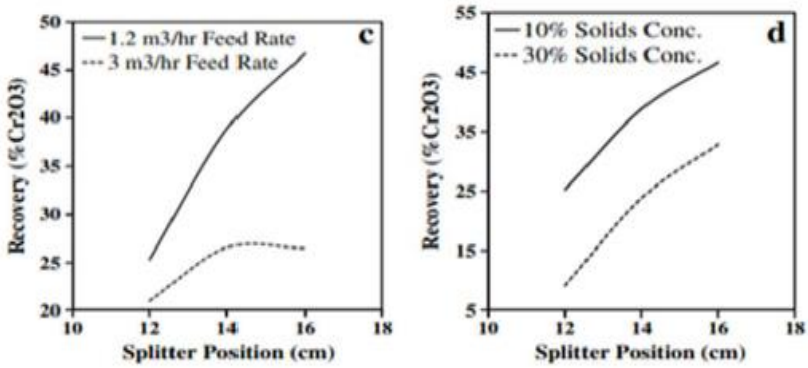

Figure 2.7: Effects of splitter position on Cr2O3 recovery (Tripathy and Murthy, 2012)

The splitters are located along the height of a spiral, on spiral turns and at the bottom of the spiral (Alaee et al., 2025). The first splitters are normally positioned from the first third of the spiral height (see Figure 2.8 below for reference).

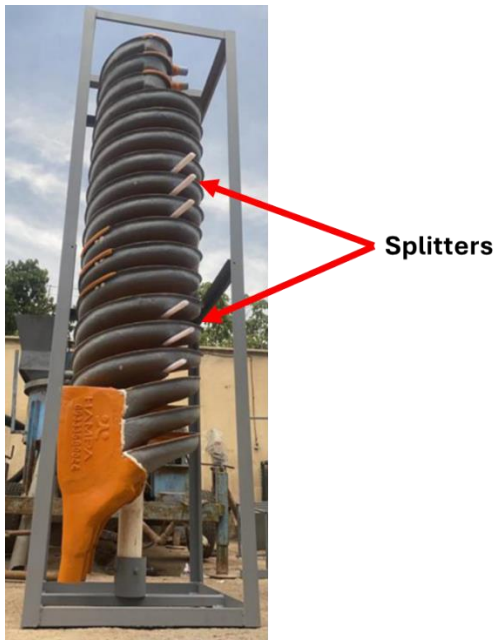

Figure 2.8: A spiral prototype showing some splitter positions (Alaee et al. 2025)

The basis of the splitter position on a spiral surface or trough is a visual band which forms on the surface as the slurry gravitates from the feed point towards the bottom end. Figure 2.4(b) above shows a calibrated splitter handle in which the first number from the outside of the spiral is considered the splitter position. The handles of the splitters are then adjusted as per the separation as seen in Figure 2.9 below to extract the heavy particles as they concentrate towards the centre column (Alaee et al., 2025).

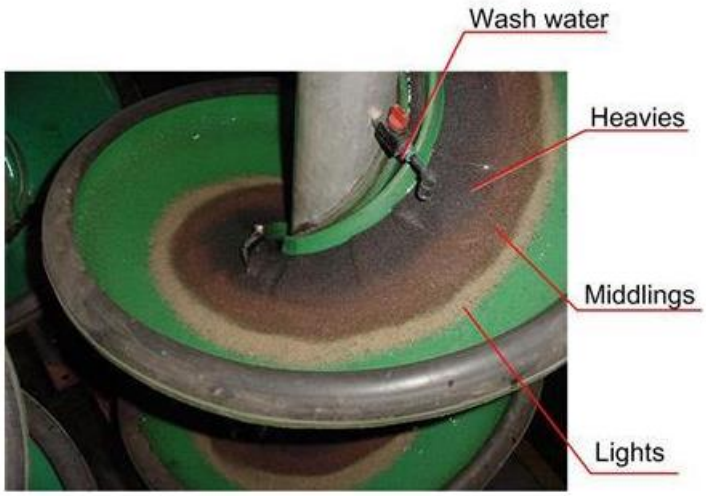

Figure 2.9: Visual bands appearing on the spiral surface due to stratification on the spiral trough (Wills and Finch, 2016)

The bottom splitters are either the same as in Figures 2.4(b) and 2.4(c) are as shown in Figure 2.10 below. They are the last sets of splitters before the separated streams are collected by different launders sitting below the spirals.

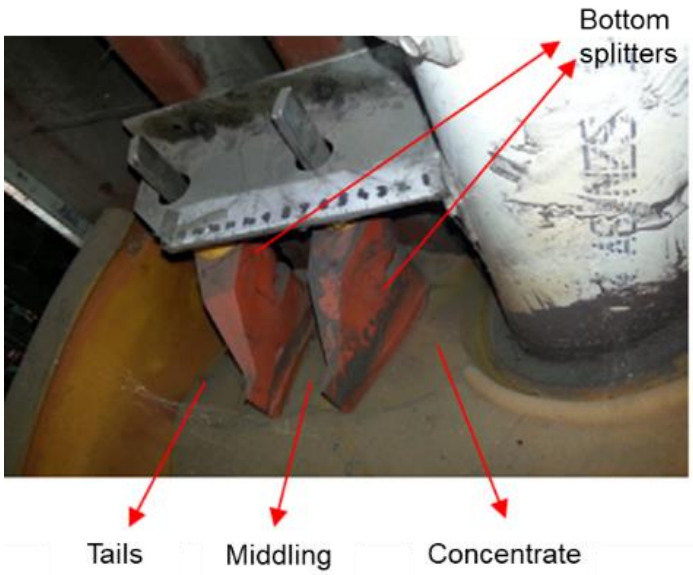

Figure 2.10: Bottom splitters of a spiral separator (Dixit et al. 2015)

2.3.5 Effects of pulp density on spiral separation

In mineral processing, high pulp densities can mean increase in throughput and process flow rates. As such, pulp density is a physical property that is used to optimise the performance of process equipment. In a ball mill for example, slurry density determines the migration of particles through the mill zones which is then related to grindability and power consumption (Tangsathitkulchai and Austin, 1989). In froth flotation, which is a physiochemical process compared to mineral sands, the effects of slurry density on the separation of nickel-copper sulphide from fine serpentine has also been reported. Here, a decrease in the density of the pulp from 40% to 20% by weight saw an increase in the recovery of nickel from 70.7% to 79.5% and an increase in copper recovery of from 82% to 85.4%. The density of the pulp therefore affected its rheology leading to improved plant performance at low density (Gao et al., 2018).

Now in terms of gravity concentration, denser pulps are often desired as they are associated with high feed rates. However, like with the feed rate, an increase in pulp density introduces inefficiency in the spiral and results to a

decrease in recovery to the concentrate as the valuable mineral is lost to the tails. This is illustrated in Figure 2.11 for Cr_2O_3 as the valuable mineral (Tripathy and Murthy, 2012). It can be seen indeed that the recovery steadily decreases as the pulp density increases irrespective of the feed rates tested, i.e., 1.2 m^3/h and 3 m^3/h.

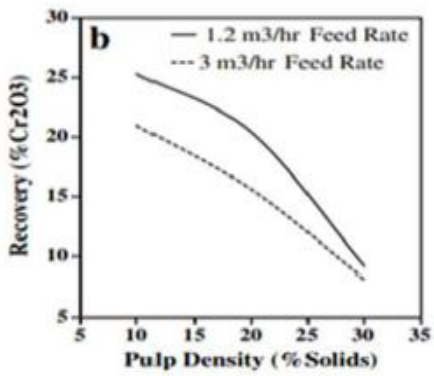

Figure 2.11: Effects of pulp density on Cr_2O_3 recovery (Tripathy and Murthy, 2012)

For the mineral of value tested (i.e., Cr_2O_3), low pulp density is preferred as this translates into higher recovery to concentrate. Low density makes room for suspended solid particles to freely move thereby leading into a clear separation of heavy minerals from light ones present in the feed. Light mineral particles therefore enjoy an almost unhindered motion, which may explain the trends in Figure 2.11.

2.3.6 Effects of feed properties on spiral separation

The properties of the feed to be treated by a spiral are central to the amenability of the feed to spiral concentration. The presence of agglomerations, near-density particles and trash minerals are some of the main factors that affect the efficiency of the spiral separation. Richardson et al. (2002) define agglomeration as the interaction between particles adhering to each other and forming clusters. This is due to mechanical interlocking, surface attraction, plastic welding, electrostatic attraction, moisture effects, and temperature

fluctuations. Near-density or near-gravity material, on the other hand, refers to the amount of material occurring within ±0.1 specific gravity cutoff range (Majumder and Barnwal, 2003). Any material with the cutoff range may report to the concentrate or the tails and contribute to contamination. Lastly, Grobler and Zietsman (2017) explain that the presence of trash minerals can outweigh the effects of particles on spiral separation. This is especially true if a significant volume of trash minerals falls within the cut-off range.

Another equally important property of the feed is particle size distribution. According to Kursun et al. (2016), particle size analysis is a key requirement in managing a beneficiation process as the size and shape of particles determine their behaviour during gravity separation. Sivamohan and Forssberg (1985) advise that the spiral should be set up to minimise the loss of heavy finer particles to the tails. This is because these fine particles, although heavy, can be easily dragged by the centrifugal force to the edge of the conduit thereby reporting to the tails as misplaced. Tripathy and Murthy (2012) highlighted the problem by analysing the chemical content of the spiral concentrate per particle size fraction. The Cr_2O_3 content was observed to vary with particle size as can be seen in Table 2.1 below.

Table 2.1: Example of chemical analysis showing Cr_2O_3 at different particle sizes (after Tripathy and Murthy, 2012)

Size (micron)	Assay value (%)			
	Cr_2O_3	$Fe_{(T)}$	Al_2O_3	SiO_2
+150	10.07	21.38	18.99	25.99
-150 +105	15.80	18.03	18.40	25.31
-105 +75	17.06	16.99	17.20	27.28
-75 +45	22.60	19.41	14.02	21.62
-45 +37	28.54	19.21	13.01	17.10
-37 +25	32.13	17.45	12.62	15.69
-25	23.81	24.94	13.02	13.47

And in the particular sample for which the chemical analysis results are reported in Table 2.1, the Cr_2O_3 content increased as particle size became finer. The opposite was noted with SiO_2 (the trash mineral) suggesting higher misplacement of SiO_2 particles to the concentrate stream at coarser particle sizes.

Considering the importance of particle size, it is not surprising why it can be measured using several techniques depending on the fineness of the material to be analysed. Richardson et al. (2002) for example presented eight such particle size analysis techniques and their respective ranges of application. The most widely used technique is sieving; it finds application in the analysis of solids of size 50 μm and coarser using a nest of sieves. Conversely, microscopic analysis is a two-dimensional technique which is used to analyse particles of up to 0.001 mm. The sedimentation and elutriation method is used to measure particle sizes smaller than 1 mm. Permeability is another particle size measuring technique that makes use of pressure difference across a packed bed to measure 1 mm and above particles. Electronic particle counters, laser diffraction analysers (for particles of size 0.1 to 600 μm), and X-ray or photo-sedimentometres are modern methods of particle sizing.

Finally, Wills and Napier-Munn (2006) argue that sieving forms part of the oldest methods of particle size analysis. In terms of its principle, a known weight of sample, wet or dry, is passed through a stack of sieves that are shaken for a given time span (usually 15 or 20 min). The mass retained of each sieve is measured to determine the corresponding percent fraction of the initial sample for that sieve size.

2.4 Beneficiation of mineral sands

Beneficiation in mineral sands occurs through a combination of mineral processing, chemical analyses and monitoring the recovery of total heavy minerals. In this section primary concentration after mining, mineral separation

for final products concentrates, the minerals of interest and gangue minerals are discussed. Gangue material or trash, with a specific gravity between 3 g/cm^3 and 4 g/cm^3 has no value. Its presence can negatively affect the spiral performance and reduce recovery of saleable minerals such as zircon (Grobler and Zietsman, 2017).

2.4.1 Production of heavy mineral concentrates

Mineral sands are extracted from mineral deposits generally found in costal environments. Referred to as heavy mineral sands, this name stems from the use of tetrabromoethane (TBE), which has a density of 2.96 g/cm^3, to separate quartz that has a density of 2.71 g/cm^3 from the minerals which have densities greater than that of the TBE (Grobler and Zietsman, 2017).

The mining of heavy mineral sands is generally done by dredging or hydraulic mining through an open pit or by dry excavation mining. Perks and Mudd (2019) provides a general outline of the beneficiation process where the run-of-mine ore is pumped through a series of preparation stages. As illustrated in Figure 2.12, these stages can include comminution, screening, hydrocyclones, thickeners, density tanks and spirals to produce a heavy mineral concentrate.

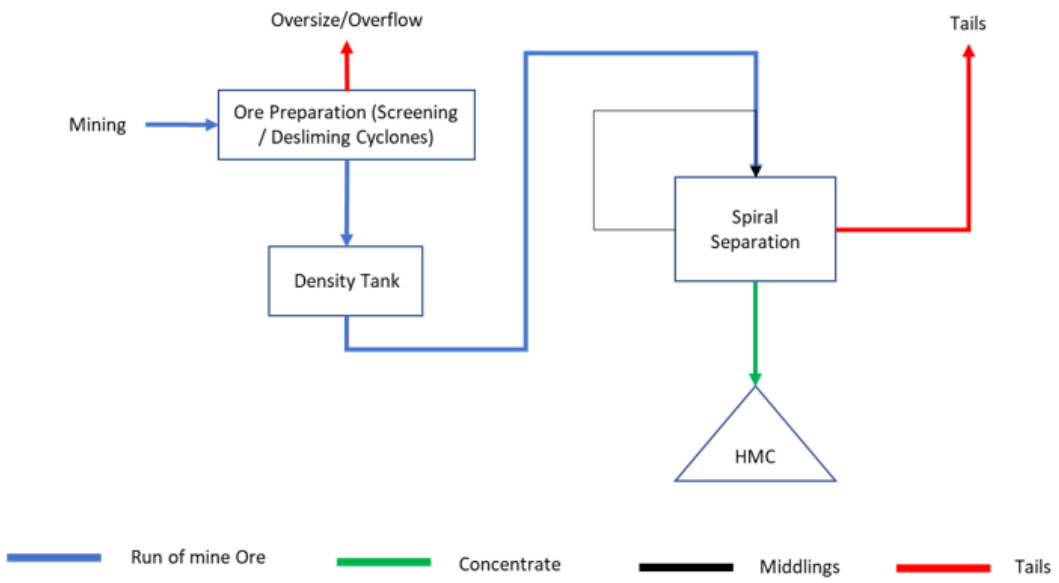

Figure 2.12: Typical mining and production of heavy mineral concentrate (adapted from Perks and Mudd, 2019)

The prepared heavy mineral concentrate (HMC) is treated in a mineral separation plant (MSP) to produce finished goods. As shown in the MSP in Figure 2.13, the HMC can be slurried and treated by wet-high-intensity-magnetic separation (WHIMS). This is done to separate the ilmenite-rich magnetic fraction from the non-magnetic fraction which is rich in zircon, rutile and leucoxene. The magnetic fraction can then be later treated preferably dry to produce the ilmenite product. The non-magnetic fraction, on the other hand, goes through a series of spiral, wet shaking tables and classification in the Wet Circuit to produce a concentrate. The concentrate from this process is then treated through electrostatic and magnetic separation dry to produce rutile, leucoxene and zircon.

It is therefore clear that if spiral separation in Figure 2.12 does not yield good-quality HMC or if a substantial amount of heavy minerals report to the tails; then, the mine will be working at a low profit margin as less goods will be produced from the MSP.

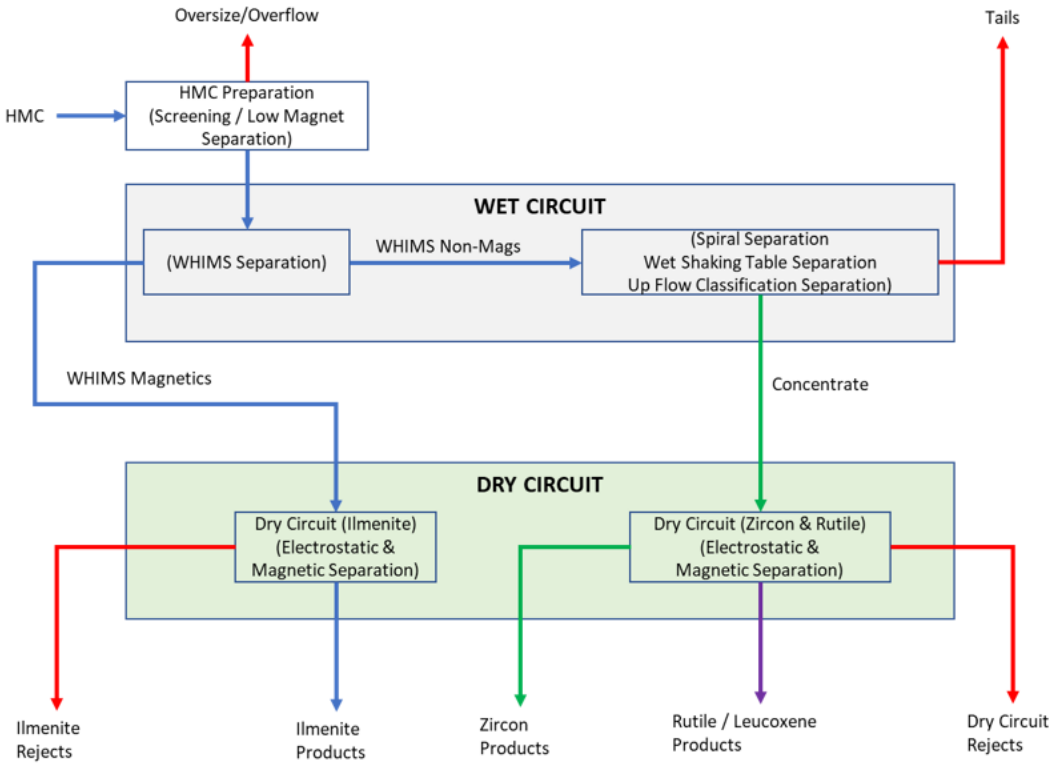

Figure 2.13: A typical HMC separation process (adapted from Perks and Mudd, 2019)

2.4.2 Common heavy sand minerals

Zircon is one of the heaviest (more accurately, it is one of the densest) minerals in the heavy sand family. It is a non-magnetic and non-conductive mineral that is available in the form of any of the zirconium silicates ($ZrO_2.SiO_2$) shown in Figure 2.14.

It has a specific density of 4.6 – 4.7 g/cm^3 with a bulk density of 3.8 g/cm^3 (Perry et al., 1997). It exhibits heaviness during gravity separation similarly to other materials (i.e., contaminants) present in the feed (Van Gosen et al., 2013). Contaminants therefore make it challenging to achieve good zircon recovery as solids-solids separation becomes difficult.

Figure 2.14: Zirconium silicate (source: Abduriyim et al., 2012)

High content of silicates in zircon-bearing feeds contributes to high intermediate stockpiles in mineral sands operations. The silicates also contribute to high zircon losses to rejects, and thus, to low production of zircon. Reprocessing poor concentrates of intermediate stockpiles may bring about a better concentrate. This implies that in order to increase the zircon recovery, the business must increase the footprint of spirals which can result into a project becoming financially not viable (Galvin et al., 2016).

The major contaminating silicates are kyanite, staurolite, quartz and tourmaline. See Figure 2.15 through Figure 2.17 for the visual samples of these silicates. Kyanite (Al_2SiO_5) is transparent, blue or white while staurolite ($Fe^{+2}Al_4[Si_4O_{11}]_2O_2(OH)_2$) is dark or reddish brown (Anthony et al., 1995).

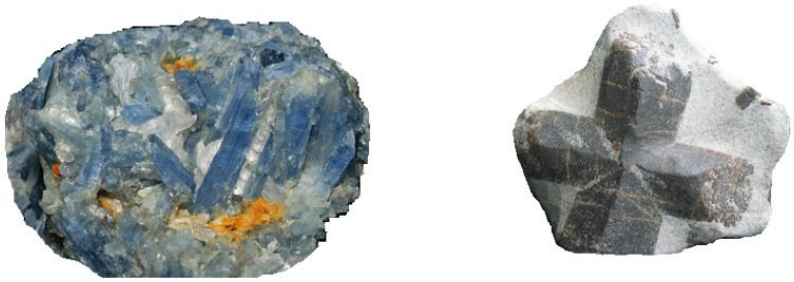

(a) (b)

Figure 2.15: (a) Kyanite and (b) Staurolite (Alderton, 2021)

Tourmaline is another heavy sand mineral. It is complex compared to kyanite and staurolite with the following generalised formula: (Na, Ca) R_3(Al, Fe)$_6B_3Si_60_{27}$(O, OH, F)$_4$, where R = Mg, Fe", Fe"', Al, Li, Mn, and Cr (Krynine, 1946). Tourmaline has three basic focal points in its mineral group: Elbaite or lithium tourmaline ($H_5NaLi_2Al_2Al_8B_4Si_80_{4l}$); Schorlite or iron tourmaline ($H_5NaFe_2Fe_2Al_8B_4Si_8O_{4l}$); and Dravite or magnesium tourmaline

($H_5NaMg_2Mg_2Al_8B_4Si_{4l}$). Although it occurs frequently in mineral deposits, it is not detected quite often.

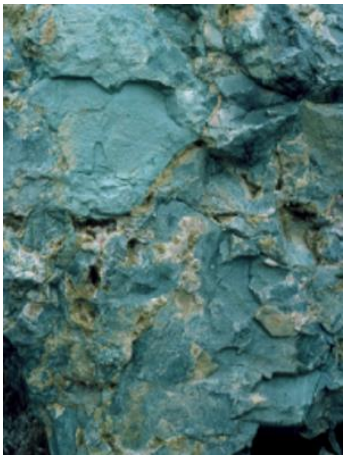

Figure 2.16: Tourmaline (source: Alderton, 2021)

Quartz is a major gangue found in heavy mineral sands. It is made up of silica (SiO_2) and can be a serious contaminant to the concentration process. Quartz can be colourless, white (see Figure 2.17), pinkish or yellowish (Anthony et al., 1946).

Figure 2.17: Quartz (Source: Pan et al., 2022)

Table 2.2 provides a summary of the average specific gravities of the heavy minerals and silicates for reference. Note that zirconium silicate has a high density of 4.7 g/cm^3.

Table 2.2: Average specific gravities of common sand minerals or associated silicates (after Wills and Napier-Munn, 2006; Perry et al., 1997; Krynine, 1946; Jones, 2006)

Heavy Mineral & Silicate	**Specific Gravity (g/cm^3)**
Zircon	4.7
Rutile	4.23
Leucoxene	3.9
Ilmenite	4.7
Kyanite	3.6 – 3.7
Quartz	2.7
Staurolite	3.6 – 3.8
Tourmaline	3.1

It is understood that the success of gravity separation including spiral concentration is dependent on the densities of the mineral species involved. According to Burt and Mills (1985), effective separation between valuable mineral and gangue material only occurs under certain conditions. This has hence led to the development of an indicator used in the characterisation of the effectiveness of the gravity separation known as separation ratio R_S.

If ρ_m, ρ_g, and ρ_l are specific gravities for minerals, gangue and liquid medium respectively, the separation ratio can be defined as follows (Burt and Mills, 1985):

$$R_S = \frac{\rho_m - \rho_l}{\rho_g - \rho_l} \tag{2.1}$$

Based on Equation (2.1), the separation is considered easy if the ratio is greater than 2.5 (i.e., R_S > 2.5). On the other hand, the gravity separation is not commercially viable if R_S is less than 1.25 (i.e., R_S < 1.25).

Applying the specific gravity values in Table 2.2 to Equation (2.1) with the liquid medium being water of specific gravity 1 g/cm^3, the theoretical separation ratios are recorded in Table 2.3 below. The specific gravities of rutile, leucoxene and

ilmenite are 4.23 g/cm^3, 3.9 g/cm^3 and 4.7 g/cm^3 respectively while kyanite and staurolite specific gravities were set at 3.7 g/cm^3 and 3.8 g/cm^3 respectively.

Table 2.3: Theoretical separation ratios from Equation (2.1)

	Zircon	**Rutile**	**Leucoxene**	**Ilmenite**
Kyanite	1.37	1.20	1.07	1.37
Staurolite	1.32	1.15	1.04	1.32
Quartz	2.18	1.90	1.71	2.18
Tourmaline	1.76	1.54	1.38	1.76

The ratios in Table 2.3 show that it would be easy to separate quartz from zircon, rutile, leucoxene and ilmenite if they were all in the sand mineral ore. Equally, separation would still occur for zircon and ilmenite from all the silicates (kyanite, staurolite, quartz, and tourmaline) although R_S is slightly above the 1.25 threshold for kyanite and staurolite. On the contrary, rutile and leucoxene are more challenging to separate from kyanite and staurolite. This means that rejecting kyanite and staurolite successfully should always mostly come with significant loss of rutile and leucoxene.

One of the shortcomings of the separation ratio R_S is that it does not account for particle size distribution even though this property is important. Accordingly, Gill (1991) was able to show that for $R_S \geq 2.5$, separation will be easy up to 75 μm in particle size. A ratio $1.75 \leq R_S < 2.5$, separation would work for particles of size between 75 μm and 212 μm. And finally, when the separation ratio drops below 1.5; then, particles must be at least 1700 μm coarse.

Gill (1991) uses a ratio to explain the separation based on specific gravity:

$$G = \frac{\rho_H - \rho_l}{\rho_L - \rho_l} \tag{2.2}$$

Where G is the Gill separation ratio; ρ_H and ρ_L are the specific gravities of the heavy component and the light component of the feed; and ρ_l is the specific gravity of the liquid carrier which is water in this study. In this case the heavy

component is the zircon particle, and the light component is the aluminium bearing particle.

2.5 Relationship between mineral recovery and concentrate grade

This section is devoted to reviewing how the performance of a plant or a processing unit such as a spiral is measured. Recovery is an important key performance indicator commonly used in operations, sub-circuits, test work, and research. Wills and Napier-Munn (2006) define recovery as the percentage of the total mineral contained in the ore that is recovered into the concentrate.

In normal practice, the overall recovery of a mineral processing circuit is constantly measured and monitored. The overall recovery must correspond to stage-by-stage recovery as the ore is upgraded from the initial feed to the final concentrate. The aim is to ensure that as many of the valuable minerals as possible that are fed into the circuit arrive at the final concentrate stream.

Mineral recovery can be expressed mathematically as concentration over feed or as concentration over combined concentration and tails. The former definition is the most used in the industry. For a spiral unit that has received feed at rate F and mineral content f, the concentrate produced at a rate C, with mineral content c, while the tails fraction is disposed of at rate T with mineral content t, the mineral recovery R is given by (Wills and Napier-Munn, 2006):

$$R = \frac{c}{f}\frac{C}{F} \tag{2.3}$$

$$R = \frac{c}{f}\frac{f-t}{c-t} \tag{2.4}$$

Note that Equations (2.3) and (2.4) are equivalent but Equation (2.4) is generally referred to as the two-product formula (Wills and Napier-Munn, 2006). Equation (2.4) only requires estimates of the grades or mineral contents of the feed, concentrate and tails. This makes the two-product formula handy

to use in a plant operation where chemical analysis of the three streams is routinely done in internal laboratory.

In Equation (2.3), the term C/F is called mass-pull or yield while the term c/f is known as the grade factor. The yield is used as a measure of efficiency of separation to produce a concentrate. However, the pursuit of high yields has been reported to lead to a contaminated product or concentrate. Figure 2.18 below illustrates this classical interaction whereby a trade-off should always be stricken between the grade and the recovery of the concentrate (Wills and Napier-Munn, 2006). Simply put, both cannot be obtained simultaneously: either the concentrate grade is high at the expense of recovery or grade suffers for greater recovery. Holland-Batt (1995) puts it this way: the spiral efficiency to separate the valuable minerals from the gangue material decreases when the mass pull to the concentrate increases.

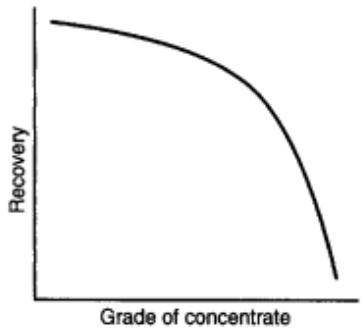

Figure 2.18: Typical recovery-grade curve (Wills and Napier-Munn, 2006)

The grade-recovery relationship is not a spiral-only phenomenon. Figure 2.19 below exemplifies a similar relationship for a flotation bank. Neethling and Cilliers (2012) describe this flotation grade-recovery curve as trade-off between "achieving a high-grade concentrate while sacrificing as little recovery as possible". They further explain that the grade-recovery relationship is used to compare flotation reagent suites, operating conditions, flotation cell designs and other influential measurable process parameters.

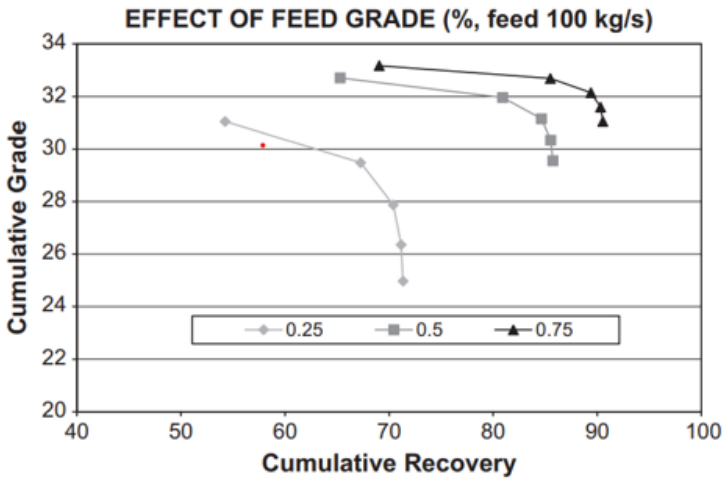

Figure 2.19: Grade-recovery for copper froth flotation (Neethling and Cilliers, 2012)

Another example is drawn from the iron recovery process. Here also, Figure 2.20 below shows the same type of relationship between iron recovery by spiral separation and concentrate grade. It shows that as the iron grade in the concentrate increased, the recovery decreased across different solid contents in the feed.

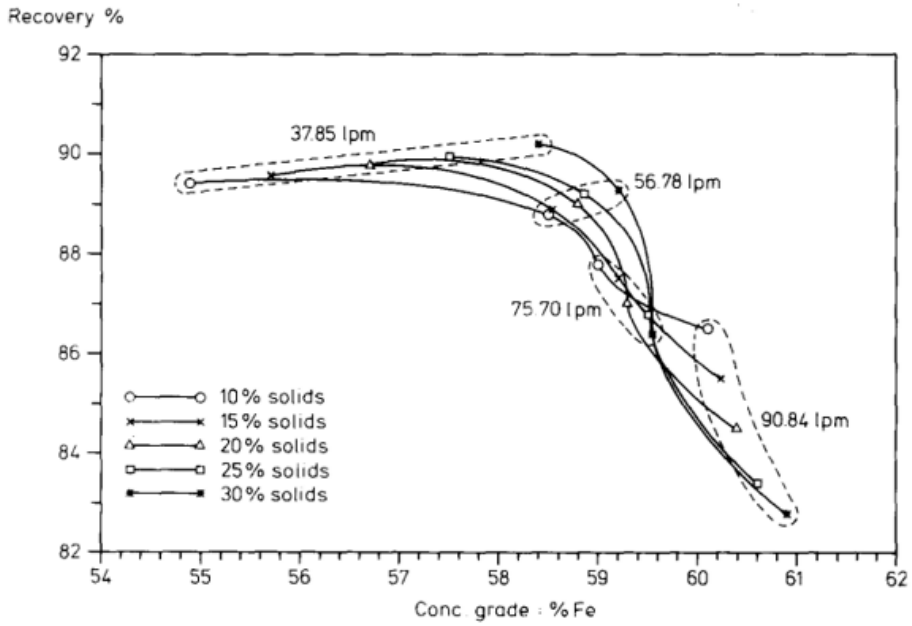

Figure 2.20: Spiral performance at different solid contents and feed rates (Sivamohan and Forssberg, 1985)

All in all, separation is not only about the equipment or the quantity of the feed to be separated, but it is also about the nature of mineral material being treated. This is the reason why the geometallurgical properties of the ore play an important role in mineral processing. QEMSCAN, one crucial geometallurgy tool is touched upon in the next section.

2.6 Detailed analysis by QEMSCAN

The quantitative evaluation of minerals by scanning electro-microscopy (or QEMSCAN) is one geometallurgical tool which is used to study and to determine the physical properties of mineral particles (Tiu et al., 2023). It provides visual imaging of the particles with high resolution as illustrated in Figure 2.21.

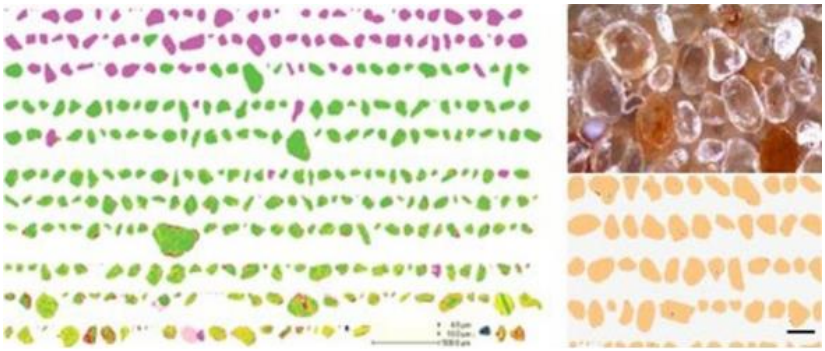

Figure 2.21: Examples of a QEMSCAN image for zircon characterisation (Ramsaywork et al., 2010; Wallmach et al., 2012)

2.6.1 Briefly about geometallurgy

Geometallurgy generally refers to a “multi-disciplinary holistic approach that aims to improve resource management by integrating geological, mining, metallurgical, environmental and economic information to generate a database that can be readily integrated into a near real-time spatial predictive model for mineral processing plants of future or existing mining operations” (Dehain et al. 2021). Philander and Rozendaal (2011) define geometallurgy as the

“determined properties of geological test samples, and the spatial distribution thereof using geostatistical techniques to aid metallurgical process modelling”. From the definition, it is understood that the fundamental to the properties draws from geology, chemistry and mineralogy to generate a block model for the deposit and subsequently determine the mine plan. It shows that geometallurgy is a collaboration between the mine and the concentrator in anticipating or looking for signs of things that may not go as planned. So, failing to determine these signs or properties in advance can result into missed opportunities or can have negative economic consequences for operations. It is why Lishchuk et al. (2020) consider geometallurgy as a very important tool used to mitigate risks on production and to improve economic performance of operations in the modern mining industry.

QEMSCAN is an ideal geometallurgical tool since it makes it possible to identify individual mineral species present in particles as well as their texture which if undetected can negatively affect the beneficiation process. It offers high-resolution of both chemical and mineral analyses in addition to particle size distribution and apparent densities of minerals (Edahbi et al., 2018).

The following section discusses how QEMSCAN analyses a sample to produce comprehensive analyses. It is an overview of main components of the machine and the sequence of analysis. It also shows how QEMSCAN can be used to identify challenges in gravity separation and to separation efficiency.

2.6.2 Components of the QEMSCAN instrument

QEMSCAN is an instrument that has capabilities of providing mineralogical, chemical, elemental and physical properties analyses of particles. Tonzetic et al. (2006) provide an image for a Zeiss EVO50 series Scanning Electron Microscopes that utilize up to four light-element X-ray detectors (Figure 2.22). The technology incorporates an automated image analysis system, utilizes Backscattered Electron (BSE) and Energy Dispersive (EDS) X-ray signals for

creation of digital images. Particle mineral analyses (PMA) produce a particle map (Grobler and Bosman, 2009). The PMA resolves particles characteristics associated with locking or liberation (Grammatikopoulos et al. 2013)

Figure 2.22: A QEMSCAN instrument (Tonzetic et al., 2006)

2.6.3 Analysis of samples by QEMSCAN

In Figure 2.23 below, Amao et al. (2016) summarise the QEMSCAN analytical process in the analysis of oncoids. Calibration is according to internal quality assurance procedures to ensure the quality of results prior to the analysis. The X-ray beam voltage of the QEMSCAN is then operated at 15 to 25 kilovolts at a beam current of about 5 to 10 nano-Amps.

For gravity separation in mineral sands about 10 milli grams of a representative sample is “exposed to a polished section and available for analysis”, (Grobler and Bosman, 2009).

The QEMSCAN system analyses the sample by capturing both backscattered electron (BSE) signals and EDS X-ray intensities. The BSE image offers material contrast based on differences in atomic number. The EDS data reveals the elemental composition at each point. After acquisition, the raw data is processed by the software which generates mineral or phase maps by

classifying each pixel according to a Species Identification Protocol (SIP) database to produce the results (Kenis et al., 2020).

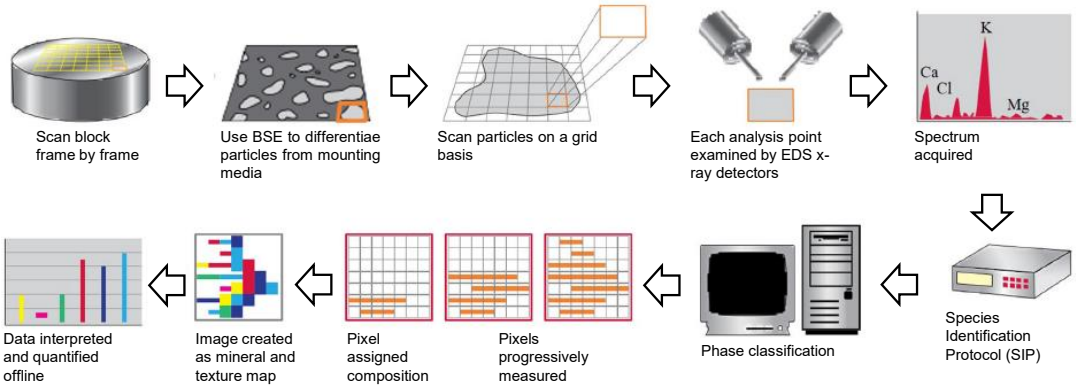

Figure 2.23: The process of analysing a sample using QEMSCAN (Amao et al., 2016)

The QEMSCAN analyses provide an advantage to the gravity separation process due to the information that details physical properties of the particles. The following section highlights the advantages.

2.6.4 QEMSCAN on gravity separation

Pascoe et al. (2007) argue that the understanding of mineralogy effects, liberation and particle size on the performance of a separator in a gravity concentration process as key benefits of QEMSCAN analysis. QEMSCAN can classify particles according to their densities and size. In Figure 2.24 below, Grobler and Bosman (2009) compare the conventional dry screening of samples to the particle mineral analysis (PMA) of the QEMSCAN over 60 samples. They emphasize that such data can be used in future calculations and comparisons.

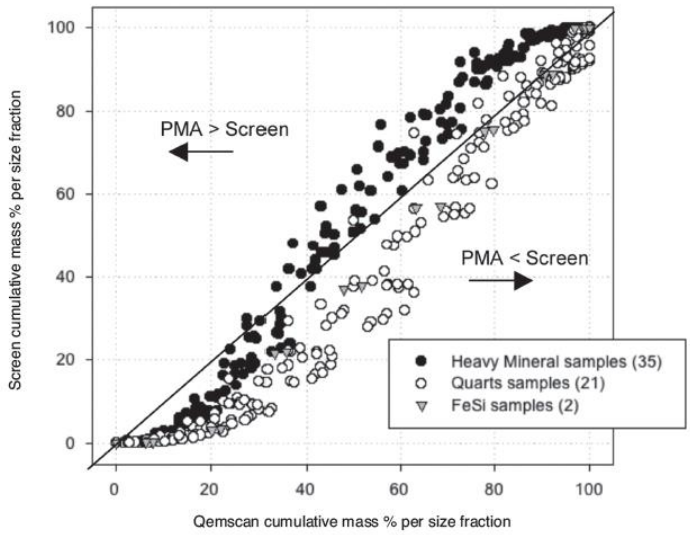

Figure 2.24: Comparing particle size from QEMSCAN and conventional dry screening (Grobler and Bosman, 2009).

Pascoe et al. (2007) developed a model based on particle size and density which can be used to compare to the gravity separation process (refer to Figure 2.25 below). The model approach consisted of a complete set of feed and products that were prepared for analysis. Minerals were identified and particle size analysed by QEMSCAN, with software (iExplorer) used for size ranges and density classes. Regression analysis was then used to generate a polynomial model for individual density and particle size classes recovery prediction. They concluded that QEMSCAN does show effects on recovery by the particle size and density.

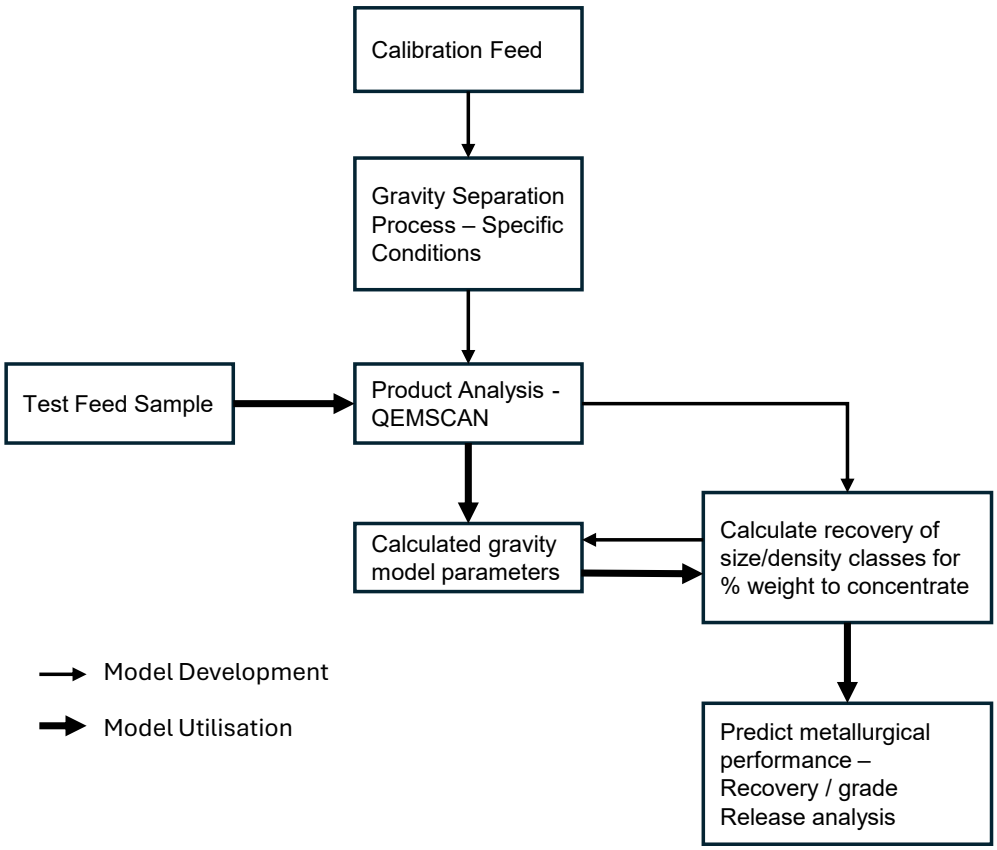

Figure 2.25: Gravity separator model (Pascoe 2007)

The model in Figure 2.25 was used to predict the recovery of Cr_2O_3 by QEMSCAN size and for cumulative Cr_2O_3 recovery to concentrate against the cumulative Cr_2O_3 grade for an Assemon ore (Figure 2.26).

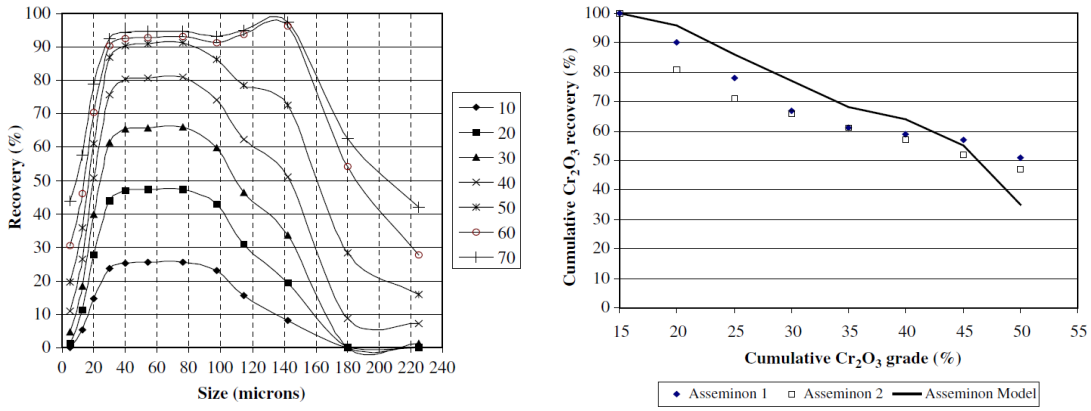

Figure 2.26: Model predictions of Cr_2O_3 recovery using QEMSCAN (Pascoe et al., 2007)

In conclusion, QEMSCAN provides analytical capability which can be used in a gravity separation process to provide additional data and analysis that compare to conventional methods. The gap identified between the conventional methods and QEMSCAN is an improvement opportunity on key performance indicators such as the recovery.

2.6.5 Gravity separation tests at pilot plant scale

A pilot plant is small production unit, set up for small scale production mostly beneficial for experimental understanding of a phenomenon under investigation. Depending on the part of the beneficiation being investigated, the pilot plant can be a complete circuit of feed preparation, feed transportation to a unit being tested, and products handling for sampling. For gravity separation a pilot plant comes with a feed sump, pump, feed control, unit being tested and sampling points. For spiral testing a pilot plant provides a testing capacity like an operational unit online, which cannot be achieved, due to the risk of production interruption or lack of space to test it. The pilot plant provides flexibility to test a spiral or different spirals in full capacity under various feed conditions, different streams and grades. It allows a stable environment with less disturbances to experiment, producing reliable results. A pilot plant is therefore used to conduct experimental work to quantify the amenability of an ore feed to spiral separation, the expected performance of the spiral (or even various designs and types of spiral concentrators), and the optimum operating conditions to be used on the full-scale operation.

A pilot-scale spiral concentrator is generally a closed-circuit setup consisting of a spiral mounted on a rig, a sump, a pump, valves and make-up water. The spiral has a feed pipe and three products discharging back to the sump as shown in Figure 2.27. The three products are the concentrate, the middlings and the tails (Dehanie and Filippov, 2016).

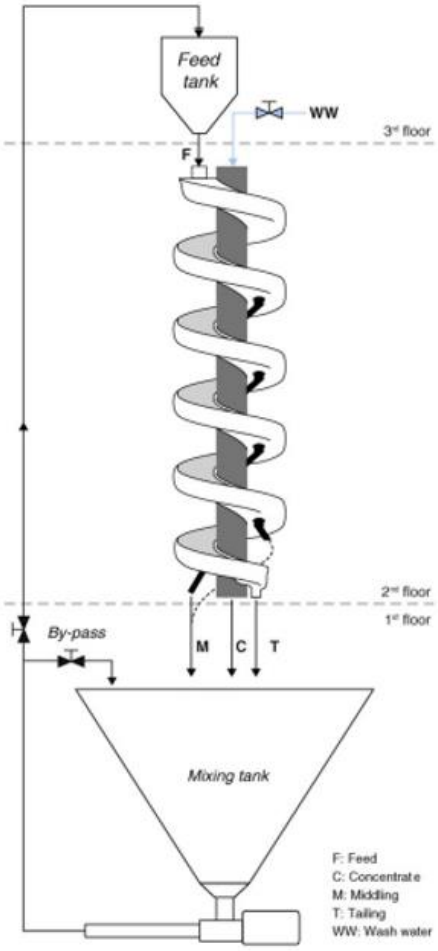

Figure 2.27: Theoretical representation of a pilot plant (Dehaine and Filippov, 2016)

De Klerk (2004) argued that the closed-loop pilot plant configuration ensures constant experimental conditions and provides the same feed to all the experiments. The benefit of a closed-circuit setup is that the feed is reconstituted in the mixing tank in Figure 2.27 for recirculation. Such can be done because the feed does not undergo major transformation in the form of dissolution and particle size reduction for example. This is the reason why pilot plant testing is commonly used for gravity separation across the industry.

Lastly, to conduct meaningful pilot tests, a representative sample must be collected from the process as alluded to sample representativity of the whole stream being sampled (Ashley and Callow, 2000). Process conditions must also be favourable, i.e., steady state, before, during and after the collection of

the sample for pilot testing. Ali (2001) also recommends that the process must not experience undesirable levels of contaminants that may negatively impact on the quality of the sample to be collected. Note here that buckets and bags are generally used to collect samples from process streams. Some sample points such as sumps from which a sample is collected do not allow bucket sampling due to possibility of compromising sample representativity and safety concerns. In this case, sampling with special bags becomes the only feasible solution (Vigoroso et al., 2025).

2.7 Developments in spiral concentration

2.7.1 Performance of the Humphrey spiral concentrator

Spiral concentrators are extensively used in the treatment of heavy mineral sand deposits to produce ilmenite, rutile and zircon amongst others. They are effective, low cost, and easy to operate units. They also require minimum maintenance and have no connected horsepower (Wills and Napier-Munn, 2006).

Concordant studies including that by Arnold et al. (2007) have identified three operating and design parameters that strongly affect the performance of a spiral. These parameters are the slurry concentration or weight fraction of solid content in the slurry, the splitter and cutter positions, and the dry feed rate expressed in tons per hour of solids fed to the spiral. The splitter and cutter positions determine how the spiral product will be divided into concentrate, middlings, and tails.

Particle size is another critical operating parameter. This is because coarse but light particles, irrespective of their densities, can easily make a way to the stream of heavy particles. Conversely, finer but heavy particles that should have reported to the heavy stream coal can be lost to the light stream (Arnold et al., 2007).

2.7.2 Special spirals: Compact Turbo and Alicoco spirals

Mineral Technologies (Pty) Ltd, an Australian company, and South Africa's Multotec (Pty) Ltd are known manufacturers of various types of spirals used in different stages of beneficiation. Other spiral manufacturers include Carpco/Outokumpu and Krebs/SWMS (Arnold et al., 2007). Table 2.4 below shows some of the spirals that are available in the market with their specifications. The specifications include the number of starts per spiral and the feed rate per start, with HC1RS and HX being the high-capacity spirals for Mineral Technologies and Multotec respectively. Pulp density and size range are two other major specifications which guide spiral selection. Spirals are commonly used to upgrade the ore from as low as 1% heavy mineral (HM) content to more than 90% HM content. In the first instance, HC1RS spirals can be used to treat feed containing less than 1% HMs while HG10 spirals may handle as much as 90% HMs (GCO, 2013). Note that the H1CRS and the HG10 spirals are both products manufactured by Mineral Technologies.

Sivamohan and Forssberg (1985) observed that in the early designs of Humphrey spirals fixed splitters resulted to overloading of inner channels which cut the concentrate as the band built on the spiral trough. Adjustable splitters enable the removal of the high-quality heavy concentrate while keeping the light tails on trajectory path to rejection. The bottom splitters eventually cut the downward flow to concentrate, middling and tails as shown in Figure 2.10 above (Wills and Finch, 2016). This means that the middling and the tails are produced at the bottom of the spiral while the concentrate is a progressive extraction of heavy particles from the top of the spiral.

As Tripathy and Murthy (2012) show in Figure 2.7 in section 2.3.4 above, a splitter movement that will increase the concentrate will result to high recovery. However, that will happen at the expense of the poor grade of the concentrate due to negative relationship between the recovery and the concentrate grade (refer to Figure 2.18 and Wills and Napier-Munn, 2006).

Table 2.4: Some Mineral Technologies and Multotec spirals in the market (Mineral Technologies, 2026; Multotec, 2026)

Spiral Maker	Spiral	Feed Rate		Volume	Number of Turns	Number of Modules	Diametere	Height	Splitter Set Per Module	Pulp Density	Size Range
		Number of Starts	tph / Start	m^3/hr	#	#	(mm)	(mm)		(%)(Typical)	(mm)(Typical)
Mineral Technologies	CT	3-6	4	6-9(12 max)		1-5		5360	1	25-60(34-45)	0.03-2.0(0.04-0.70)
	MG12	1-3	5(3-3.5)	8(4-6)	12		680	5960	3	25-60(30-45)	0.03-2.0(0.04-0.70)
	MG6.3	1-3	4(2-3)	8(4-6)					1		0.03-2.0(0.04-0.70)
	HG10i	1-3	4.5(1.5-3)	3.5-5(5.5 max)						30-60(30-45)	0.03-2.0
	HC33	1-3	3-6(9)	6-9(12 max)					5	30-50	0.03-2.0
	HC1RS	1-4	8	12				7800			
Multotec	HX	2-4	4-7(4-9)		2.5-5						0.04-1.5
	SC	2-3	4-9		3-8					High	0.04-1.5
	SX4	1-3	1-3		4						0.1-2.0
	MX7	1-3	2.5-3.5		7						0.1-2.0
	SX7	1-3	1.8-2.5(1-2.5)		7					1.4-1.55 (35%)	0.1-2.0

A recent addition to the Mineral Technologies family is the Compact Turbo spiral. This type of spiral which physically looks different to the classical spirals is illustrated in Figure 2.28(a) below. It is called the Compact Turbo spiral because it is compact and lightweight.

The Compact Turbo spiral was introduced to the market in March 2021 as an alternative solution to the different ongoing problems faced by mines (Mineral Technologies, 2021). The Compact Turbo spiral is a new product which is being trialled in the field to addressed some of the problems associated with the Humphrey spiral design (refer to Figure 2.3). According to Mineral Technologies (2021), the Compact Turbo spiral is able to handle feed containing as much as 40% of heavy minerals. For comparison, the Humprey spiral concentrator can only take a maximum of 20% heavy minerals (Wills and Napier-Munn, 2006).

The Compact Turbo spiral has a column height of 5360 mm. It accommodates four assemblies packed with five modules each, with each assemble handling 4 tph per start. It is designed to handle between 25% and 60% of solids in the feed, with typical range at 35% to 45% where its efficiency is optimum. It can handle between 0.03 mm and 2.0 mm particle sizes and 6 m^3/h to 9 m^3/h volumetric flow rate that must not exceed 12 m^3/h (Mineral Technologies, 2021).

The challenge which the spirals face is when there are changes in mineral behaviour or an increase in trash minerals in the feed. This results in difficulty to achieving valuable mineral recoveries and may require QEMSCAN investigation to establish the problem for example in zircon-aluminium separation (Grobler and Zietsman, 2017). With inefficient spirals resolving these issues may mean an increase in footprint, which translates to other costs such as maintenance. Richards et al. (2000) highlight the fine particles as another problem which the Humphrey spirals face. Under turbulent conditions

which can be due to inconstant feed rate they state that finer particles below 75 microns are dragged to the tails and consequently lost.

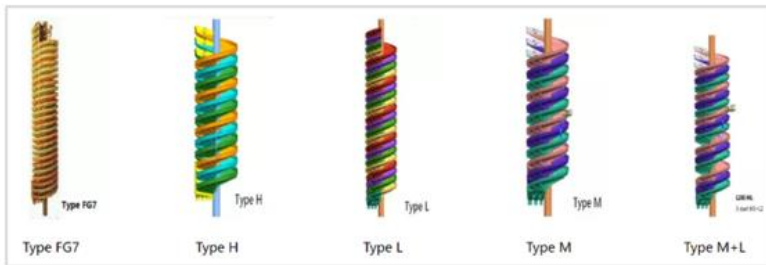

(a) (b)

Figure 2.28: (a) A Compact Turbo spiral by Mineral Technologies (Pty) Ltd and (b) Alicoco spirals by Alicoco Mineral Technology Co. Ltd

Based in Guangzhou City, China, Alicoco Mineral Technology Co. Ltd, or Alicoco for short, has also developed spirals (refer to Figure 2.28b above) purported to be efficient in rejecting aluminium silicates and in producing a zircon-rich concentrate from conventional Wet Circuits at good recovery. There is no literature providing the performance of the Alicoco spiral so far. As Arnold et al. (2007) state “some spirals manufacturers claim to incorporate proprietary features into their spiral designs that are intended to improve separation performance; and many studies suggest that there is actually little difference in the various designs”.

Refer to Figure 2.29 below for a Type H Alicoco spiral which was used in this research work. It has a column height of 3 m, a diameter of 1 230 mm, and it is available in single to triple starts. It handles between 0.03 mm to 0.30 mm particle sizes in the density range of 10% to 55% solids percentage in the feed, at the volume of 5 m^3/h to 15 m^3/h per start. Equation (2.5) converts the volumetric flow rate to mass flow rate (Wills and Finch, 2016):

$$\mathrm{M} = \frac{\mathrm{Qs}(\rho-1)}{\mathrm{s}-1} \qquad (2.5)$$

If Q is the volumetric flowrate between 5 m^3/h and 15 m^3/h; ρ is 1.08 t/m^3 (10% solids) to 1.72 t/m^3 (55% solids); and s is solids specific gravity at 4.17g/cm^3. Note that the mass flow rate M which the Type H Alicoco spiral can handle is between 1.62 tph and 14.18 tph.

Type H spiral can be used as a rougher, a cleaner, recleaner or a finisher scavenger spiral. It is applicable in various mineral processing operations including mineral sands where it is used for zircon, rutile and ilmenite recovery with heavy mineral concentration in the feed ranging from 0.01% to 98%.

Figure 2.29: A Type H Alicoco spiral installed in the Spiral Rig at GCO

According to Mineral Technologies (2021) the Compact Turbo spiral also outperforms the MG12 type spiral which has a capacity of up to 5.0 tph per start. GCO has tested and recently installed the MG12 spiral. MG12 has outperformed other spiral types such as MG6.3 and HC1RS from Mineral Technologies. This implies that the Compact Turbo spiral promises exceptional recoveries when handling different mineral sands feed types and when applied in different scavenger duties. However, there is currently no literature available for these spirals and this research work will contribute to availing such theory.

Refer to Table 2.4 above and Figure 2.30 below for the MG12 spiral. The MG12 spiral has a typical capacity between 3 tph and 3.5 tph and can handle up to 5 tph. It processes feed with pulp density of 25% to 60%, typically performing well between 30% and 45%. It handles a particle size range of 0.03 mm to 2.0 mm and up to 8 m^3/h of slurry volume.

Figure 2.30: The MG12 spiral separator installed at the Spiral Rig at GCO

The MG12 spiral is also compared to the MG6.3 and HC1RS spiral separators. The MG6.3 spiral is commercially specified as having a typical capacity of 1.8

tph to 2.8 tph, handling between 30% to 60% solids with manual splitter adjustments along the spiral height (GCO, 2013).

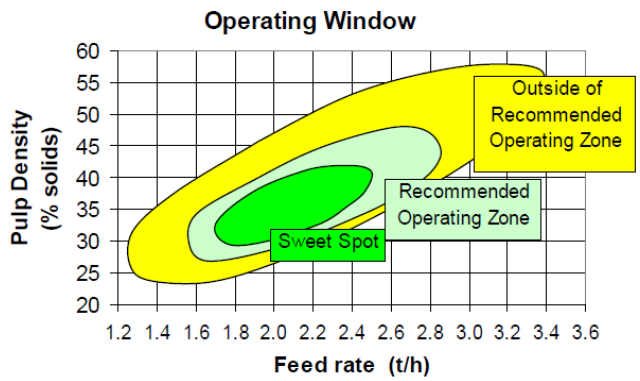

Figure 2.31: The theoretical performance of an MG6.3 type spiral as determined by feed rate and pulp density (GCO, 2013)

Mineral Technologies (2021) compared the MG12 and the MG6.3 spirals and showed that the MG12 spiral outperforms the MG6.3 across the feed range. Figure 2.32 below shows that at 4.0 tph the MG6.3 recovery of a heavy mineral is at 75% compared to 92% by the MG12 spiral. The MG12 can still recover more than 86% of heavy mineral at 4.6 tph where the recovery of the MG3.6 has decreased significantly.

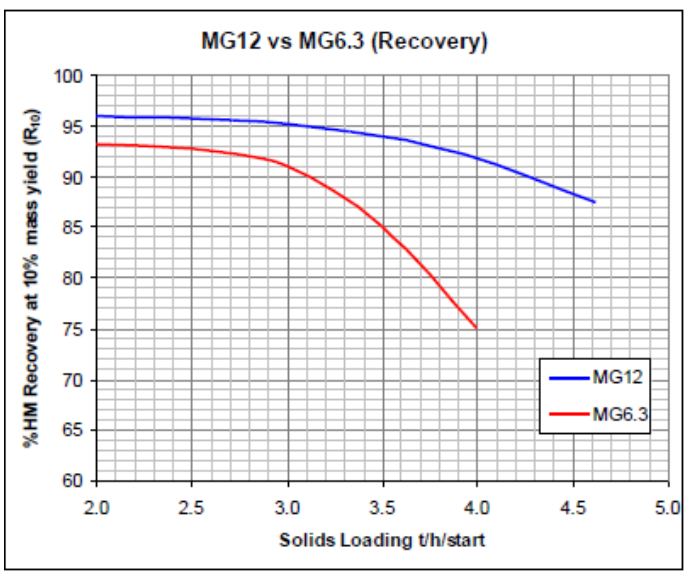

Figure 2.32: Comparing the MG12 and the MG6.3 spiral separators (Mineral Technologies, 2021)

High capacity (HC) spirals include HC1RS and HC33. Table 2.4 shows the specifications of these spirals operating in the same range of tph and volumetric flow rate with HC1RS absolute and 8 tph and 12 m^3/h respectively. Figure 2.33 below shows that it is not recommended to operate the HC33 above 6.2 tph per start whereas the HC1RS pushes the envelope and is recommended to operate above 8.0 tph.

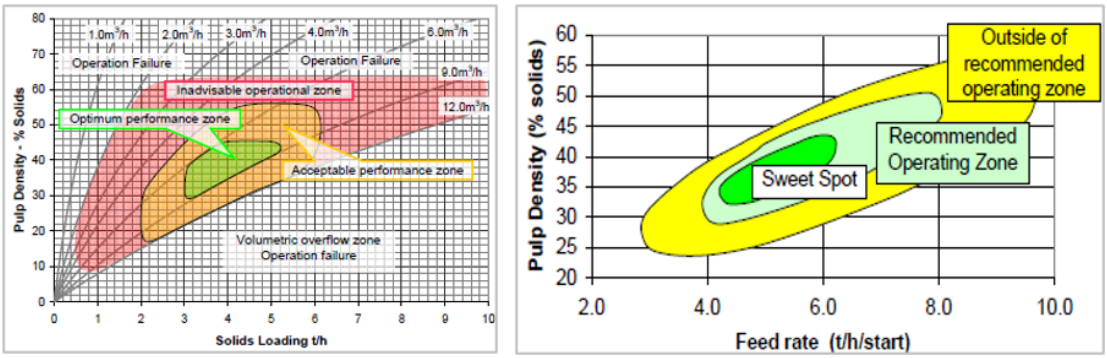

Figure 2.33: Operating windows for (Left) the HC33 spiral separator and (Right) the HC1RS (Mineral Technologies, 2021)

In the work by Ramsaywork et al. (2010), an optimum profit point with increasing metallurgical efficiency had to be determined to make a choice between MG4 and HC spirals (Walklate and Fourie, 2006). In this situation it was the MG4 which was the best spiral with the conclusion that the spiral selection is dependent on ore characteristics. The MG4 spiral can handle up to 40% heavy mineral in the feed, at 2 tph per start, at 8 m^3/h volumetric flow rate with up to 3 starts per spiral. Similar to other Mineral Technology spirals it can handle up to 2.0 mm particle size.

2.8 Concluding remarks

Gravity separation is an old phenomenon that dates back 3000 years ago. Its history of development includes hydrosizers, cyclones, jigs, sluices, shaking tables and spirals.

This literature review has primarily focused on spiral separators. The review has highlighted that the specifications of a spiral separator are selected and sized based on the properties of the ore particles to be treated. In addition to this, feed rate, splitter position and solid content in the slurry are key parameters that determine the performance (i.e., recovery) of a spiral concentrator. The slope angle of the spiral helical, the presence of near-density particles, and the presence of trash mineral, on the other hand, all affect the separation efficiency of the spiral. Furthermore, from the literature review, it became clear that optimum separation points must be established for a spiral considering the inverse relationship between mineral recovery and concentrate quality.

The evolution of gravity separation has been driven by improvement in separation efficiency and processing costs per ton of material being handled. Falling ore body grades ask for spiral separations which can handle high feed volumes at economic recovery of valuable minerals. An increase in gangue materials down the process negatively affects the mineral recoveries and requires highly efficiency spirals than can reject the trash minerals without losing the valuable ones.

The Alicoco and Compact Turbo spirals are new in the market and there is currently no scientific literature on them. From the manufacturers, Mineral Technologies (Pty) Ltd and Alicoco Mineral Technology Co. Ltd, the two spirals promise to be a solution to problems associated with Humphrey spirals. These problems include the challenging zircon-aluminium separation which Grobler and Zietsman (2017) highlighted. Indeed, when the aluminium content increases down the scavenging line of a processing plant, zircon becomes difficult to recover. This research study aims to test the Compact Turbo and Alicoco spirals where agglomerates, near-density particles, and the inability of the Humphrey spiral to separate the zircon from aluminium are prevalent in some form or another.

Chapter 3 Experimental procedures, pilot testing and data collection methodology

3.1 Introduction

The main objective of this study was to explore the improvement of the quality of the tertiary concentrate (Con 3) from the Wet Circuit of the Mineral Separation Plant (MSP) at Grande Côte Opérations (GCO). It is posited that by reducing the content of aluminium and increasing the recovery of zircon in the Wet Circuit, increased operational performance may ensue. Such desired outcome was pursued by testing specifically the Compact Turbo and Alicoco spirals to determine their abilities to improve mineral recovery.

This chapter covers the details of the procedure followed for the collection of relevant data. The experimental work is presented in line with the chronological steps below:

- Collection of a bulk sample from the Wet Circuit
- Drying of the sample.
- Pilot testing of the performance of the Compact Turbo, Alicoco, MG12, and HG10 spirals
- Preparation of samples collected from the pilot setups for laboratory assaying
- Particle size analysis of the samples from the pilot test work

The starting point was the collection of a feed sample large enough for all pilot tests presented later in this chapter. This feed sample was constituted by diverting to sampling bags the underflow stream of the CL003 classifier as per the label in Figure 1.2 of Chapter 1. Details of the protocols associated with each chronological step outlined above are presented in the subsequent sections. And before all that, the Wet Circuit is presented in the next section for easy reference.

3.2 The Wet Circuit of Grande Côte Opérations

In Chapter 1, GCO is described as a mineral sands miner that operates a mine with a Wet Concentrator Plant (WCP) that produces a heavy mineral concentrate (HMC). It also operates a Mineral Separation Plant (MSP) which processes the HMC to final products, i.e., zircon, ilmenite, rutile, and leucoxene. The Wet Circuit in Figure 3.1 below, which is the same as Figure 1.2 in Chapter 1, is the first stage of the MSP which separates the HMC to magnetic fraction which is ilmenite-rich, and to non-magnetic fraction which is rich in zircon, rutile and leucoxene.

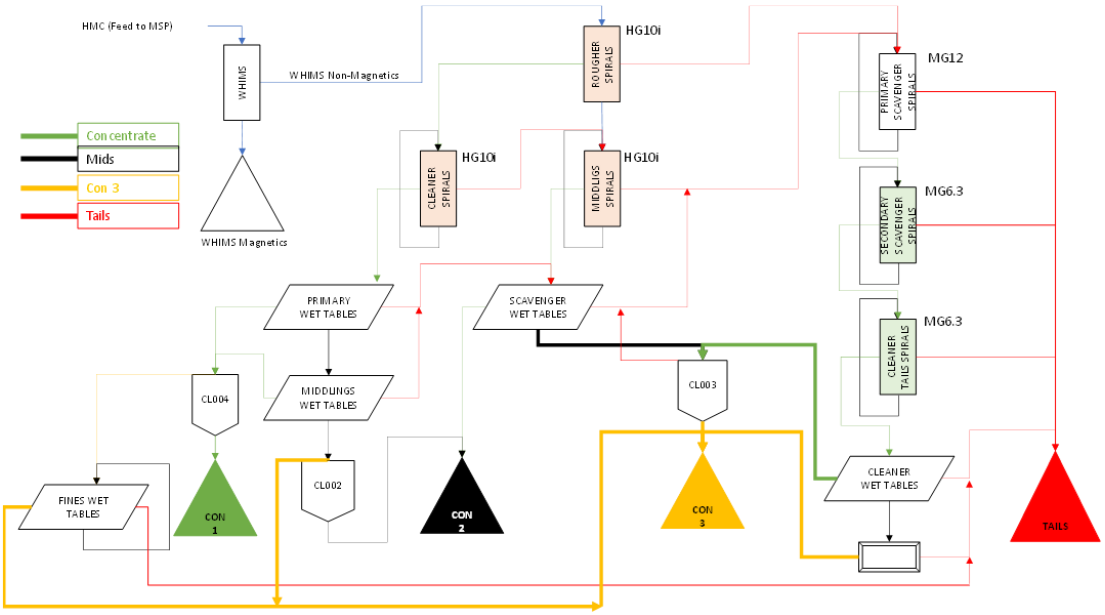

Figure 3.1: The Wet Circuit of the Mineral Separation Plant at Grande Côte Opérations

Spirals and other gravity separators in Figure 3.1 are used to treat the non-magnetic fraction. This then allows the production of intermediate concentrates rich in zircon, rutile and leucoxene. The intermediate concentrates then undergo further separation to final products in a dry circuit not shown in in this research work.

The problem is that the desired 87% recovery of zircon to primary (Con 1) and secondary (Con 2) concentrates combined, anticipated during the feasibility

study (AMC, 2010), has not been reached since production began in the past ten years. The situation is exacerbated by the fact that more zircon than planned reports to the tertiary concentrate (Con 3) and ends up in a low-grade zircon product. In addition to this, past attempts to adjust the circuit to produce more zircon to the primary and secondary concentrates have resulted in more trash contaminating the zircon concentrates. Note that trash minerals are the aluminium silicates, i.e., kyanite, staurolite and silica. These silicates negatively affect the final stage of zircon production in the dry circuit by displacing the content of ZrO_2 in the final product. Therefore, the Wet Circuit prepares the feed for the subsequent dry circuit by ensuring that the silicates are at minimum levels.

3.3 Collection of the bulk sample from the Wet Circuit

3.3.1 Description of the tertiary concentrate stream

As Figure 3.1 shows, the tertiary concentrate (referred to as Con 3) is made up of four streams: the concentrate from the fines wet table, the overflow from classifier CL002, the oversize from a screen, and the underflow from classifier CL003.

Previous circuit balances (see Table 3.1 below) show that there is no flow coming from the screen. One notes that the underflow (U/F) of classifier CL003 has the highest content of aluminium oxide or alumina (Al_2O_3) at 11.69% and makes up 61% of Con 3. The underflow stream also has the lowest content of ZrO_2 at 11.67% compared to 45.17% for the concentrate from the Fines Wet Tables. Distribution calculations show that about 45.7% of Al_2O_3 arriving to the Rougher Spirals (see Figure 3.1 for reference) report to this stream. This is why the classifier CL003 underflow is the target of this research as it has the highest content of Al_2O_3 compared to all the streams in the Wet Circuit while it is also rich in ZrO_2.

Table 3.1: Indicative properties and assays of the stream to be sampled (GCO, 2022)

			Laboratory Assays				Distribution from Rougher Spirals Feed		
Streams	**Flow Rate**	**Mass Split**	**ZrO_2**	**TiO_2**	**Fe_2O_3**	**Al_2O_3**	**ZrO_2**	**TiO_2**	**Al_2O_3**
	tph	**%**	**%**	**%**	**%**	**%**	**%**	**%**	**%**
Fines Wet Tables Concentrates	0.25	3.17	45.17	26.98	2.59	0.80	1.5	1.4	0.2
CL003 U/F	4.82	61.09	11.69	32.90	10.56	11.69	7.3	33.6	45.7
CL002 O/F*	2.82	35.74	25.83	37.07	7.03	4.46	9.5	22.2	10.2
Total	**7.89**	100	**17.81**	**34.21**	**9.05**	**8.76**	**18.2**	**57.1**	**56.1**
Design	5.74	100	12.60	40.50	2.41	13.20	7.3	52.7	37.7
Note: * O/F stands for overflow									

Finally, as argued by Grobler and Zietsman (2017), it becomes difficult to recover the zircon when the aluminium content increases down the scavenging line of a process. The complication of cleaning the classifier underflow of contaminants is therefore expected at the Wet Circuit. This is because the tertiary classifier feed is from the scavenger spirals and wet shaking tables which implies that it has already undergone several stages of processing.

3.3.2 Preparing the plant conditions for adequate bulk sampling

The Production Department at the MSP is responsible for running the Wet Circuit. A discussion was held with the production team in advance to let them know of an intention to collect a bulk sample from the underflow stream of the tertiary classifier. This was to ensure that there was no planned downtime which could affect plant stability during the sampling time.

After receiving clearance to proceed with the exercise, the Wet Circuit was allowed to process only the HMC produced by the WCP at the mine. The plant was run for 3 h to eliminate any contamination that could affect the Wet Circuit performance and the quality of the sample to be collected. In addition to this, process conditions were allowed to reach steady state as shown in Figure 3.2

before the batch of sample was taken. Sampling at steady state meant that each equipment in the circuit performed with little to no fluctuations. Under these operating conditions, Ali (2001) explains that the process cannot reach undesirable levels of contaminants levels. This would ensure that that the composition of the feed and product streams would remain sufficiently constant; hence, the decision taken at the Wet Circuit.

The plant performance trends were monitored to ensure stability using the internal process monitoring software tool. From top to bottom, Figure 3.2 illustrates the satisfactory level of stability for the following parameters: Con 1 yield, Wet Circuit feed rate (CV054) with moisture, Con 1 production rate, Con 2 production rate, Con 3 production rate, Tails rejection rate, Wet Circuit feed dry rate, WHIMS magnetics production rate and WHIMS non-magnetic production rate

Lastly, when the feed hopper was full and all indicators in Figure 3.2 were no longer increasing or decreasing, the process was deemed at steady state. This paved the way for the collection of the large batch of sample that took place on 04 November 2023 between 13:45 and 14:25.

3.3.1 Sampling point of the underflow stream from the tertiary classifier

The tertiary classifier, coded as CL003, is situated on the first floor of the Wet Circuit. Its underflow gravitates through the underflow connecting pipe to a tertiary concentrate sump that is accessible from a platform on the ground floor. The pipe entering the sump is marked as CL003 U/F for the tertiary classifier underflow.

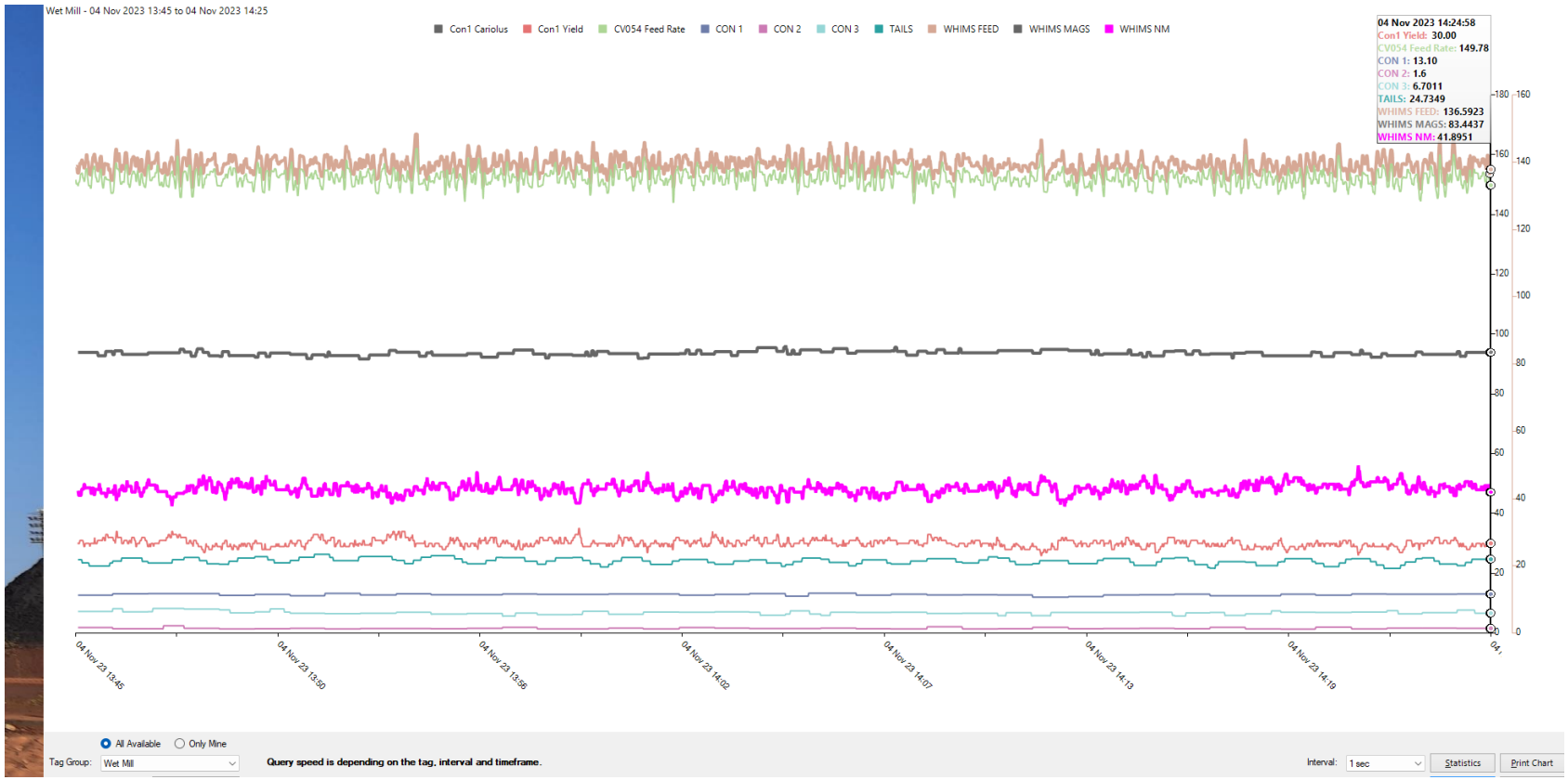

Figure 3.2: Production trends of the Wet Circuit displaying steady-state conditions before and during bulk sampling

Figure 3.3(a) below shows the underflow stream pipe entering a sump feed box on top of the sump. The feed box has a rubber cover that prevents splashing, and thus loss of mineral value, as the slurry enters the sump. Figure 3.3(b) shows the pipe inside the feed box as it discharges the slurry into the sump. This is the point where the bulk sample was collected.

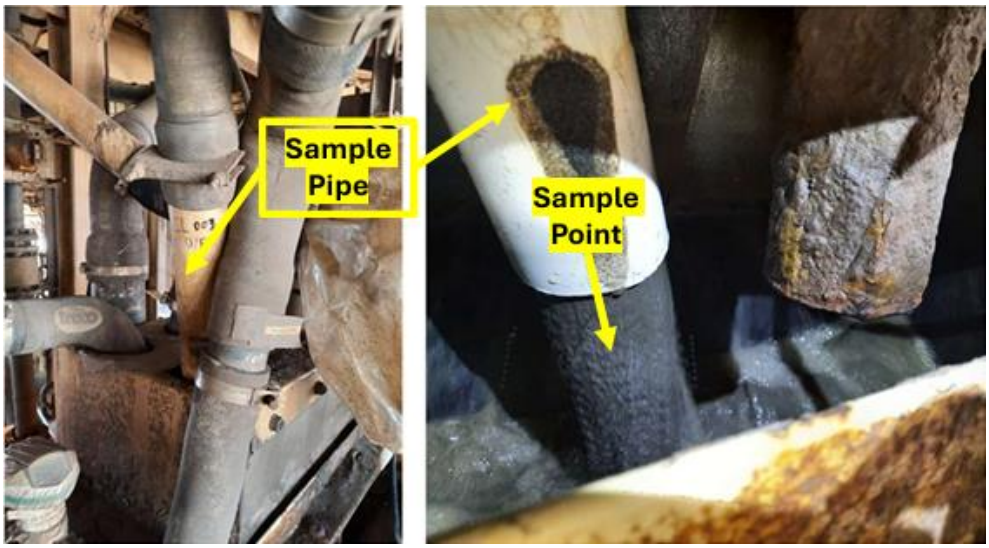

(a) (b)

Figure 3.3: (a) Underflow of the tertiary classifier as it enters the dedicated sump and (b) sampling point where the slurry discharges into the sump

3.3.2 Collection of a bulk sample from the Wet Circuit

Initially, sampling was done on 27 May 2023 after the WCP battled to produce the HMC for many months. A new sampling was then executed on 04 November 2023. The new sampling was motivated by three reasons: there was continued low production of HMC at the WCP, prevailing downtime experienced at the MSP during the first campaign, and an insufficient sample initially collected that was later discarded into the Wet Circuit.

Due to the nature of the stream in Figure 3.3(b) above, to comply with safety requirements (Vigoroso et al., 2025), and to prevent compromising the quality of the sample being taken to ensure representativity it was not possible to use

a 10-litre bucket to collect the sample. A number of labelled calico bags was used instead as shown in Figure 3.4.

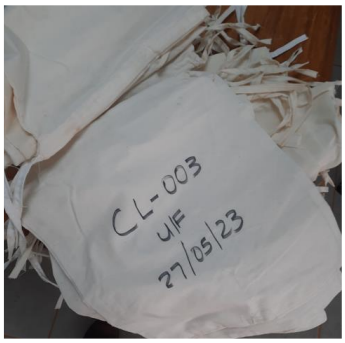

Figure 3.4: A labelled calico bag used to collect small samples from the classifier CL003 underflow stream

Two people were required for sampling, one holding the rubber cover of the feed box while the other held the calico bag and collected the bulk sample from the sampling point (Figure 3.3b). The pipe discharging into the feed box was repositioned in a way to prevent any mixing of the underflow with other materials making up the tertiary concentrate being discharged into the sump. Afterwards, each calico bag was opened and comfortably placed directly under the pipe discharge, collecting the discharged slurry until it could hold approximately 5 kg of wet classifier CL003 underflow material without overflowing. The calico bag was then removed and closed once enough sample had been collected. The sample in each calico bag was collected for 3 – 5 s to ensure that the bag did not overflow.

A total of 70 sample bags were collected as illustrated in Figure 3.5 to produce a bulk sample of about 350 kg. Based on previous test work on the spiral rig, it takes about 80 kg of sample to conduct a full pilot test to completion.

Figure 3.5: Sample collected in 70 calico bags making about 350 kg of bulk sample

Upon completing the sampling campaign, the calico bags were packed on a drying trolley and put into an oven. The samples were then allowed to dry at 120°C over two days. Thereafter, the dry samples were removed from the oven and transferred from the trolley to a container where they were kept. The container is kept locked and clean to comply with housekeeping and quality requirements for GCO. This ensured that there was no contamination.

After all the precautionary measures, the next step was to test carefully prepared fractions from the bulk sample using the Compact Turbo and Alicoco spirals at the rig. The goal was to establish which of the spirals is more efficient in separating zircon from the silicates. The following section presents the experimental programme, the tools used, and the protocols followed for the test work at the spiral rig.

3.4 Pilot testing programme

GCO exclusively uses spirals from Mineral Technologies in its WCP at the mine and in its Wet Circuit at the MSP.

Generally, testing of a new spiral at GCO is achieved in two ways: online testing and pilot testing. With the first setup, the spiral is installed in a duty where it receives the feed going to other spirals of that stage or duty in the plant. But, in case the plant setup does not allow such online testing, a pilot plant or the test rig is used to test a recreated slurry which is pumped through the spiral in a closed-circuit setting. The latter was used for the purpose of this research study.

Preparations to conduct the necessary pilot tests involved checking that there was enough water by opening the water valve and filling up the sump. Then, electricals were tested by starting the pump through a control panel, watering each spiral and stopping the pump. Once these steps were completed, the dry samples stored in the container were transported to the spiral rig area for the test work to begin.

The spiral rig fitted with the selected spirals tested as part of this research study is presented in the next section.

3.4.1 Presentation of the spiral rig fitted with the spirals

The spiral rig at GCO is situated in the vicinity of the Wet Circuit about 300 m away from the container where the calico bag samples were stored. The spirals to be tested were either installed on the rig or kept on the floor at the base of the rig as the rig can only handle three spirals at a time. The Alicoco spiral, the Compact Turbo spiral, and the HG10 spiral were installed simultaneously as shown in Figure 3.6(a) below. The Compact Turbo and the MG12 spirals fitted in one position on the rig and were therefore tested one after another.

(a) (b)

Figure 3.6: The two spiral rigs used for spiral test work at GCO – (a) Spiral rig fitted with the Alicoco spiral, the Compact Turbo spiral, and the HG10 Spiral; and (b) Spiral rig fitted with the MG12 spiral and the HG10 spiral

Each spiral was connected to one of the two sumps and to the pumps. Pumps were used to send the slurry from the sumps to the top of the spiral being tested. From there, the slurry would gravitate down the spiral height, separating into three fractions before discharging into the same sump in a closed-circuit setting. The three fractions from the spiral separation that were recombined in the sump are the concentrate, the middlings, and the tails. The pump has a CMG Marathon Electric 3 phase motor with 380 – 415 V, 50 Hz, 5.5 kW duty and 1440 revolutions per minute (rpm).

All the experiments were conducted in the open space outside the Wet Circuit building. This means that the spiral rig was exposed to the sun, the rain, and windy conditions to name a few. As such, tests were carried out only on days when there was no rain to avoid further dilution of the slurry.

3.4.2 Equipment and tools used for the rig test work

This section is devoted to presenting the list of equipment and tools that was used to support the pilot test work.

Starting off with the tools, a hand-held scale (see Figure 3.7) below was used to weigh a bucket and calico bags during the preparation of the slurry feeds to the spirals. The hand-held scale was also used during sampling of the product streams of the spirals. Figure 3.7 shows a stopwatch and a calico bag that were used in tandem to collect timed product samples. A calico bag prevents slimes or particles less than 45 μm from passing through it, letting only water. This setup together with the hand-held scale enabled the later estimation of flowrates from the mass of the sample and the time recorded. The calico bag served to retain samples including slimes while allowing water to pass through. The bag can also withstand high temperatures during the drying process.

(a) (b) (c)

Figure 3.7: Tools used to collect timed fraction samples (a) stopwatch, (b) calico bag and (c) hand-held scale

In terms of the list of equipment, Table 3.2 provides a summary of the spirals tested as well as all the items used for the research work.

Table 3.2: List of equipment used for the experimental test work programme

#	EQUIPMENT	USAGE
1	Compact Turbo Spiral	Research
2	Alicoco Type H Spiral	Research
3	MG12 Spiral	Research
4	HG10 Spiral	Additional research
5	Bucket	Density measurement
6	Calico bag	Sampling and drying of Wet Circuit and Rig samples.
7	Stopwatch	Taking of timed samples
8	Handheld weighing scale	Density checks and wet weight measurement
9	Splitter	To split samples for various analysis
10	Screens, shaker, and brush	Particle size distribution
11	Desk weighing scale	Particle size distribution
12	Oven	Drying of samples in calico bags

The Compact Turbo spiral handles 4 tph per start at 25% to 60% solids weight with particle size distribution between 0.03 mm to 2 mm in the feed. The

equipment tested was therefore selected based on its ability to compete with the current equipment that handles the feed with properties at this range.

The Alicoco Type H spiral can handle between 1.62 tph to 14.18 tph per start at 10% to 55% solids weigh with particle size 0.03 mm to 0.3 mm in the feed. The MG12 spiral handles the feed of up to 5 tph per start of 25% to 60% solids weight and the particle size distribution between 0.03 mm and 2 mm. The HG10 spiral can process the feed rate between 1.5 tph and 3 tph with 4.5 tph maximum with 30% to 60% solids weight and the particle size distribution of 0.03 mm to 2 mm.

The conditions under which the tests were conducted were selected to represent the plant requirements instead of targeting the supplier operating ranges for each spiral that was tested.

It is important to highlight that the bulk sample from the tertiary classifier underflow was treated by the pilot spirals. The feedstock is therefore a down-the-process stream. It is for this reason that the HG10 spiral was added to the test work arsenal to interrogate its purported ability to handle already refined streams (MacHunter and Pax, 2007). So, although beyond of the initial work, the inclusion was to enrich the research and provide preliminary data on the quest to improving operations at GCO.

3.4.3 Experiments in closed-circuit configuration

The experiments were conducted in a closed circuit around the sump and the spiral. Such a closed-loop configuration provides an advantage of keeping the experimental conditions as stable as possible. The same feed is also recycled and reused through all the experiments conducted under various operating conditions (de Klerk, 2004).

In the closed-circuit experiment used in this research study as shown in Figure 3.8, the spiral is positioned directly above the sump. The slurry is

pumped from the sump to the top of the spiral. It then gravitates down the spiral column and separates in the process to produce a concentrate (C), middlings (M), and tails (T) which all discharge into the sump.

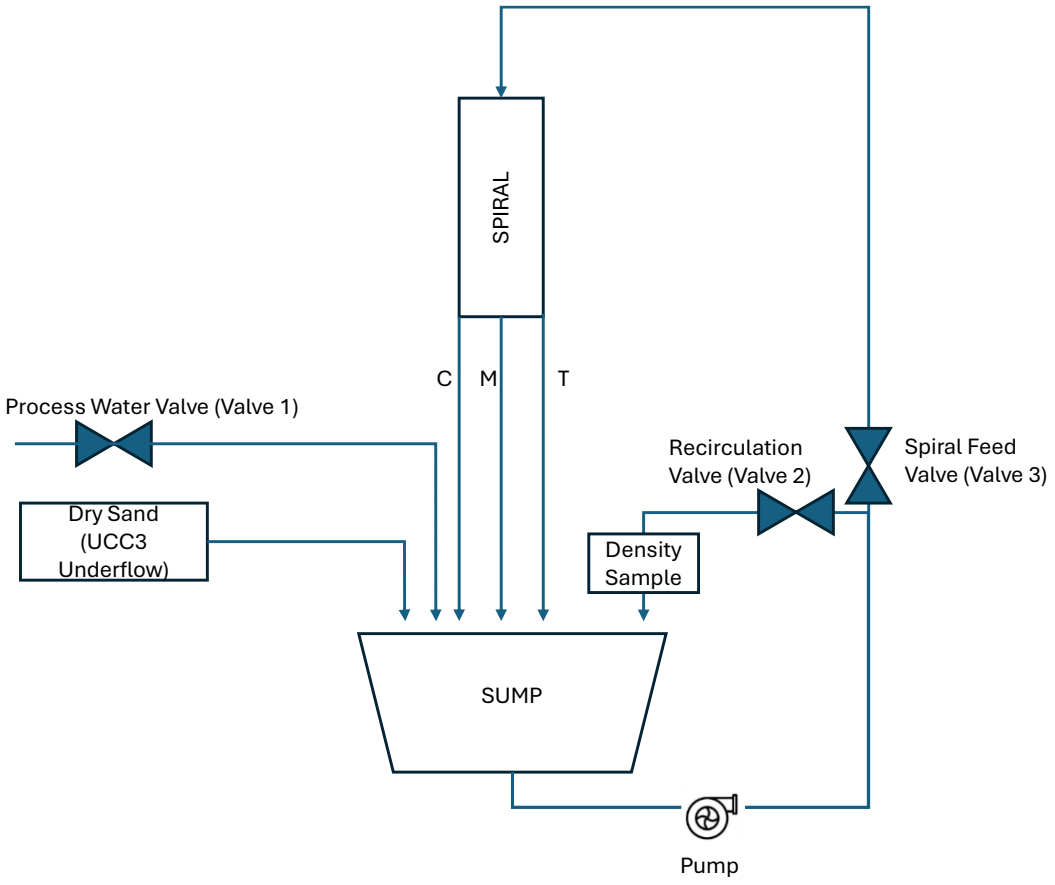

Figure 3.8: The closed circuit used for spiral pilot testing at GCO

The sump in Figure 3.6 has a total volume of 1 m^3. The total of 350 kg sample can however make up the slurry of 30% to 40% solids in the feed at the volume of 0.50 m^3. The speed of the pump varies between 1000 rpm and 1440 rpm to increase or decrease the feed rate to the spirals.

3.4.4 Preparation of the slurry feeds for pilot testing

The slurry feeds were prepared by mixing a predetermined mass of dry sample from the bulk with process water in the sump installed at the spiral rig in Figure 3.6 above. The calico bags were picked up randomly, opened, weighed, and

poured into the sump. It was assumed that the grade in the feed was uniform due to the sample having been collected under steady state conditions. Then, process water was added at different proportions depending on the required density of the final slurry feed.

The first slurry feed was prepared at 30% solid content by weight by mixing 0.50 m^3 of water (500 kg) with 214 kg of solid. The sum of 500 kg of water and 214 kg of sample is 714 kg of slurry. The 214 kg of samples is 30% of the slurry as required. In the same way, slurry feeds successively at 35% and 40% solid content by weight were prepared. The same experiments were run for all three slurry concentrations (i.e., 30%, 35%, and 40%) that correspond to a slurry density of 1.30 g/cm^3, 1.36 g/cm^3 and 1.44 g/cm^3 respectively.

The choice of the range of the solid concentration in the slurry feed (i.e., 30% to 40%) was made to mimic the current concentrations observed at the Wet Circuit.

3.4.5 Experimental procedure used for the closed-circuit configuration

The following procedure was followed in preparation for the experiments to be conducted with the selected spirals set in closed circuit. First, the process water valve (Valve 1 in Figure 3.8) was opened to fill water into the sump. The recirculating valve (Valve 2) was then opened to enable the water to return to the sump. The spiral feed valve (Valve 3), on the other hand, was kept closed during the preparation of the slurry feed. After this, the pump was started as the water level rose to the half mark of the sump volume. Valve 1 was then closed. Second, the stirrer at the bottom of the sump was started the agitation of the slurry. A pre-weighted number of calico bags containing dry samples were opened one after the other. Each bag was held above the sump to ensure that it did not drop into the sump. The sand from the bags was then slowly poured into the sump. Last, an empty bucket was weighed using the handheld scale to establish its weight. After that, a slurry sample was collected into the

bucket from the discharge after the recirculation valve (i.e., Valve 2 in Figure 3.8). The bucket with the slurry content was weighed and the weight of the empty bucket was deducted from the total weight. The net weight of the content was representative of the mass of slurry collected. The bucket with the slurry content was then left to settle for 5 min. After the solids had settled, the water was decanted to another empty bucket while ensuring that solid particles did not get entrained. This left behind a thicker slurry that was weighed together with the bucket. The weight of the wet solid content was calculated after discounting that of the bucket from the total. Dry solids were estimated to represent 80% of the thick slurry as guided by past routine tests (Geneyton and Diack, 2020). The weight of the dry solids was divided by the weight of the slurry to establish the percentage solids. The wet solids and the decanted water were then added back to the sump. Based on the estimated solid content of the initial slurry sample from the recirculation valve, dry solids from another calico bag or process water from Valve 1 was added to correct the slurry density to the desired value. This cycle entailing slurry sample collection, density measurement, and top-up of water or dry solids was repeated until the required solid content was reached. Note that three solid contents of slurry were prepared for this study: 30%, 35%, and 40% by weight.

The next step was to run the actual pilot tests themselves. For each solid content, the spiral feed valve (i.e., Valve 3 in Figure 3.8) was opened, and the recirculating valve (Valve 2) was closed. This enabled the slurry to be pumped to the top of the spiral for the separation to start. The pump speed was increased as the solids content in the slurry increased. It was 1100 revolutions per minute (rpm) from 30% solids (1200 rpm for 35% solids and 1300 rpm for 40% solids) in the slurry. This adjustment of the pump speed was necessary to prevent the chocking of the feed line to the spirals. An inspection was done to ensure that the entire surface of the spiral was wet to enable good separation as the closed circuit reached steady state. After confirming that separation was taking place without spillage or blockages, three empty calico bags each were

weighed beforehand were used to collect the slurry of the concentrate, the middlings, and the tails simultaneously. Each bag load was weighed and then left to settle. For the MG12 spiral the concentrate was made up of the combined super-concentrate and the concentrate. The mass of the thick slurry was calculated as a net weight content. Using in-house practice, the weight of the dry solids was considered to be 80% of the thick slurry. This enabled the solid contents to be estimated for the concentrate, the middlings, and the tails. This information was further used to determine the flow rates of the sampled streams and the constituted feed by mass balance. The split of the concentrate was determined by dividing the concentrate mass by the determined feed mass. The determined feed mass forms part of the practical performance assessment of the spirals. The concentrate splitter of the spiral shown in Figure 3.9 below (also refer to Figure 2.4 and Figure 2.10) was adjusted to obtain the desired split, i.e., 80%, 85% or 90%. Refer to Table I1 in Appendix I for the splitter positions along the spiral stages for the MG12, HG10 and the Compact Turbo spirals at 30%, 35% and 40% feed pulp densities. The splitter positions in Table I2 in the Appendix are for the HG10 and the Alicoco spirals at low feed pulp densities.

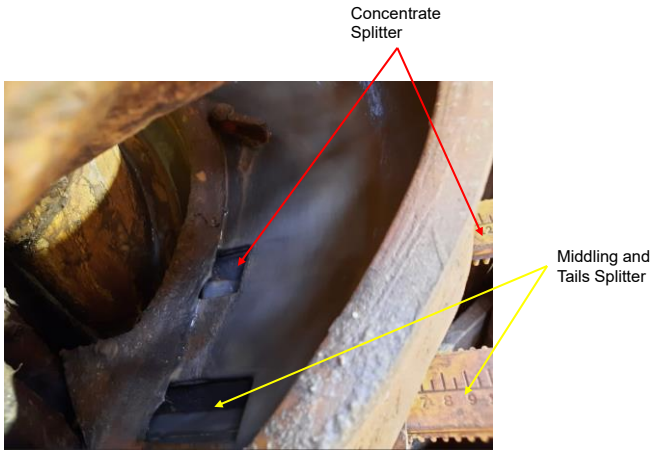

Figure 3.9: Splitter positions for the MG12 spiral separator at GCO

This testing and sample collection protocol described for 30% solids by weight in the feed was repeated for the solid contents set at 35%, and then, at 40%.

When all the tests were completed, the various samples collected in calico bags were taken to the GCO Laboratory for drying. They were then prepared for chemical and mineralogical analysis, as well as particle size analysis. These steps are covered in the next section.

3.5 Laboratory characterisation of pilot test samples

All the calico bags samples collected were sent to the laboratory for further processing. The workflow entailed drying, X-Ray analysis, determination of total heavy mineral content, identification of mineral assemblage, particle size distribution, and QEMSCAN analysis. Laboratory preparation, testing, characterisation, and analysis were done for samples collected from each spiral: Compact Turbo, Alicoco, MG12, and HG10.

3.5.1 Sample drying

Before drying the various product samples collected from the pilot testing programme, these were weighed to later determine their respective solid contents. For the 30% solid samples, the following orders of magnitude of masses were recorded: 2 – 5 kg for concentrates, 0.1 – 0.7 kg for middlings, and 0.05 – 0.50 kg for tails. At 35% solid, 4 – 6 kg for the concentrate sample sizes, 0.06 – 1.00 kg for middlings, and 0.1 – 1.0 kg for tails. At 40%, sample sizes were between 4 kg and 6kg for the concentrates, 0.2 kg and 2 kg for the middlings, and 0.08 kg and 2.00 kg for the tails.

After weighing, all the product samples were placed on trolley-trays in the GCO Laboratory. The trolley-trays were then placed in the oven (refer to Figure 3.10) and allowed to dry 24 h thereby ensuring moisture had been removed completely from the samples.

Figure 3.10: A Marc Technologies drying oven (2 m^3, 415 V, 50 Hz) at GCO laboratory

Finally, the dry product samples were moved to the splitter room to prepare them for submission to the chemical laboratory for analysis. Preparation for chemical and mineralogical analysis amongst others are presented in the following section.

3.5.2 Chemical and mineralogical analysis of product samples

Each dry product sample was first weighed on the Kern scale in Figure 3.11 below to determine their respective mass. For that, a sample receiving bowl was put on the scale which was then reset to zero. A calico bag with dry sample was opened and carefully emptied into the receiving bowl while ensuring no spillage. The mass of the sample was then read off and recorded.

Figure 3.11: A 15-kg Kern weighing scale at GCO Laboratory

After the weighing was done, the rotary splitter in Figure 3.12 was used to split each sample to proportions needed to characterise the chemical and mineral contents. Note here that the splitter in Figure 3.12 is a Quantachrome Instruments sieving riffler, it can handle a 10 kg sample and split it through its eight sample receivers.

Figure 3.12: A Quantachrome Instruments sieving riffler splitter (220 V, 50/60 Hz) at GCO Laboratory

In terms of protocols, the splitter was switched on. As it rotated, a selected product sample was gradually poured into the cylinder from the top. The content of the cylinder then discharged into the eight sample receivers. Depending on the size of a sample needed for later analysis, the splitting was repeated until the required size was obtained. Based on the requirement of instruments available in the GCO Laboratory, 100 g of sample was required for mineral analysis and for chemical analysis by X-Ray Fluorescence (XRF). The Quantitative Evaluation of Minerals by Scanning Electro-microscopy (QEMSCAN), on the other hand, required 30 g to conduct mineral, density and particle size analyses. Particle size analysis by sieving required 100 – 200 g. The manual or riffle splitter in Figure 3.13 below was used to further split samples from Figure 3.12 to the required final masses. Similarly to the rotating

splitter in Figure 3.12, sample splits can be poured back to the manual sampler in Figure 3.13 a number of times until the required sample size is reached.

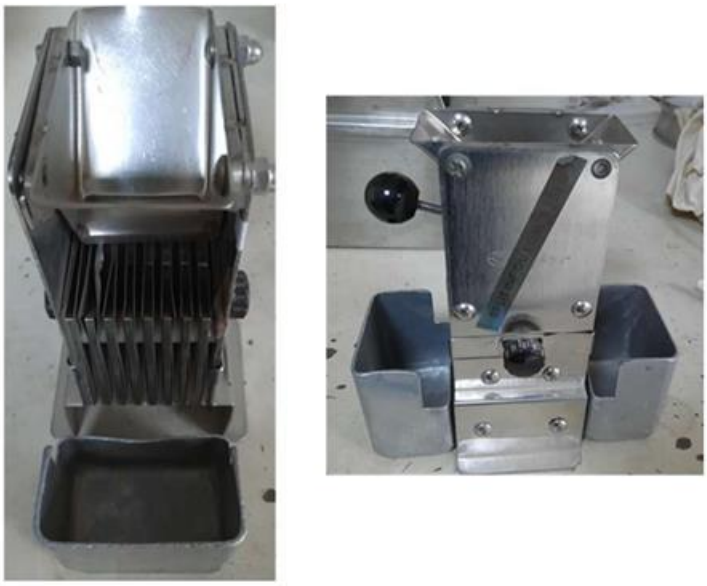

Figure 3.13: The manual splitter that can split a 100-g sample at the GCO Laboratory

Once the preparation of the adequate sample size was complete, the various splits were individually submitted to the GCO Laboratory for XRF analysis. A sample submission sheet accompanied the samples to the laboratory, which stated the name of the person under which the results would be reported in the internal Laboratory Information Management System (LIMS). Note that GCO has two XRF machines which are both capable of reading any sample submitted to the Laboratory depending on availability at the time of submission. Figure 3.14 shows one of the two XRF machines that were both used as part of this research work.

Figure 3.14: One of the two X-Ray Fluorescent (XRF) machines stationed at the GCO Laboratory

In addition to XRF analysis, all concentrate splits were submitted for total heavy mineral (THM), mineralogy analysis, and QEMSCAN analyses. It must be highlighted that all concentrate splits and selected middlings and tails splits were submitted to Eramet Ideas in France for these specialised analyses. The QEMSCAN machine in Figure 3.15 below was used for the purpose.

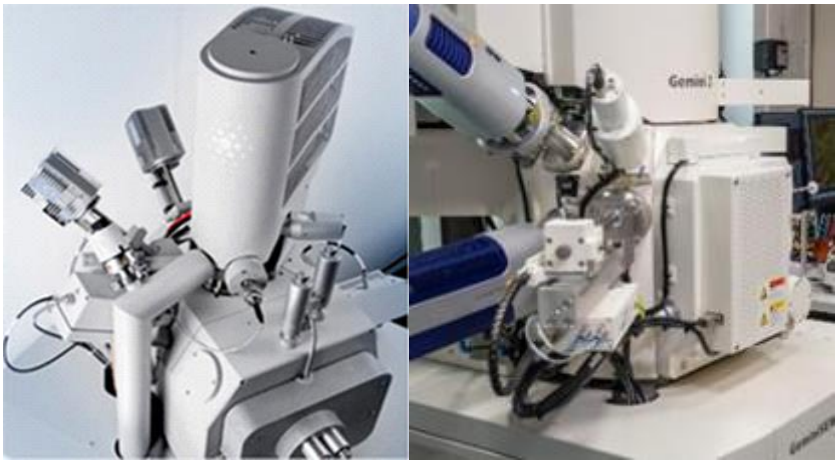

Figure 3.15: A QEMSCAN machine at Eramet Ideas, France

Finally, for each product sample, another split was prepared and kept for particle size analysis covered in the next section.

3.5.3 Particle size analysis

Screening, also known as sieving, was conducted using the screen shaker and the nest of sieves in Figure 3.16 below. A screening time of 15 min and a variable shaking frequency was applied to all product samples. The following screen apertures in microns (μm) were used for particle size analysis: 600, 300, 250, 212, 180, 150, 125, 106, 90, 75, and 53 microns.

Figure 3.16: A stack of screens on the shaking machine at the GCO Laboratory

After the shaking machine had stopped screening, each screen was weighed on the zeroed Kern scale in Figure 3.11 above. The combined mass of the screen and the sample was recorded. The sample was removed from the screen; then, a small brush was used to extract all the particles stuck in the apertures of the sieve. Thereafter, the screen was weighed. The difference

between the two masses was determined as the fraction retained on the screen after sieving. The masses of all the fractions of the initial sample retained on each screen were determined in this way and recorded for later processing.

3.6 Problems experienced during the experimental work

The research work experienced several problems which resulted in delays in sampling and processing of data. The main problems are highlighted below.

Shortage of Heavy Mineral Concentrate from the Wet Concentrator Plant caused instability in the Wet Circuit. As a result, a bulk sample could not be taken for months in 2022 and 2023. The delays in obtaining a bulk sample from the Wet Circuit were caused by breakdowns at the Wet Concentrator Plant which supplies the Wet Circuit with the heavy mineral concentrate. Consequently, the Wet Circuit could not reach steady state for the collection of a good bulk sample for a long time. Now when operations stabilised, the initial sample collected in May 2023 was insufficient for the necessary pilot test work. Successful bulk sampling was later done in November 2023 when a sample equivalent to 350 kg was taken for pilot testing.

GCO conducted infill geology drilling during the course of the year 2023 to confirm the grade along the mine path. In 2024, geology samples received priority in the GCO Laboratory. This delayed the chemical and mineralogical analysis of samples linked to this research study. And the laboratory became partially available; repeatability analysis could not be done; it was only limited to the split increments from the density run associated with each feed slurry. The delays alluded to here caused some splits, especially for the Compact Turbo and the HG10 spirals, to go missing while they were waiting for particle size analysis. As a remedy, corresponding tests were redone which may have not been very similar in slurry feed properties to those initially done with the Alicoco and the MG12 spirals.

In terms of the pilot tests, the Alicoco spiral was not able to handle the desired slurry feed. The Compact Turbo spiral was able to handle the feed well initially at 30% solid content by mass. But it did so partially at 35% and 40% as it experienced beaching as the experiment progressed. The same was observed with the HG10 spiral although it handled the slurry feed better than the Compact Turbo spiral except at 40% solids due to beaching. Only the MG12 handled all the solid concentrations (30%, 35%, and 40%) in the slurry feeds tested well. Because of all this, attempts to further dilute the slurry feed did not help. Note here that beaching refers to the accumulation of solid particles in the slurry feed on the surface of the spiral.

The use of calico bags to sample the concentrate, middlings and the tailings of the spirals in the spiral rig could have effects on the totality of the mass balance due to small particles remaining within the bags. However, due to the drying of the samples and diligence in emptying the bags the effects were expected to be minimal and negligible.

The combination of adjusting the splitters, increasing the pump speed to prevent choking the feedlines to the spirals, and sampling uncertainty might have resulted to variability in actual splits feed rate, with the analysis of the latter (feed rate) focusing on the operational conditions that resulted to its variability.

While there is data limit for the Alicoco Type H spiral, the failure of the spiral to handle the operational conditions is the result of the test work in itself. Data is limited to tests conducted outside this experimental work for comparison and performance assessment.

All in all, despite some of the unexpected challenges mentioned above, the experimental work was conducted successfully. Relevant data was collected the results of which are presented in the next chapter.

Chapter 4 Performance of the Alicoco, the Compact Turbo, the MG12, and the HG10 spiral separators

4.1 Introduction

The intention of feeding a slurry to a spiral separator is to recover valuable minerals in the beneficiation process while rejecting gangue material. This chapter presents the results of the pilot test work conducted in Chapter 3. The various types of data generated as part of the experimental tests were logged onto the Laboratory Management Information System (LIMS) in use at GCO. The data includes the physical, chemical, and mineralogical properties of all the samples collected around the Alicoco, the Compact Turbo, the HG10, and the MG12 spiral separators. Figure 4.1 below illustrates a display of the LIMS used at GCO. Relevant data properly codified and captured can be easily retrieved and exported to a Microsoft® Excel® spreadsheet for processing.

The mineralogy results were communicated electronically via an e-mail from the GCO Laboratory and from Eramet Ideas in Paris, France. The Eramet Ideas results were obtained by analysing the samples using QEMSCAN (i.e., quantitative evaluation of minerals by scanning electro-microscopy) to provide mineralogical, chemical, particle size and density analyses.

The results which are discussed in this chapter show the performance of four spirals: Compact Turbo, MG12 and HG10 spirals from Mineral Technologies and the Alicoco Type H spiral from Mineral Technology Co. Ltd.

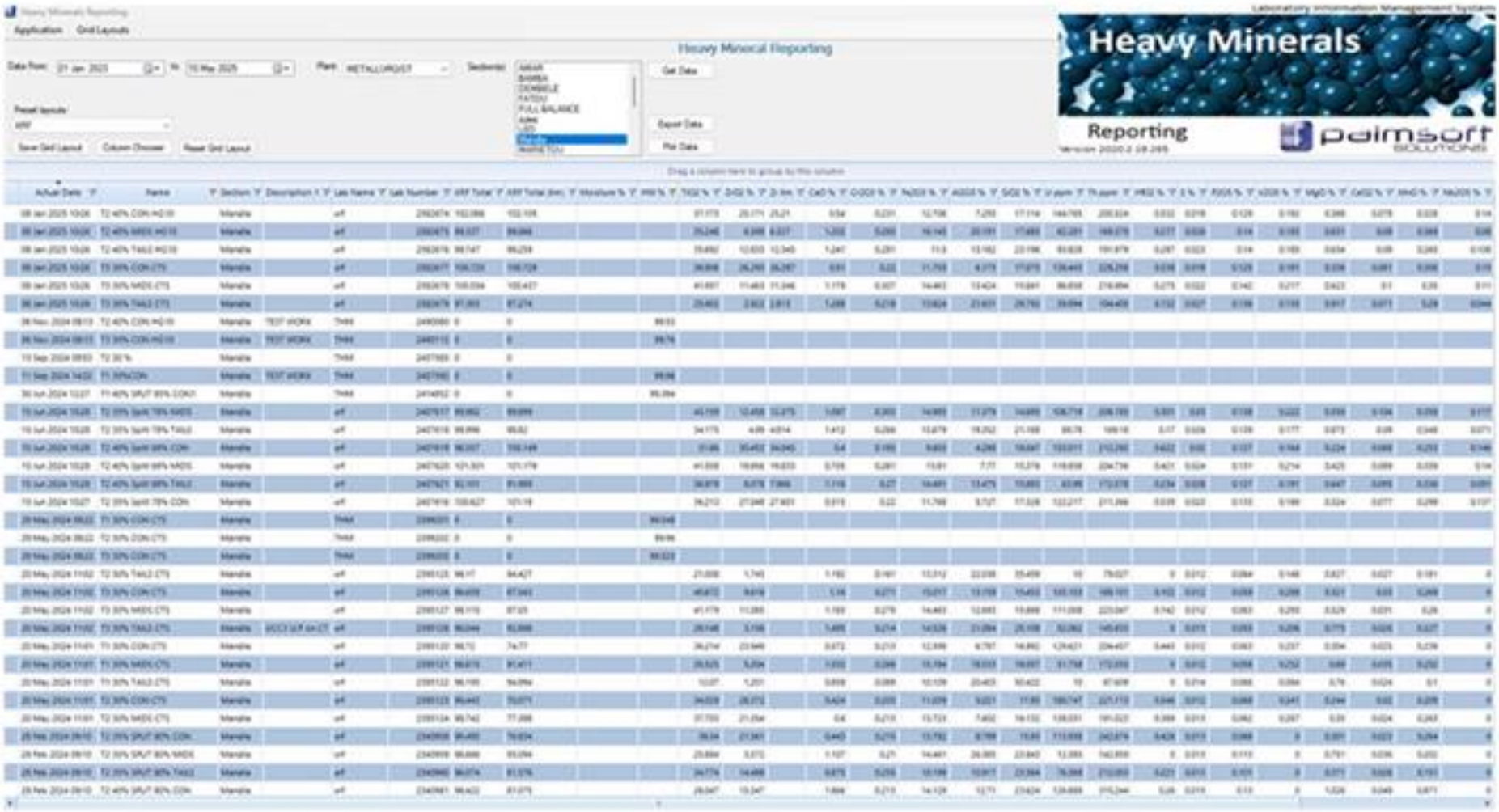

Figure 4.1: A screenshot of the Laboratory Information Management System (LIMS) at GCO

The HG10 spiral was included in the test due to its proven ability to handle feed that has already been processed like in cleaner stages (MacHunter and Pax, 2007). The MG12 spiral is touted mostly as the spirals with ability to handle raw feed to achieve high capacity, to achieve good concentrate grades and recoveries and improved metallurgical performance (Walker, 2016). This research is set to generate knowledge about the Compact Turbo spiral as there is currently no research available on it.

The Alicoco spiral, which was also the focus of the research, was not able to handle any of the tests as set out in the plan. Results from a separate test which was conducted in 2022 are included to indicate its ability of this spiral to handle the Classifier 3 underflow stream (see Appendix E).

The following section discusses the performance of the Compact Turbo, MG12 and the HG10 spirals using the recovery of ZrO_2 and Al_2O_3 as key performance indicators.

4.2 Recovery performance of the spirals

The recovery of ZrO_2 and Al_2O_3 by the three different spirals from Mineral Technologies is compared. Each spiral was fed a slurry which had percentage solids content varying from 30%, to 35% and to 40% by weight. In each solids content level in the feed the mass pull to the concentrate was set to 80%, to 85% and to 90% to get more recovery to the concentrate.

Wills and Napier-Munn (2006) calculate the percent solid content in a slurry using the formula:

$$x = \frac{s\,(\rho - w)}{\rho\,(s - w)} \times 100\% \qquad (4.1)$$

where x is the percent solid content by weight in the slurry feed (30%, 35% and 40% were tested in this research study); ρ is the density of the slurry [kg/m^3]; s is the density of the solids [kg/m^3]; and w is the density of water as the mixing fluid [kg/m^3].

Re-arranging Equation (4.1) and solving for slurry density ρ, the following can be obtained:

$$\rho = \frac{s\,w}{[s - x\,(s - w)]} \tag{4.2}$$

In terms of the present study, the specific density of the tertiary classifier underflow was determined to be $s = 4.17$ g/cm^3 while that of water is $w = 1$ g/cm^3. Substituting these in Equation (4.2) at $x = 30\%$, 35% and 40%, the corresponding densities of slurry feeds tested are $\rho = 1.30$ g/cm^3, 1.36 g/cm^3 and 1.44 g/cm^3.

At 30% solids or 1.30 g/cm^3 pulp density and for the 0.50 m^3 water volume in the sump the amount of solids added to make up the slurry was 214 kg. At the same 0.50 m^3 volume of water in the sump, 269 kg of solids make up the 35% solids in the slurry or 1.36 g/cm^3 pulp density. To make up 40% of solids in the slurry of 1.44 pulp density with 0.50 m^3 of water, 333 kg of solids were added.

These slurry densities are in line with the spiral designs densities in Table 2.4 and are in line with the slurry densities to the separation stages at the Wet Circuit (GCO, 2022).

4.2.1 Separation recoveries at 30% solid content in the slurry feed

The solids content in the feed remained constant at 30% and a spiral split was adjusted to increase the concentrate. The increase was from 80%, to 85% and then to 90%. The detailed results are in Appendix A, showing flow rates, quality and recovery or distribution of the chemical content to different spirals products.

Referring to Figure 4.2 below, it can be seen that as the mass pull or split to the concentrate increased from 80% to 90%, the recovery of ZrO_2 was increasing from the HG10 and the MG12 spirals. The recovery of the Compact Turbo spiral, on the other hand, sharply increased from 88.65% at 80% split to reach a maximum of 97.5% recovery to concentrate before dropping.

As for the Alicoco spiral, it experienced beaching and could not handle the stream; that is why, it does not feature in Figure 4.2.

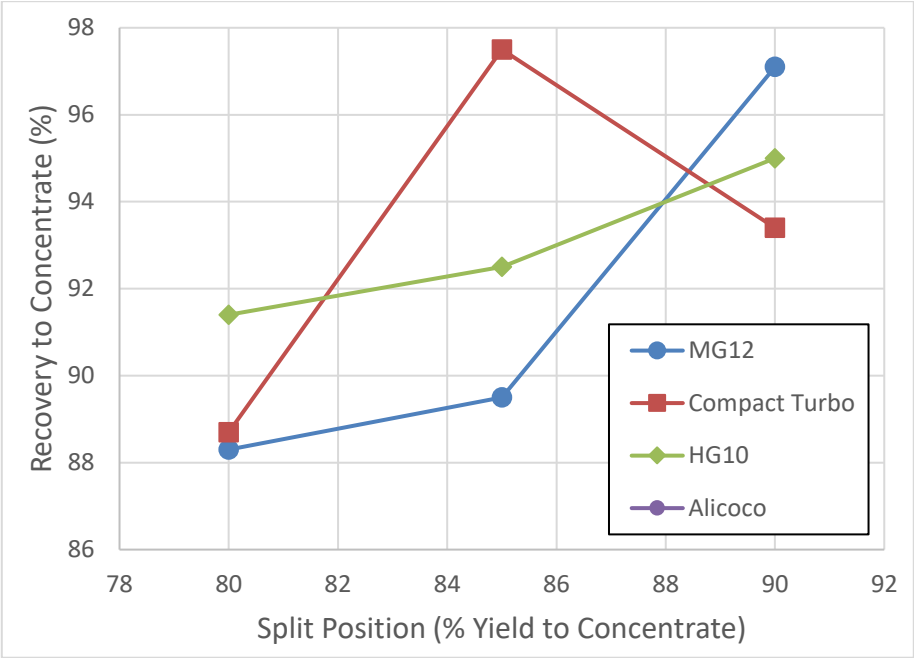

Figure 4.2: Recovery of ZrO_2 to the concentrate at 30% solid concentration in the slurry feed

In terms of comparison, Figure 4.2 shows differentiated ZrO_2 recoveries at 85% yield to concentrate with Compact Turbo at 97.5% while MG12 recorded the lowest recovery at 89.5%. When tested at 80% yield, the lowest and highest ZrO_2 recoveries were 88.3% and 91.4% corresponding to MG12 and HG10 respectively. At 90% yield the MG12 spiral recorded the highest ZrO_2 recovery of 97.06%, followed by the HG10 spiral at 94.99% and the Compact Turbo at 93.38%.

Referring to Figure 4.3 below as the mass pull or split to the concentrate increased from 80% to 85% and then to 90% the recovery of Al_2O_3 increasing from the minimum of 60.10% by the Compact Turbo spiral to 87.7% maximum by the HG10 spiral.

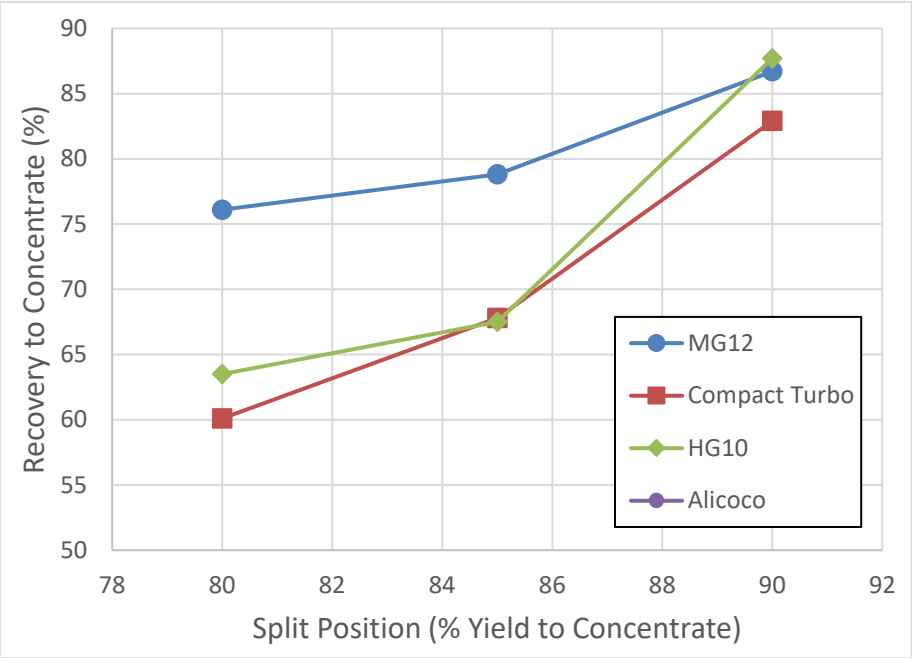

Figure 4.3: Recovery of Al_2O_3 to the concentrate at 30% solid concentration in the slurry feed

In Figure 4.3, the recovery of the contaminant, which is Al_2O_3, to the concentrate was the lowest consistently in all the splits of the Compact Turbo spiral, followed by the HG10 spiral and then the MG12. The Compact Turbo and HG10 spirals performance was close in rejecting aluminium at 80% yield to the concentrate. The Compact Turbo spiral recovered 60.09% Al_2O_3 compared to 63.49% by the HG10 spiral, both which were lower than 76.01% by the MG12. The Compact Turbo and HG10 spirals rejected almost 40% of Al_2O_3 compared to 24% by the MG12.

At 85% yield to the concentrate the Compact Turbo and HG10 spirals recovered 67.51% and 67.81% Al_2O_3 respectively compared to 78.84% by the MG12. And at 90% yield to the concentrate, the Compact Turbo spiral was clearly the best performer, recovering 82.94% Al_2O_3 compared to 86.70% and 87.66% by MG12 and HG10 respectively. The Compact Turbo spiral was therefore a better separator of the ZrO_2 and Al_2O_3 at 30% solids in the feed at the mass pull of 85% to the concentrate.

The performance of the spirals was investigated further by increasing the content of solids in the feed and repeating the above analysis. The recovery of ZrO_2 and the rejection of Al_2O_3 at 35% solids in the feed to the spirals is discussed in the following section.

4.2.2 Separation recoveries at 35% solid content in the slurry feed

The detailed results are summarised in Appendix B, showing flow rates, quality and recovery or distribution of the content to different spirals products.

When the solids content remained constant at 35% in the slurry feeding the spirals and the yield to the concentrate increased from 80% to 85% and then to 90% the recovery of ZrO_2 increased from the minimum of 88.51% to 96.11% maximum by the MG12 spiral (Figure 4.4).

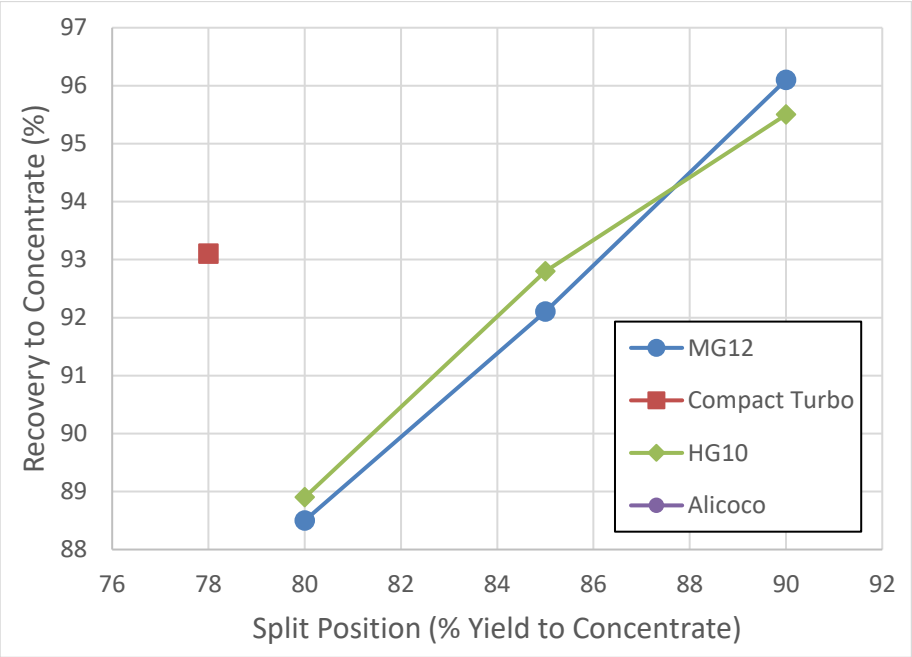

Figure 4.4: Recovery of ZrO_2 to the concentrate at 35% solid concentration in the slurry feed

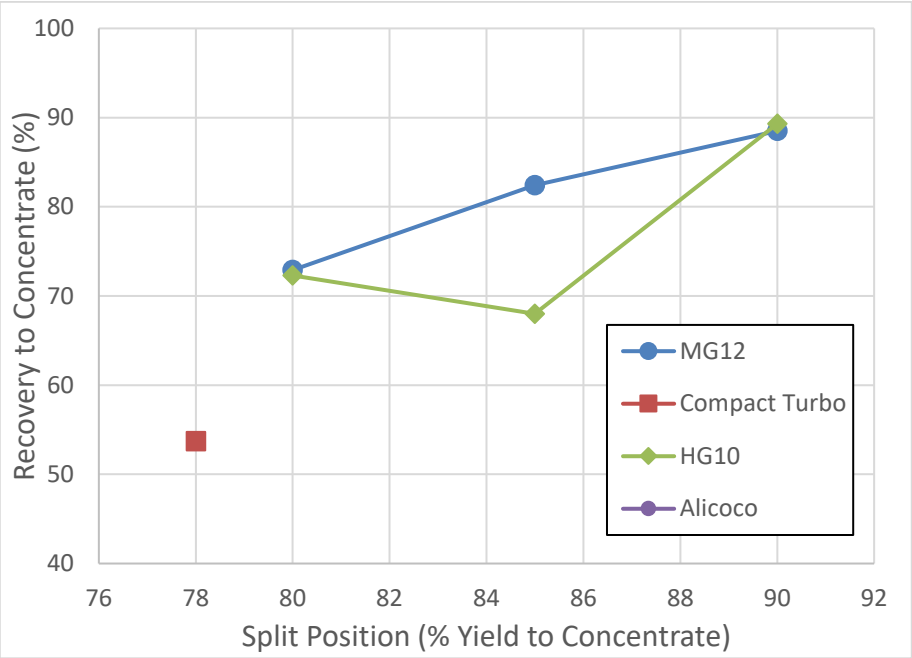

Figure 4.5: Recovery of Al_2O_3 to the concentrate at 35% solid concentration in the slurry feed

It can be seen in Figures 4.4 and 4.5 that the Compact Turbo spiral was not able to achieve 80% yield due to beaching and no separation. The maximum split that could be achieved was 77.70% or 78% to concentrate when the content of the solids increased from 30% to 35%. At this 78% yield the ZrO_2 recovery to the concentrate was 93.08%. The Al_2O_3 recovery was at 53.71%.

At 80%, the HG10 spiral recovered 88.94% of ZrO_2 and 72.32% of Al_2O_3 to concentrate. It performed slightly better than the MG12 spiral which recovered 88.51% of ZrO_2 and 72.87% of Al_2O_3. And when the yield increased to 85% the HG10 spiral maintained a better separation than the MG12, recovering 92.80% of ZrO_2 compared to 92.06% by the MG12. It recovered 67.95% of Al_2O_3 compared to 82.38% by the MG12.

At 90% yield to the concentrate, the MG12 was a better performer recovering more ZrO_2 at 96.11% and less Al_2O_3 at 88.50. The HG10 spiral recovered 95.47% of ZrO_2 and 89.29% of Al_2O_3 to concentrate.

The Alicoco spiral experienced beaching and was not able to handle the stream. The Compact Turbo spiral equally experienced beaching and blockage of the concentrate when the split was increased beyond 78%.

The overall results show that while the Compact Turbo spiral had the best recovery of ZrO_2 to the concentrate and the rejection of Al_2O_3 compared to the HG10 and MG12 at 80%, the HG10 performances at 80% and 85% are the best for this set of results. The restricted split by the Compact Turbo spiral limit further recovery of minerals to concentrate as compared to the HG10 and MG12 spirals.

The solids content in the feed was further increased from 35% to 40%, repeating the same analyses as in the above two sections. The aim of increasing the feed was to establish the ability of each spiral to handle concentrated solutions which come with high feed rates or desired capacities in the operations. The results are discussed in the section below.

4.2.3 Recovery performance at 40% solids level in the feed

The detailed results are available in Appendix C, showing flow rates, quality and recovery or distribution of the content to different spirals products.

When the solids content in the slurry feed to the spirals was kept constant at 40% with the yield to the concentrate increasing from 80%, to 85% and then to 90% the recovery of ZrO_2 increased from the minimum of 86.26% by the Compact Turbo spiral to 97.10% maximum by the MG12 spiral. The Al_2O_3 recovery also increased from 42.78% by the Compact Turbo spiral to 90.76% by the MG12 (Figure 4.6 below).

Figure 4.6: Recovery of ZrO_2 to the concentrate at 40% solid concentration in the slurry feed

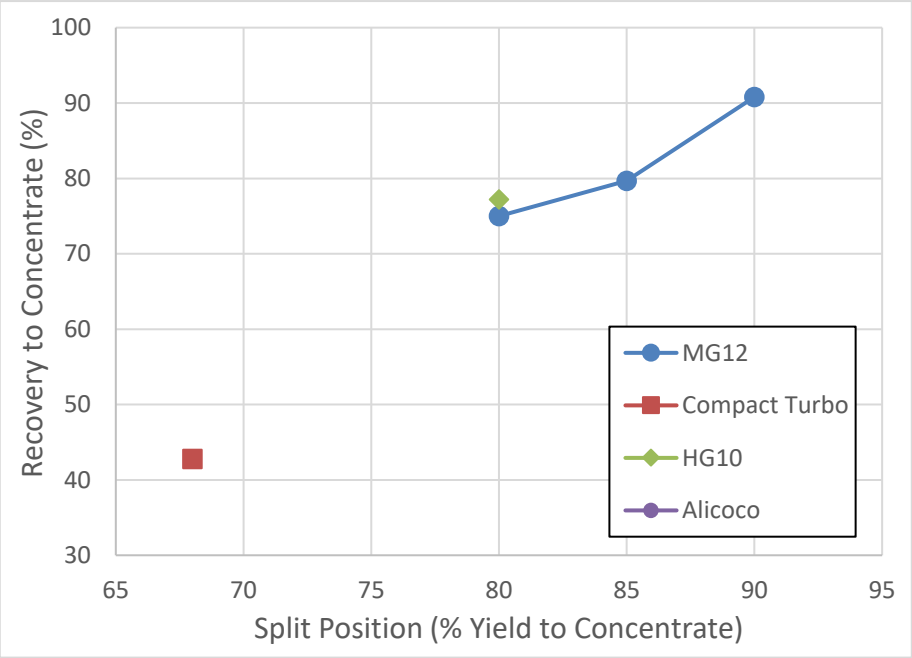

Figure 4.7: Recovery of Al_2O_3 to the concentrate at 40% solid concentration in the slurry feed

What can be noted from Figures 4.6 and 4.7 is that the Compact Turbo spiral was not able to achieve 80% yield due to beaching and blockage of the concentrate at the split position. The maximum split that could be achieved was 68.27% or 68% to concentrate. At this yield the ZrO_2 recovery to the concentrate was 86.26%. The Al_2O_3 recovery was at 42.78%.

At 80% yield to the concentrate, the HG10 spiral achieved the ZrO_2 recovery to the concentrate of 89.15%. The Al_2O_3 recovery was at 77.22%. The MG12 achieved 89.57% of ZrO_2 and 75.04% of Al_2O_3 recoveries to the concentrate. It should be noted that the HG10 spiral was not able to achieve 85% and 90% yield due to beaching and no separation.

At 85% yield to the concentrate, the MG12 achieved 89.70% of ZrO_2 and 79.72% of Al_2O_3 recoveries. And at 90% yield to the concentrate, the MG12 achieved 97.10% of ZrO_2 and 90.76% of Al_2O_3 recoveries.

The Compact Turbo and H10 spirals struggled to perform at 40% solids in the feed while treating the classifier 3 underflow. The MG12 was able to handle feed but the high recovery of Al_2O_3 to the concentrate demonstrates poor rejection of the contaminant and loss of spiral separation efficiency. Similar to the performance of the spirals at 35% solids in the feed, the restricted split by the Compact Turbo and the HG10 spirals limit further recovery of minerals to concentrate as compared to the MG12 spiral.

The recovery is not the only measure of the performance for the spiral. The quality of the streams coming out of the spirals and the feed rate to the spirals are other key indicators of a spiral performance. As it is known that the good recovery is always at the expense of poor quality to the product when factors such as feed rates increase (Neethling and Cilliers, 2012.), the quality is scrutinised in the following section.

4.3 Quality performance of the spirals

Section 4.2 above has demonstrated that when the split increases to the concentrate, the recoveries of ZrO_2 and Al_2O_3 to the concentrate increase. The increasing recovery is expected to have negative effects on the quality of the concentrate due to the inverse relationship between the recovery and the quality (Neethling and Cilliers, 2012; Wills and Napier-Munn, 2006).

The quality results are presented below at different solids content in the slurry feed and at different yields to the concentrate.

4.3.1 Quality performance at 30% solids level in the feed

The qualities of all the streams from the spirals at 30% solids in the spiral feed, which is equivalent to 1.30 g/cm^3 pulp density, and at the splits of 80%, 85% and 90% to the concentrate were analysed in an X-ray fluorescent (XRF) machine at the GCO Laboratory. The results are for ZrO_2 and Al_2O_3 as detailed in Appendices A, B and C. The concentrates were further analysed for mineralogy, using a mineral assemblage solver tool, also in the GCO Laboratory, for the mineral content of zircon, kyanite, silicates, etc. The detailed mineralogy results are in Tables D1 to D3 of Appendix D.

In Table 4.1 below the concentrate with the highest ZrO_2 content of 28.37% was from the Compact Turbo spiral at 80% split and with a reconstituted feed of 25.45% ZrO_2. The Compact Turbo spiral also reported the lowest Al_2O_3 content of 5.02%. The ZrO_2 and Al_2O_3 by the MG12 were 24.42% and 9.41% respectively. For the HG10 they were 24.87% and 6.12% respectively.

Table 4.1: The quality performance of the spirals at 30% solids and 80%, 85% and 90% split to the concentrate

		LABORATORY ASSAYS AT 30% SOLIDS (1.30 g/cm^3 PULP DENSITY) IN THE FEED							
Compact Turbo spiral									
YIELD	Con tph	**ZrO_2**	**Al_2O_3**	**THM**	**Zircon**	**Kyanite**	**Staurolite**	**Silicates**	**Quartz**
80%	1.99	28.37	5.02	99.36	36.53	5.16	3.77	4.63	0.64
85%	2.35	23.95	6.79	99.49	43.55	3.68	3.06	2.70	0.51
90%	2.60	9.62	13.16	99.52	36.58	4.57	3.93	4.51	0.48
MG12 spiral									
YIELD	Con tph	**ZrO_2**	**Al_2O_3**	**THM**	**Zircon**	**Kyanite**	**Staurolite**	**Silicates**	**Quartz**
80%	2.59	24.42	9.41	99.42	36.22	5.62	3.32	2.64	0.58
85%	2.65	23.39	9.69	99.37	37.95	0.36	7.28	4.67	0.63
90%	2.98	25.51	8.65	99.27	42.95	0.35	6.15	2.75	0.73
HG10 spiral									
YIELD	Con tph	**ZrO_2**	**Al_2O_3**	**THM**	**Zircon**	**Kyanite**	**Staurolite**	**Silicates**	**Quartz**
80%	2.40	24.87	6.12	99.49	43.55	3.91	3.04	2.61	0.51
85%	2.38	26.66	5.57	99.47	36.83	6.64	2.56	2.17	0.53
90%	2.41	23.75	8.56	99.76	35.12	4.39	6.37	3.69	0.24
Alicoco spiral									
YIELD	Con tph	**ZrO_2**	**Al_2O_3**	**THM**	**Zircon**	**Kyanite**	**Staurolite**	**Silicates**	**Quartz**
80%									
85%	0.06								
90%									

In Table 4.1, when the split increased from 80% to 85% and then to 90% while the solids in the feed remained at 30%.

Looking at the Compact Turbo spiral, it can be seen that at 80% split, the ZrO_2 content was 28.37%. At 85% split, it was 23.95% and then 9.62% at 90% split. Also, the 9.62% results could be an outlier possibly ascribed to laboratory contamination. The Al_2O_3 was 5.02% at 80% split, 6.79% at 85% and 13.16% at 90% split. The kyanite and staurolite which are the sources of Al_2O_3 were respectively 5.16% and 3.77% at 80% split, 3.68% and 3.06% at 85% split, and

4.57% and 3.93% at 90% split. They decreased while the Al_2O_3 increased. This also puts questions on laboratory tools especially for mineralogy solver.

As for the MG12 spiral, at 80% split the ZrO_2 was 24.42% at 80% split. At 85% the ZrO_2 was 23.39% and at 90% split it was 25.51%. The Al_2O_3 was 9.41% at 80% split, 9.69% at 85% split and 8.65% at 90% split. The kyanite was 5.62% at 80% split and then it decreased significantly to below 1% at 85% and 90% splits, which may be another outlier. The staurolite was 3.32% at 80% split, 7.28% at 85% split and 6.15% at 90% split.

Now in terms of the HG10 spiral, at 80% split the ZrO_2 was 24.87%. At 85% the ZrO_2 was 26.66% and then at 90% it was 23.75%. The Al_2O_3 was 6.12% at 80%, 5.57% at 85% and then 8.56% at 90% split. The kyanite and staurolite were respectively 3.91 and 3.04% at 80%, 6.64% and 2.56% at 85% split; and 4.39% and 6.37% at 90% split. An important note is that the silicates and the quartz are constant in all the splits per spiral with the Compact Turbo spiral showing higher values compared to the MG12 and the HG10 spirals.

With the Alicoco spiral: the sample collected was too small to be analysed due to beaching and no separation.

The complete tabulated results available in Appendix A1 show that the Al_2O_3 prefers to go to the tails in the Compact Turbo spiral at 22.04% content with 1.74% ZrO_2. This leaves the room to increase the ZrO_2 recovery to the concentrate by taking a bit from the middlings fraction to the concentrate without inviting a lot of contamination by Al_2O_3. The tails for the MG12 contain 9.29% Al_2O_3 and 6.14% ZrO_2 with the Al_2O_3 concentrating in the middlings at 13.95%. The HG10 tails contain 11.47% Al_2O_3, and high ZrO_2 at 15.31%, with high content of Al_2O_3 in the middlings. Further information is also available in Appendices A1 and A2.

Overall, the quality of the concentrate deteriorated as the split increased thereby inviting more Al_2O_3 and reducing the ZrO_2 content in the concentrate.

The Compact Turbo spiral offered better quality performance compared to the MG12 and the HG10 spirals.

The above results show the spiral performance when the content of the solids in the feed was at 30%. In the following section the performance is studied with the solids content increasing to 35%.

4.3.2 Quality performance at 35% solids level in the feed

The qualities of all the streams from the spirals at 35% solids or 1.36 g/cm^3 pulp density in the spiral feed and at the splits of 80%, 85% and 90% to the concentrate are presented in Table 4.2 below. The complete table of results is presented in Appendix B1 for chemical analysis, and in Tables D1 to D3 of Appendix D for mineralogy analysis.

Table 4.2: Quality performance of the spirals at 35% solids or 1.36 g/cm^3 pulp density and 80%, 85% and 90% split to the concentrate

		LABORATORY ASSAYS AT 35% SOLIDS (1.36 g/cm^3 PULP DENSITY) IN THE FEED							
Compact Turbo spiral									
YIELD	Con tph	**ZrO_2**	**Al_2O_3**	**THM**	**Zircon**	**Kyanite**	**Staurolite**	**Silicates**	**Quartz**
78%	2.87	27.05	5.73	99.78	40.51	3.26	3.40	2.76	0.22
MG12 spiral									
YIELD	Con tph	**ZrO_2**	**Al_2O_3**	**THM**	**Zircon**	**Kyanite**	**Staurolite**	**Silicates**	**Quartz**
80%	3.12	25.61	8.53	99.77	36.26	0.35	6.73	4.96	0.23
85%	3.45	24.43	9.06	99.71	36.19	0.36	7.65	2.29	0.29
90%	3.24	21.82	8.80	99.70	35.86	0.36	7.72	2.32	0.30
HG10 spiral									
YIELD	Con tph	**ZrO_2**	**Al_2O_3**	**THM**	**Zircon**	**Kyanite**	**Staurolite**	**Silicates**	**Quartz**
80%	2.79	21.56	8.80	99.78	35.17	4.49	5.84	3.61	0.22
85%	2.79	24.42	6.43	99.23	36.29	4.16	5.78	3.84	0.77
90%	2.83	22.53	9.55	99.46	33.35	5.32	6.47	3.87	0.54

In Table 4.2 at 35% solids in the feed and 78% split to the concentrate the ZrO_2 quality of the concentrate produced by the Compact Turbo spiral was 27.05%.

The closest comparison to the MG12 and the HG10 spirals were at 80% yield with 25.61% ZrO_2 by MG12 and 21.56% by HG10 spirals. Al_2O_3 was the lowest in the concentrate in the Compact Turbo spiral at 5.73% compared to 8.53% and 8.80% in the MG12 and HG10 concentrates respectively.

When the split increased to 85% and 90% while the solids in the feed remained 35%, the following was observed:

- **Compact Turbo spiral:** it could not handle the increase in split at 35% solids due to beaching and blockages.
- **MG12 spiral:** the ZrO_2 decreased to 24.43% and to 21.82%. The Al_2O_3 increased to 9.06% and then decreased to 8.80%.
- HG10: the ZrO_2 increased to 24.42% and then decreased to 22.53%. The Al_2O_3 decreased to 6.43% and then increased to 9.55%.
- **Alicoco spiral:** the sample collected was too small to be analysed due to beaching and no separation.

For the MG12 spiral the kyanite results remain very low while the staurolite showed an increase from 6.73% to 7.72% overall. It was in line with the increase of the Al_2O_3. The HG10 spiral also indicated an increase in kyanite and staurolite in line with the increase of Al_2O_3, from 8.80% to 9.55%. Detailed reports of supporting results can be found in Appendices A1 and B2. Suffice to say that results show that the Al_2O_3 concentrated in the middlings for the MG12 and HG10 spirals while it favoured tails in the Compact Turbo spiral.

4.3.3 Quality performance at 40% solids level in the feed

The qualities of all the streams from the spirals at 40% solids or 1.44 g/cm^3 pulp density in the spiral feed and at the splits of 80%, 85% and 90% to the concentrate are presented in Table 4.3 below. The full report of results is presented in Appendix C1 for chemical analysis and in Tables D1 to D3 of Appendix D for mineralogy analysis.

Table 4.3: The quality performance of the spirals at 40% solids or 1.44 g/cm^3 pulp density in the feed and 80%, 85% and 90% split to the concentrate

		LABORATORY ASSAYS AT 40% SOLIDS (1.44 g/cm^3 PULP DENSITY) IN THE FEED							
Compact Turbo spiral									
YIELD	Con tph	**ZrO_2**	**Al_2O_3**	**THM**	**Zircon**	**Kyanite**	**Staurolite**	**Silicates**	**Quartz**
68%	3.32	30.45	4.29	98.68	40.45	4.07	4.25	3.85	1.32
MG12									
YIELD	Con tph	**ZrO_2**	**Al_2O_3**	**THM**	**Zircon**	**Kyanite**	**Staurolite**	**Silicates**	**Quartz**
80%	3.75	25.08	7.30	99.27	36.03	4.09	10.56	2.61	0.73
85%	3.65	20.57	8.44	99.67	38.32	0.36	6.84	2.16	0.33
90%	3.14	22.93	8.35	99.86	37.94	0.67	6.16	2.10	0.14
HG10									
YIELD	Con tph	**ZrO_2**	**Al_2O_3**	**THM**	**Zircon**	**Kyanite**	**Staurolite**	**Silicates**	**Quartz**
80%	2.84	15.35	12.71	99.35	38.02	3.34	6.10	3.51	0.85
85%									
90%									

In Table 4.3 above, at 40% solids in the feed the Compact Turbo spiral could only handle 68% maximum split to the concentrate. The HG10 was able to handle only the 80% maximum split while the MG12 handled all the splits successfully.

For the Compact Turbo spiral at 68% split to the concentrate, the ZrO_2 quality of the concentrate produced was 30.45% with Al_2O_3 being the lowest among all the concentrates at 4.29%.

At 80% split to the concentrate, the MG12 achieved 25.08% ZrO_2 quality and the HG10 achieved 15.35% ZrO_2. The Al_2O_3 was 7.30% and 12.71% in the MG12 and HG10 concentrates respectively. Compared to the previous performances at 30% and 35% solids levels in the feed the HG10 performance deteriorated when the solids content increased to 40%.

When the split increased to 85% and 90% while the solids in the feed remained 40%, the following was observed for each of the spirals tested:

- **Compact Turbo spiral:** it could not handle the increase in split at 40% solids due to beaching and blockages.
- **HG10 spiral:** it could not handle the increase in split at 40% solids due to beaching and blockages.
- **MG12 spiral:** the ZrO_2 was 25.08% at 80% split, decreased to 20.57% at 85% and then increased to 22.93% with the overall decreasing trend. The Al_2O_3 increased from 7.30% to 8.44% and then decreased to 8.35% as the split increased.
- **Alicoco spiral:** it could not handle the increase in split at 40% solids due to beaching and no separation.

Appendix D1 shows that in the Compact Turbo spiral concentrate kyanite and staurolite were high at 4.07% and 4.25% respectively compared to the concentrates at 30% and 35% solids content in the feed. The HG10 spiral (refer to Appendix D3) indicates the presence of the two contaminants with the staurolite at 6.10% relative to the Al_2O_3 of 12.71%. The MG12 in Appendix D2 offers a better trend at the 40% solids results although kyanite has mixed results, and staurolite decreased as the Al_2O_3 increased. QEMSCAN offers an insight on kyanite and staurolite in the Compact Turbo spiral concentrates.

In addition to high recovery of valuable minerals, rejection of contaminants, and good quality of the product, a spiral feed rate influences the recovery and plays a role is selecting the equipment which is suitable for beneficiation. The following section discusses effects of operational feed rate variation to determine a better performing spiral.

4.4 Spirals operational feed rate variation

The overall performances of the Compact Turbo, the MG12 and the HG10 spirals include all the tests that were conducted for the 30% (1.30 g/cm^3 pulp density), 35% (1.36 g/cm^3 pulp density) and 40% (1.44 g/cm^3 pulp density) content of solids in the feed. The operational performances cover all the splits

achieved from 68%, 78%, 80%, 85% and 90%. The datasets are limited to these overall results as explained in Section 3.6 in the previous chapter.

4.4.1 Compact Turbo spiral operational feed rate

Figure 4.8 below shows that for the Compact Turbo spiral, the recovery of ZrO_2 increased from 88.65% with an increasing feed rate from 2.50 tph at the density of 1.30 g/cm^3 and 80% split, to peak at 97.45% when the feed rate was 2.75 tph at 1.36 g/cm^3 density and 85% split. It then started to decrease until it reached 86.26% when the feed rate was 4.86 tph at 1.44 g/cm^3 and 68% split.

The recovery of Al_2O_3 followed the same trend as that of the ZrO_2. It was 60.09% at 2.50 tph, peaked at 82.94% at 2.97 tph and then it decreased to 42.78% at 4.86 tph.

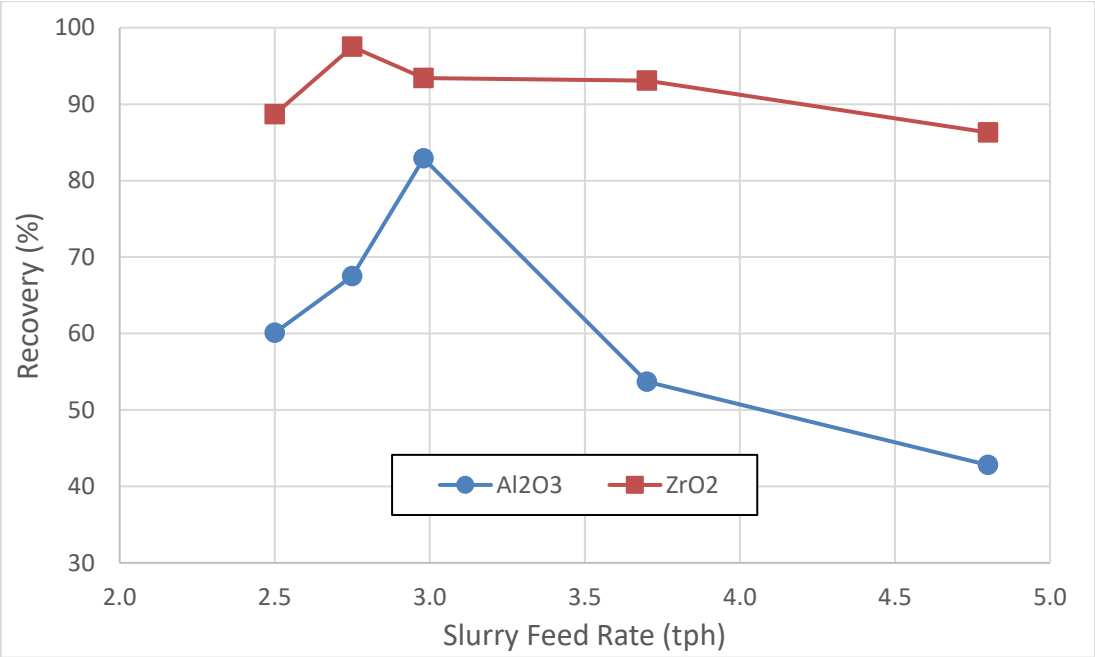

Figure 4.8: Effects of slurry feed rate on the recovery of ZrO_2 and Al_2O_3 to the concentrate by the Compact Turbo spiral

The best recovery of 97.45% at feed rate of 2.75 tph for the Compact Turbo spiral was achieved at 30% solids (1.30 g/cm^3 pulp density), at 85% split to the

concentrate with qualities of 23.95% ZrO_2 and 6.79% Al_2O_3 in the concentrate (see Table A2 in Appendix A for further reference). Table 4.1 above shows that the kyanite was 3.68%, staurolite was 3.77%, silicates 4.63% and quartz at 0.64%. The Al_2O_3 rejection to the middlings and tails was 32.49% (recovery to the concentrate was 67.51%).

4.4.2 MG12 spiral operational feed rate

The picture of the recoveries of the ZrO_2 and Al_2O_3 by the MG12 spiral is the same as that of the Compact Turbo spiral. Figure 4.9 below shows that for the MG12 spiral the ZrO_2 recovery was initially 88.30% at 3.17 tph feed rate when the density and the split were 1.30 g/cm^3 and 80% respectively. It increased and peaked at 97.10% at 3.36 tph when the density and the split were 1.44 g/cm^3 and 90% respectively and then started to decline until it reached 89.57% at 4.53 tph when the density and the split were 1.44 g/cm^3 and 80% respectively.

The Al_2O_3 recovery to the concentrate followed the trend of the ZrO_2 just like it was observed with the Compact Turbo spiral. At the same feed rates as in the Compact Turbo spiral it was initially 76.01%, peaked at 90.76% and then decreased to 75.04%.

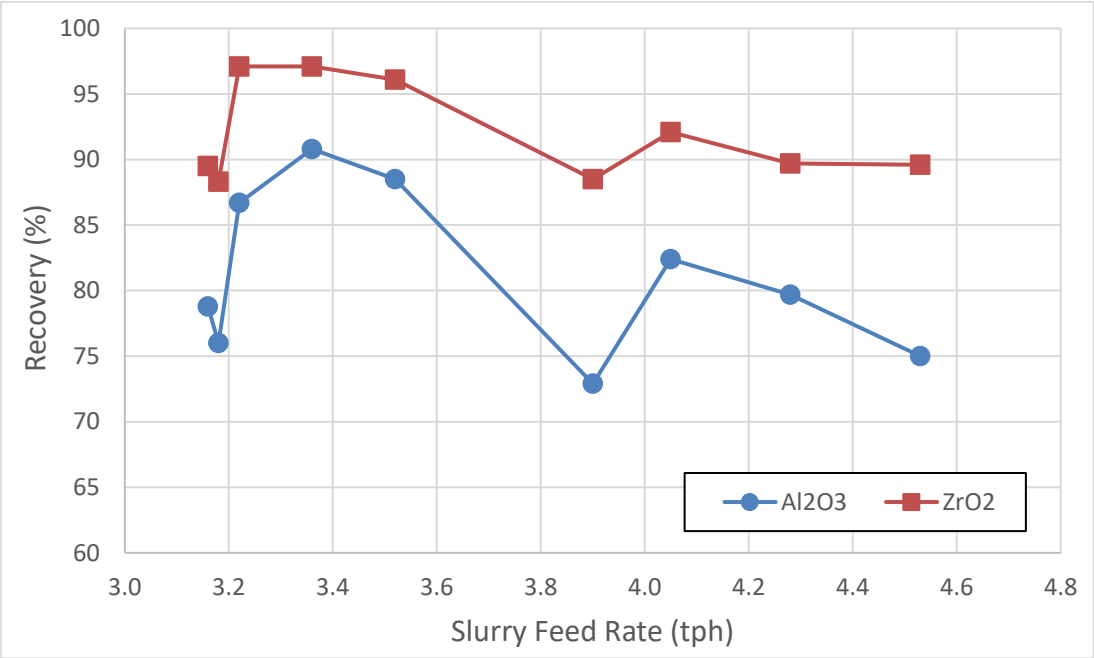

Figure 4.9: Effects of slurry feed rate on the recovery of ZrO_2 and Al_2O_3 to the concentrate by the MG12 spiral

Here, the best recovery of 97.10% at feed rate of 3.36 tph in Figure 4.9 was obtained when the solids level in the spiral feed was at 40% and the split to the concentrate was 90% (additional information is available in Table C3 of Appendix C). The ZrO_2 in the concentrate was 22.93%, the Al_2O_3 was 8.35% and the Al_2O_3 rejection was 9.24%, i.e. 90.76% recovery of Al_2O_3 to the concentrate.

Table 4.3 above shows that kyanite was at 0.67%, the staurolite 6.16%, the silicates 2.10% and the quartz 0.14%.

4.4.3 HG10 Spiral operational feed rate

Figure 4.10 below shows that the HG10 spiral displays a different performance behaviour compared to the Compact Turbo and the MG12 spirals. The recoveries of both the ZrO_2 and the Al_2O_3 show declining trends as the feed rate increases. At 2.64 tph (1.30 g/cm^3 and 90% split) the recoveries were 97.06% and 86.70% for ZrO_2 and Al_2O_3 respectively. They respectively

decrease to 88.94% and 74.74% when the highest feed rate of 3.75 tph was reached at 1.36 g/cm^3 and 80% split.

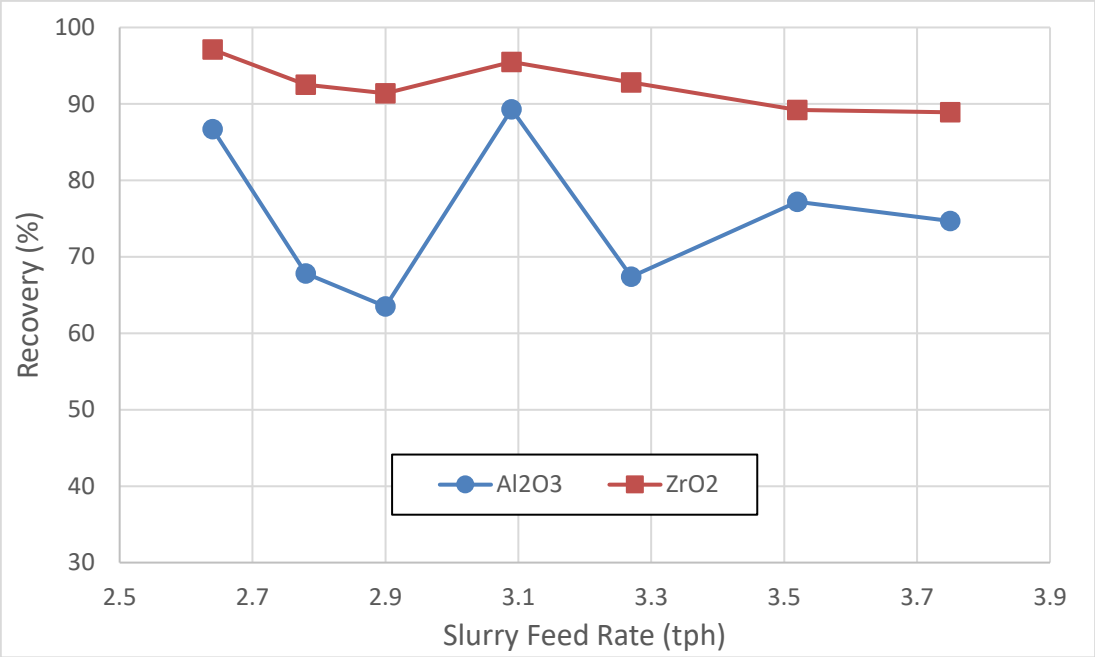

Figure 4.10: Effects of slurry feed rate on the recovery of ZrO_2 and Al_2O_3 to the concentrate by the HG10 spiral

Table A3 in Appendix A shows that the best recovery of 97.06% at the feed rate of 2.64 tph was achieved at 30% solids in the feed, 90% split to the concentrate with the ZrO_2 quality of 23.75%, Al_2O_3 quality of 8.56% and the Al_2O_3 rejection of 12.34% (87.66% recovery to the concentrate).

Table 4.1 shows that kyanite was 4.39%, staurolite was 6.37%, silicates 3.69% and quartz 0.24%.

4.5 Problems observed with the Alicoco spiral

The Alicoco spiral was not able to separate the slurry at 30% (1.30 g/cm^3 pulp density), at 35% (1.36 g/cm^3 pulp density) and at 40% (1.44 g/cm^3 pulp density) solids as the spiral started to beach. The solids content for the Alicoco spiral was decreased to below 30% compared to 30%, 35% and 40% by other Mineral

Technologies spirals but it was still not able to achieve any separation. Refer to Figure 4.11 below for the Alicoco spiral beaching conditions during the testing.

Figure 4.11: Alicoco spiral unable to separate slurry even when water was added at the top of the spiral to reduce beaching

In 2022, the Alicoco spiral was tested on the same material, and its performance was compared against the HG10 spiral. The following results were obtained as reported in Tables 4.4 to 4.6 below.

In the first test in Table 4.4 the Alicoco spiral treated a slurry with 22.32% solids by weight (1.20 g/cm^3 pulp density) compared to 28% (1.27 g/cm^3 pulp density) by the HG10 spiral. The yield to the concentrate for the Alicoco spiral was 57.62% compared to 47.45% by the HG10. The ZrO_2 and Al_2O_3 were 11.13% and 10.64% respectively in the Alicoco concentrate. They were respectively 14.40% and 11.93% for the HG10 spiral. The HG10 concentrate quality was better than that of the Alicoco spiral. The Alicoco recovered 63.23% of ZrO_2 and 90.29% of Al_2O_3 compared to 80.295 ZrO_2 and 35.30% Al_2O_3 by the HG10. Therefore, the Alicoco spiral concentrated the Al_2O_3 more than the ZrO_2, creating an undesirable situation.

Table 4.4: Test 1 results for Alicoco and HG10 spirals separating Classifier 3 Underflow in 2022

			LABORATORY ASSAYS		RECOVERY	
Alicoco spiral						
Test 1: 22.32% Solids	**TPH**	**YIELD %**	**ZrO_2 %**	**Al_2O_3 %**	**ZrO_2 %**	**Al_2O_3 %**
Con	1.00	57.62	11.13	10.64	63.23	90.29
Mid	0.20	17.81	11.76	2.85	20.65	7.49
Tails	0.34	24.58	6.65	0.61	16.12	2.22
Feed (calc)	1.55	100.00	10.14	6.79	100.00	100.00
HG10 spiral						
Test 1: 28% Solids	**TPH**	**YIELD %**	**ZrO_2 %**	**Al_2O_3 %**	**ZrO_2 %**	**Al_2O_3 %**
Con	1.01	47.45	14.40	11.93	80.29	35.30
Mids	0.29	13.67	5.05	19.54	8.12	16.65
Tails	0.83	38.87	2.54	19.82	11.60	48.04
Feed (calc)	2.13	100.00	8.51	16.04	100.00	100.00

In Test 2 (refer to Table 4.5 below), the Alicoco spiral treated a slurry with 19.60% solids by weight (1.18 g/cm^3 pulp density) compared to 25% (1.23 g/cm^3 pulp density) by the HG10 spiral. The yield to the concentrate for the Alicoco spiral was 59.58% compared to 57.39% by the HG10 spiral. The difference between two yields, 2.19%, was small compared to that of Test 1, which was 10.17%.

The ZrO_2 and Al_2O_3 quality contents were 11.10% and 10.97% respectively in the Alicoco concentrate. They were respectively 13.59% and 9.16% in the HG10 spiral concentrate. The HG10 concentrate quality was better than that of the Alicoco spiral, showing an upgrade from the calculated feed of 9.06% ZrO_2 and 13.34% Al_2O_3. The Alicoco recovered 67.34% of ZrO_2 and 90.20% of Al_2O_3 compared to 86.13% ZrO_2 and 39.39% Al_2O_3 by the HG10. More than half of the Al_2O_3 (51.54%) that arrived at the HG10 spiral reported to the Tails compared to only 4.60% which was rejected by the Alicoco spiral. Test 2 confirmed the Test 1 results.

Table 4.5: Test 2 results for Alicoco and HG10 spirals separating Classifier 3 Underflow in 2022

			LABORATORY ASSAYS		RECOVERY	
Alicoco						
Test 2: 19.60% Solids	**TPH**	**YIELD %**	**ZrO_2 %**	**Al_2O_3 %**	**ZrO_2 %**	**Al_2O_3 %**
Con	2.02	59.58	11.10	10.97	67.34	90.20
Mid	0.51	15.05	10.86	2.50	16.63	5.20
Tails	0.86	25.37	6.21	1.31	16.03	4.60
Feed (calc)	3.39	100.00	9.82	7.25	100.00	100.00
HG10						
Test 2: 25% Solids	**TPH**	**YIELD %**	**ZrO_2 %**	**Al_2O_3 %**	**ZrO_2 %**	**Al_2O_3 %**
Con	1.13	57.39	13.59	9.16	86.13	39.39
Mids	0.16	8.23	5.11	14.71	4.65	9.08
Tails	0.68	34.37	2.43	20.01	9.22	51.54
Feed (calc)	1.97	100.00	9.06	13.34	100.00	100.00

In the third test in Table 4.6 below the Alicoco spiral treated a slurry with 14.85% solids by weight (1.13 g/cm^3 pulp density) compared to 26% (1.25 g/cm^3 pulp density) by the HG10 spiral. The yield to the concentrate for the Alicoco spiral was 64.82% compared to 70.08% by the HG10.

The ZrO_2 and Al_2O_3 were 11.29% and 11.64% respectively in the Alicoco concentrate. They were respectively 11.44% and 14.38% for the HG10 spiral. The higher than Alicoco's yield for the HG10 saw the Al_2O_3 concentrate content increased compared to Test 1 and Test 2. The Alicoco concentrate quality was better than that of the HG10 spiral in terms of Al_2O_3.

The Alicoco recovered 74.63% of ZrO_2 and 96.19% of Al_2O_3 compared to 91.33% ZrO_2 and 66.90% Al_2O_3 by the HG10. The Alicoco recovered Al_2O_3 better than it recovered the ZrO_2 as it rejected 10.93% ZrO_2 to the tails compared to 1.08% Al_2O_3.

Table 4.6: Test 3 results for Alicoco and HG10 spirals separating Classifier 3 Underflow in 2022

			LABORATORY ASSAYS		RECOVERY	
Alicoco						
Test 3: 14.85% Solids	**TPH**	**YIELD %**	**ZrO_2 %**	**Al_2O_3 %**	**ZrO_2 %**	**Al_2O_3 %**
Con	1.66	64.82	11.29	11.64	74.63	96.19
Mid	0.51	13.16	10.72	1.63	14.39	2.73
Tails	0.71	22.02	4.89	0.39	10.98	1.08
Feed (calc)	2.87	100.00	9.80	7.85	100.00	100.00
HG10						
Test 3: 26% Solids	**TPH**	**YIELD %**	**ZrO_2 %**	**Al_2O_3 %**	**ZrO_2 %**	**Al_2O_3 %**
Con	1.45	70.08	11.44	14.38	91.33	66.90
Mids	0.05	2.36	1.95	25.28	0.52	3.97
Tails	0.57	27.55	2.60	15.93	8.15	29.13
Feed (calc)	2.07	100.00	8.78	15.06	100.00	100.00

Appendix F provides complete sets of results for the Alicoco (Table F1) and the HG10 (Table F2) spirals. In Table F1, the Alicoco spiral recovered 72.36 of TiO_2 better than 63.23% of ZrO_2 in Test 1. The Alicoco spiral also rejected SiO_2 (45.43%) and free SiO_2 (56.91%) to tails better than it rejected the Al_2O_3 (2.22%). In Tests 2 and 3 the trends stay the same with the worst Al_2O_3 rejection of 1.08% in Test 3. The TiO_2 recovery and SiO_2 rejection are however not any better than those by the Compact Turbo spiral, the MG12 spiral, and the HG10 spiral (refer to Appendix A for more details). Overall, the Alicoco spiral operated much better at low densities and recovered more Al_2O_3 than ZrO_2. This performance is however not yielding the desired results of high-capacity favouring high pulp density and high aluminium rejection. The results serve as evidence for operability and practical limitations of the Alicoco spiral.

The following section considers the particle size distribution of the concentrates for the Compact Turbo, the MG12 and the HG10 spirals and of the tertiary

classifier underflow. The Alicoco spiral is not part of the particle size distribution analyse due to beaching and blockages during the tests.

4.6 Particle size distributions of various streams

Figure 4.12 below shows the particle size distribution of the feed to the spirals, which is the classifier 3 underflow; and of the concentrates from the Compact Turbo, the MG12 and the HG10 spirals. The graphs show cumulative percentage of a sample that has passed through or is below the screen aperture size.

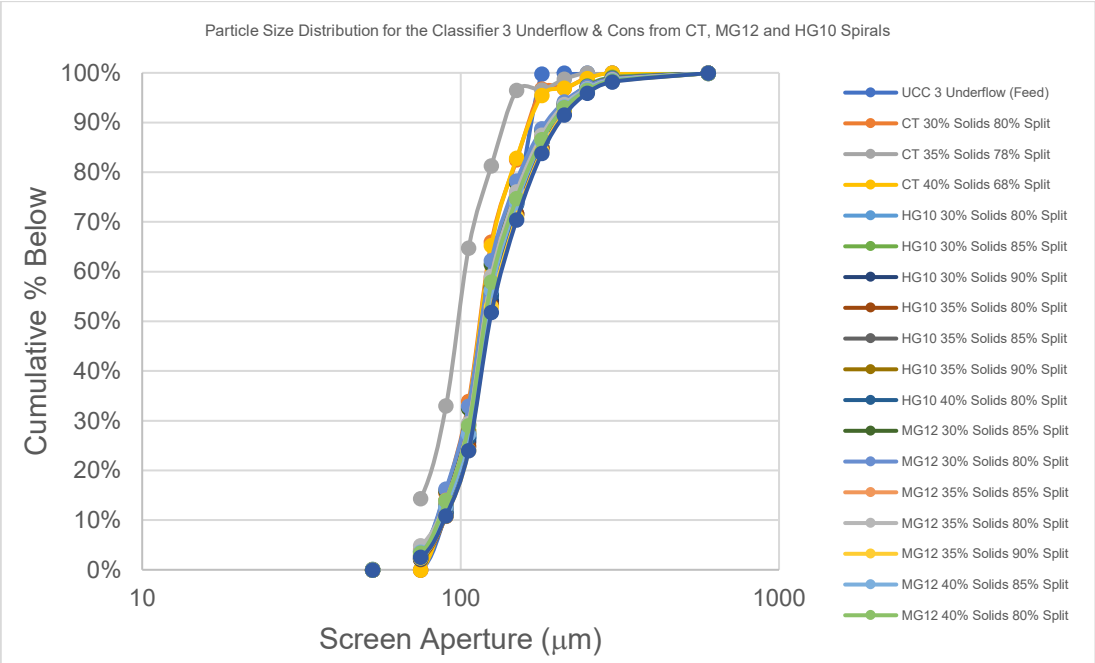

Figure 4.12: The particle size distribution of the feed to and the concentrates from the spirals

The far-left grey trend is of the Compact Turbo spiral concentrate with 35% solids in the feed, at 78% split to the concentrate. It is followed by the Compact Turbo spiral concentrate with 40% solids, at 68% split to the concentrate. The feed to the spirals, although it pitches at the top at 180 µm it remains on the far right together with the MG12 spirals trends.

The d_{50} sizes of the spirals are presented in Tables 4.7 to 4.9 below. They are compared to the d_{50} of the feed to the spirals, which is the classifier 3 underflow of 121.50 μm. Individual charts for the various spirals tested are also available in Appendix E.

The d_{50} for the Compact Turbo spirals concentrates (Table 4.7) was 115.53 μm for the 30% feed solids 80% split, 116.18 mm for the 35% feed solids 78% split; and 116.04 μm for the 40% solids 68% split to the concentrate. Compared to the d_{50} in Table 4.8 and Table 4.9 the concentrates from the Compact Turbo spiral are finer than those from the MG12 and the HG10 spirals. Compared to the feed to the Compact Turbo spiral, there is an average difference of 5.59 μm between the feed of 121.50 μm to these concentrates in Table 4.7. The Compact Turbo spiral was able to reject big particles.

Table 4.7: The d_{50} sizes for the Compact Turbo spiral concentrates

	Split to the Concentrate		
Feed Solids	**80%**	**78%**	**68%**
	d_{50} (μm)	**d_{50} (μm)**	**d_{50} (μm)**
30%	115.53		
35%		116.18	
40%			116.04

The d_{50} sizes from the MG12 spirals concentrates ranged from 117 μm minimum to 123.77 μm (124 μm) in Table 4.8. They straddled the feed, with the 30% feed solids concentrate at 117 μm and the d_{50} becoming higher (concentrate becoming courser) as the solids content in the feed and the split to the concentrate increased, reaching 124 μm at 40% solids content and 90% split to the concentrate. There is a possibility that the fine particles were lost to the tails in the MG12 spiral.

Table 4.8: The d_{50} sizes for the MG12 spiral concentrates

	Split to the Concentrate		
Feed Solids	**80%**	**85%**	**90%**
	d_{50} (μm)	**d_{50} (μm)**	**d_{50} (μm)**
30%	117	117	
35%	119	119	123
40%	120	121	124

The d_{50} sizes of the HG10 spiral concentrates range from 121 μm to 123 μm compared to 121 μm by the feed to the spiral (refer to Table 4.9 below). They are higher than all the Compact Turbo spirals d_{50} sizes, and higher than some of the MG12 spiral d_{50}s. Similar to the MG12 spiral, there is a possibility of losing fine particles to the tails and sending the larger ones to the concentrates.

Table 4.9: The d_{50} sizes for the HG10 spiral concentrates

	Split to the Concentrate		
Feed Solids	**80%**	**85%**	**90%**
	d_{50} (μm)	**d_{50} (μm)**	**d_{50} (μm)**
30%	121	121	122
35%	123	121	120
40%	121		

The chemical analyses of the samples at the GCO Laboratory as presented in the above sections show that the Compact Turbo spiral produced the concentrates that have high ZrO_2 and low Al_2O_3 contents. Samples of the best the concentrates from the Compact Turbo spiral together with the classifier 3 underflow sample were sent to Eramet Ideas Laboratory in Paris for further analysis to understand the particle behaviour in the form of mineralogy, particle size and of the density. Eramet Ideas analysed the samples by QEMSCAN.

4.7 QEMSCAN quality analysis for the feed and Compact Turbo concentrates samples

QEMSCAN provided mineralogy analysis of the classifier 3 underflow and for the Compact Turbo spiral concentrates at 30% weight solids (1.30 g/cm^3 pulp

density) and 85% split, 35% weight solids (1.36 g/cm^3 pulp density) and 78% split; and at 40% weight solids (1.44 g/cm^3) at 68% split. Figure 4.13 to Figure 4.16 show the QEMSCAN images of the samples. The results are presented in Table 4.10 below. The full report is also available in Table G1 of Appendix G for further scrutiny.

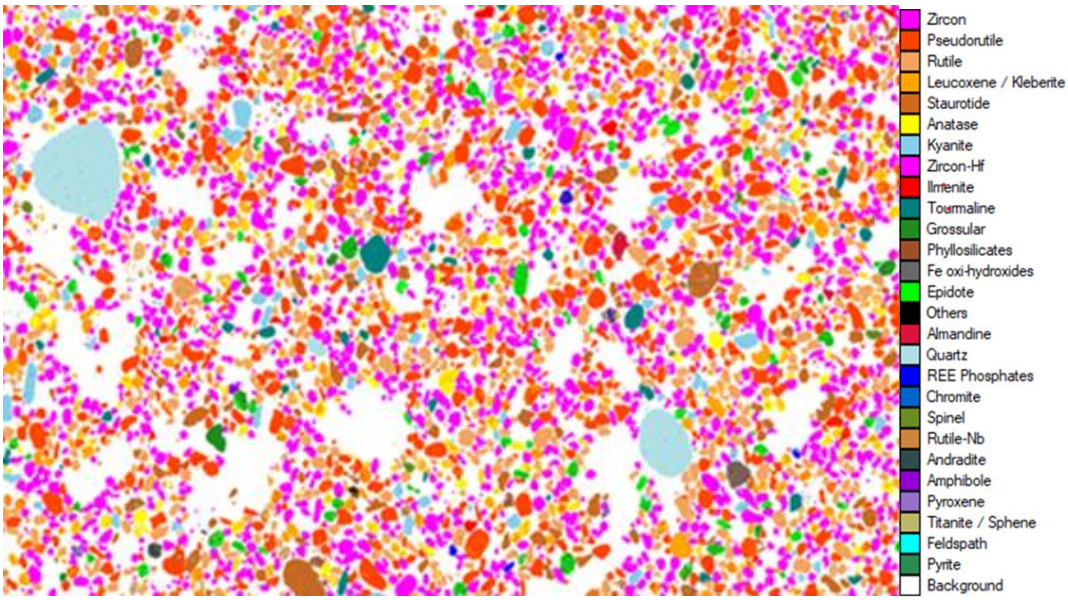

Figure 4.13: The QEMSCAN image of the classifier 3 underflow (spirals feed)

Figure 4.13 is the QEMSCAN image of the classifier 3 underflow or feed to the spiral. The larger particles indicate the presence of quartz (powder-blue) particles in the feed to the spirals. The majority of particles are zircon, rutile, leucoxene and the aluminium-bearing particles of staurolite and kyanite.

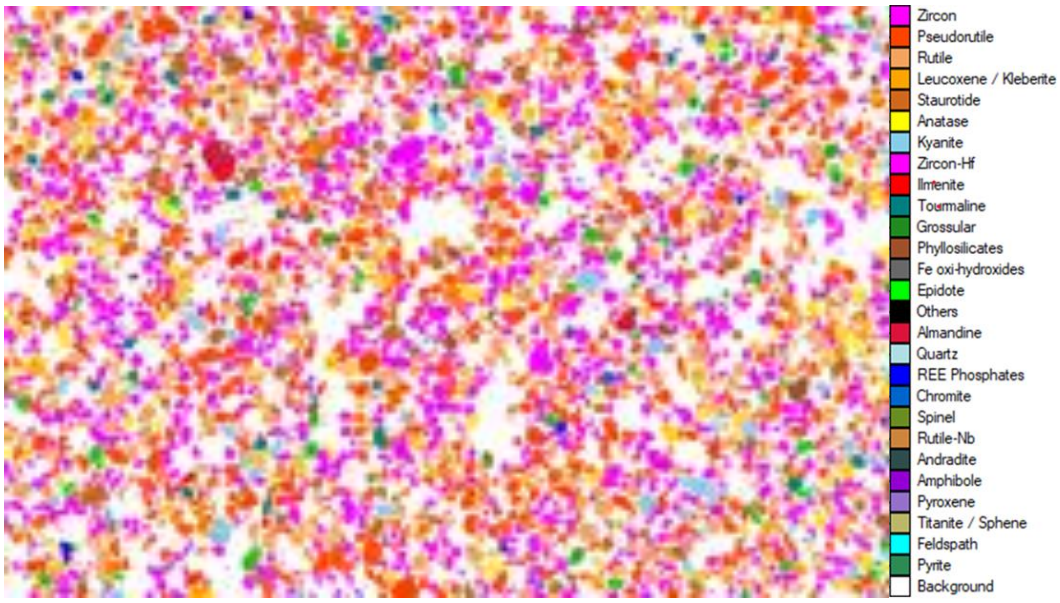

Figure 4.14: The QEMSCAN image of the 30% solids (1.30 g/cm^3 pulp density) and 85% split concentrate

Figure 4.14 is the QEMSCAN image of the 30% solids 80% split concentrate. The larger particles of quartz (powder-blue) as seen in the feed to the spirals are no longer present with dominant particles being those of zircon, rutile, leucoxene and the aluminium-bearing particles of staurolite and kyanite.

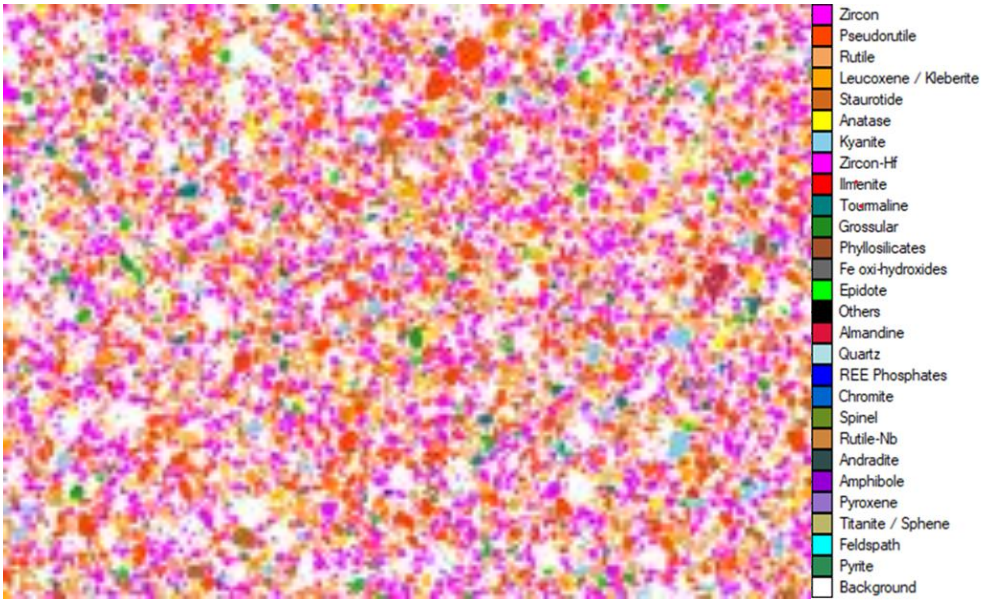

Figure 4.15: The QEMSCAN image of the 35% solids (1.36 g/cm^3 pulp density) and 78% split concentrate

Figure 4.15 is the QEMSCAN image of the 35% solids 78% split concentrate. Similar to the 30% solids 80% split concentrate the larger particles of quartz (powder-blue) as seen in the feed to the spirals are no longer present with dominant particles being those of zircon, rutile, leucoxene and the aluminium-bearing particles of staurolite and kyanite.

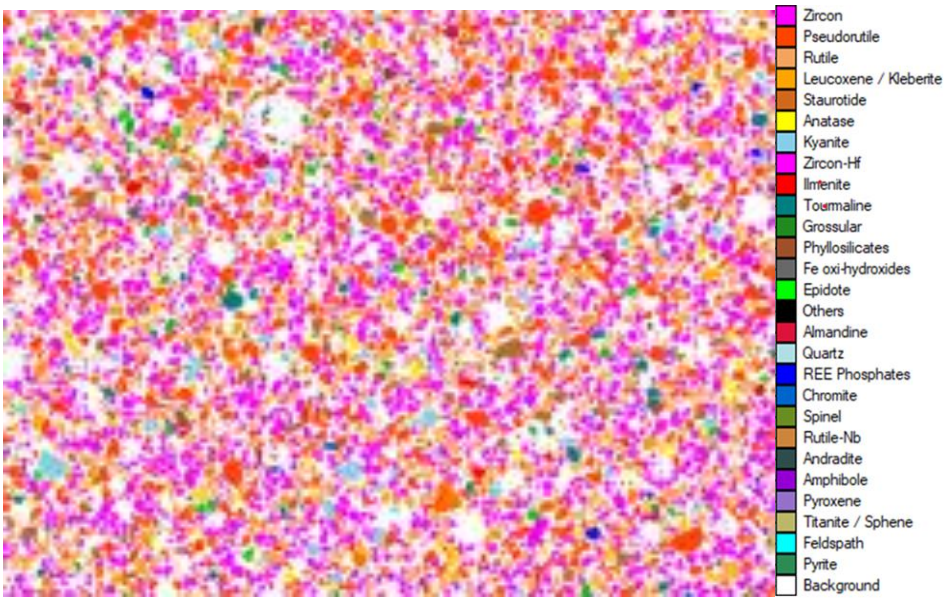

Figure 4.16: The QEMSCAN image of the 40% solids (1.36 g/cm^3 pulp density) and 68% split concentrate

Figure 4.16 is the QEMSCAN image of the 40% solids 68% split concentrate. Similar to the other two concentrates the larger particles of quartz (powder-blue) as seen in the feed to the spirals are no longer present with dominant particles being those of zircon, rutile, leucoxene and the aluminium-bearing particles of staurolite and kyanite.

The mineralogy results are summarised in Table 4.10 below showing a trend from the feed to each concentrate as the separation improved. Refer to Figure G1 in the Appendix G for the graphical representation of the trends.

Table 4.10: The QEMSCAN mineralogy analysis, showing the quality of the Compact Turbo spiral feed and the concentrates

	Mass Fractions (%)			
Mineral Name	**Feed**	**30% Solids & 85% Split**	**35% Solids & 78% Split**	**40% Solids & 68% Split**
Zircon	32.32	32.38	35.74	38.78
Pseudorutile	19.97	22.85	20.78	19.14
Rutile	17.37	17.13	16.53	17.02
Leucoxene / Kleberite	6.84	7.79	7.36	6.55
Staurolite	5.71	4.12	4.36	3.68
Kyanite	3.34	2.80	2.46	2.32
Quartz	2.41	0.35	0.31	0.25
Ilmenite	0.80	1.25	1.09	1.07
Phyllosilicates	0.71	1.02	0.93	0.99

Table 4.10 shows that there was an increase in the zircon mineral content from 32.32% in the feed to 32.38% in the 30% solids and 85% split concentrate, to 35.74% in the 35% solids and 78% split concentrate; and to 38.78% in the 40% solids and 68% split to the concentrate. Both staurolite and kyanite decreased as the zircon content improved. The difference between the 5.71% staurolite in the feed and the 3.68% in the 40% concentrate is 36% reduction. The corresponding kyanite reduction was 31%. There was 90% reduction of quartz from 2.41% in the classifier underflow to 0.25% in the 40% concentrate. Other minerals of interest such as rutile and leucoxene were rejected at 2% and 4% respectively to the middlings and tails while the ilmenite to the 40% concentrate improved by 34%.

At elemental level, the QEMSCAN results in Table G2 of Appendix G show a decrease of alumina (Al) from 4.23% in the classifier underflow to 3.18% in the 40% concentrate. This is 25% reduction. The zirconium (Zr) increased from 15.77% to 19.23% which was a 22% increase.

4.8 QEMSCAN particle size distribution for the feed and Compact Turbo concentrates samples

Figure 4.14 below shows the particle size analysis by QEMSCAN. The mass percentage is shown in the secondary-axis, and the cumulative percentage is on the primary axis.

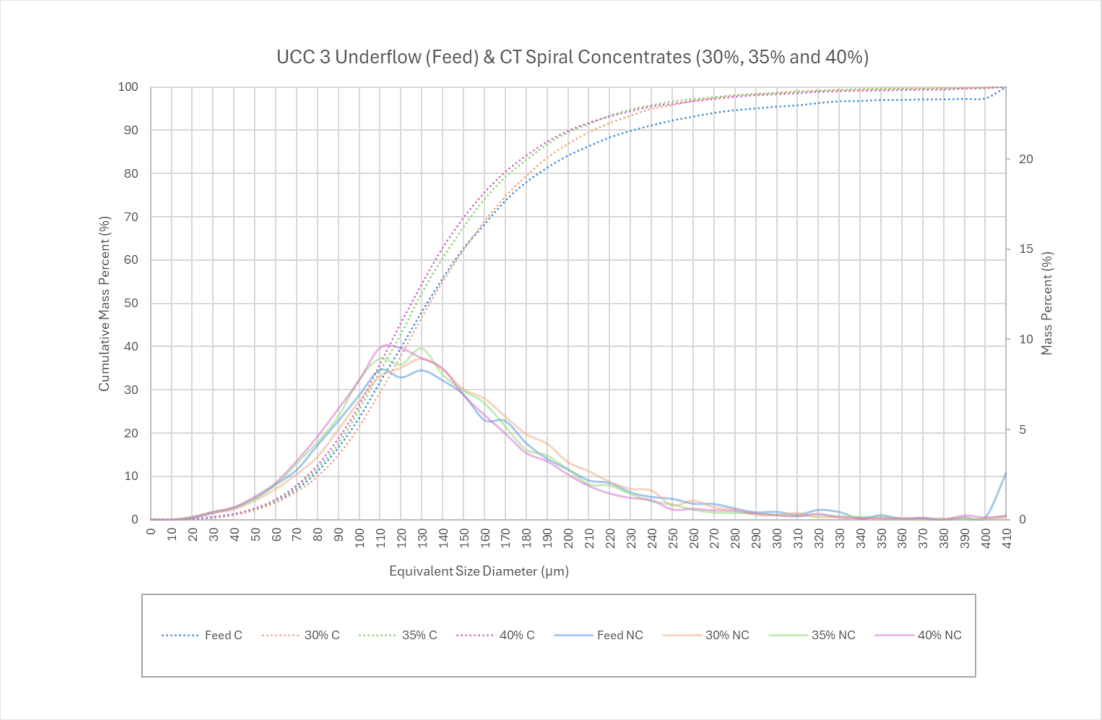

Figure 4.17: QEMSCAN sizing of the tertiary classifier underflow and the Compact Turbo spiral concentrates at 30%, 35% and 40% solids in the spiral feed

The QEMSCAN size analysis shows all the samples depicting multiple peaks between 110 µm and 130 µm. The feed lying to the right of Figure 4.17:

- For the classifier underflow or the feed to the spirals, the peaks are at 8% by mass of the sample each.
- The 30% concentrate had mild peak at 7.8% by mass and one major at 9%.
- The 35% concentrate peaked at 9% and at 10% by mass.
- The 40% concentrate has the first peak at 10% and the second one at 9% mass percentage.

Table 4.11 below shows the d_{50} and the d_{80} sizes from Figure 4.17. The table shows the results for the samples (classifier underflow, 30% concentrate, 35% concentrate and 40% concentrate) as well as the particles of the minerals within the samples.

Table 4.11: The d_{50} and the d_{80} of the classifier underflow and the Compact Turbo spiral concentrates

	Sample		Zircon		Staurolite		Kyanite	
Sample	**d_{50} (μm)**	**d_{80} (μm)**	**d_{50} (μm)**	**d_{80} (μm)**	**d_{50} (μm)**	**d_{80} (μm)**	**d_{50} (μm)**	**d_{80} (μm)**
Classifier Underflow	132	186	105	137	130	195	140	193
30% Solids	133	181	105	137	85	126	135	179
35% Solids	128	171	98	130	94	143	129	180
40% Solids	125	169	94	129	86	124	132	177

The classifier underflow sample had a d_{50} of 132 μm and the d_{80} of 186 μm. After separating the sample at 30% solids in the feed, there was no change on the d_{50} but the d_{80} decreased to 181 μm in the concentrate. At 35% solids in the feed, the d_{50} decreased to 128 μm, and the d_{80} was 171 μm in the concentrate. At 40% solids in the feed, the d_{50} decreased to 125 μm and the d_{80} to 169 μm in the concentrate.

The zircon particle size in the classifier underflow behaved the same as in the concentrate samples. The d_{50} of zircon particles in the feed was the same as of the zircon particles in the 30% concentrate at 105 μm. It then decreased to 98 μm at 35% solids and 94 μm at 40% solids. It was the same with the d80 being the same at 137 μm.

The staurolite particles had a d_{50} of 130 μm and the d_{80} of 195 μm in the feed. At 30% solids concentrate, the d_{50} was 85 μm and the d_{80} was 126 μm. The d_{50} was 94 μm and the d_{80} was 143 μm at 35% solids concentrate; and then respectively 86 μm and 124 μm at 40% solids concentrate.

The size for the kyanite particles behaved similarly to the samples and the zircon particles. In the classifier underflow, the d_{50} was 140 μm and the d_{80} was 193 μm. In the 30% concentrate the d_{50} was 135 μm and the d_{80} was 179 μm. In the 35% solids concentrate, the d_{50} was 129 μm and the d_{80} was 180 μm. In the 40% solids concentrate, the d_{50} was 132 μm and the d_{80} was 177 μm.

The behaviour of the zircon and aluminium-bearing particles in terms of the density was also studied under the QEMSCAN. The results are illustrated in Figure 4.18 and in Table 4.12 below.

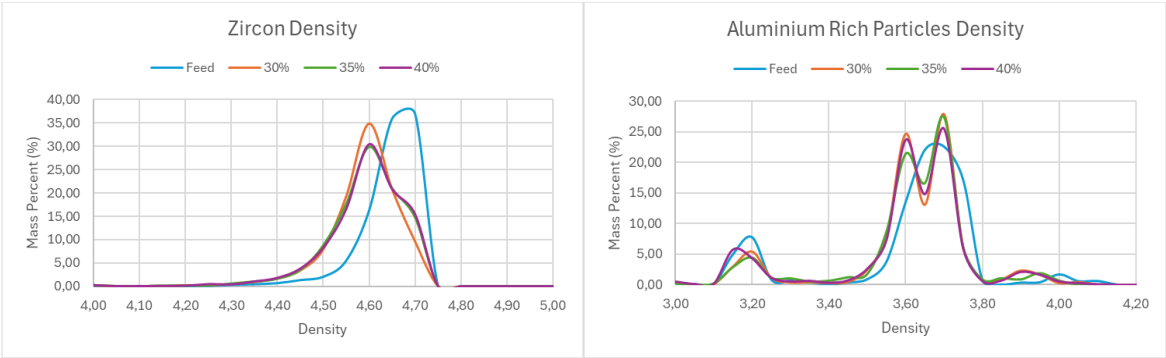

(a) (b)

Figure 4.18: The density of (a) the zircon particles in the samples and (b) aluminium bearing particles

Figure 4.18(a) shows that the density of the zircon particles was between 4.20 g/cm^3 and 4.80 g/cm^3, with the peaks at 4.60 g/cm^3 and 4.69 g/cm^3. For the aluminium-bearing particles in Figure 4.18(b) the density varied between 3.10 g/cm^3 and 4.00 g/cm^3. The summary for the zircon particles is given in Table 4.12 below.

The average density of the zircon particles in the classifier underflow was 4.70 g/cm^3 with 35% of the mass of the particles with this density. For all the concentrates, the average density was 4.60 g/cm^3. Mass fractions were 35% for the 30% solids concentrate; and 30% for both the 35% solids and the 40% solids concentrates.

Table 4.12: Summary of the density of the zircon particles of the classifier underflow and the Compact Turbo spiral concentrates

Sample	Density		
	Mass %	Peak 1 (g/cm^3)	Range (g/cm^3)
Classifier Underflow	35%	4.70	4.20 – 4.75
30% Solids Concentrate	35%	4.60	
35 % Solids Concentrate	30%	4.60	
40% Solids Concentrate	30%	4.60	

The density range for the zircon particles in all the samples was 4.20 – 4.75 g/cm^3 as seen on Figure 15(a).

The summary of the density of the particles that bear aluminium is shown in Table 4.13 below.

As shown in Figure 4.18(b), the aluminium-bearing particles had four clear peaks. The first peaks happened in the average density of 3.20 g/cm^3, covering a range of 3.10 – 3.40 g/cm^3 representing below 10% mass in all the feed, 30% concentrate, 35% concentrate and 40% concentrate samples.

The second and the third peaks for the concentrates covered a range of 3.40 – 3.80 g/cm^3. The second peaks occurred at 3.60 g/cm^3 representing 24.90% mass for the 30% concentrate; at 3.62 g/cm^3 and representing 22% mass for the 35% solids concentrate; and 3.62 g/cm^3 representing 24% for the 40% solids concentrate. The second peak for the feed sample to the spirals occurred at 3.65 g/cm^3 representing 23% of the sample mass.

The third peaks for the concentrate samples occurred at the density of 3.68 g/cm^3 and it represented 24% mass of each sample. The third and last visible peak for the feed sample to the spirals occurred at 4.10 g/cm^3 with a mass less than 1%.

The range for the fourth peaks for the concentrate samples was 3.80 – 4.14 g/cm^3.The fourth peaks occurred at 3.90 g/ cm^3 and 2% mass for the 30% solids concentrate; 3.94 g/ cm^3 at less 2% mass for the 35% solids concentrate; and at 3.90 g/ cm^3 at less than 2% mass for the 40% solids concentrate.

Table 4.13: Summary of the density of the aluminium-bearing particles of the classifier underflow and the Compact Turbo spiral concentrates

Sample	Density							
	Peak 1		Peak 2		Peak 3		Peak 4	
	Mass (%)	Density (g/cm^3)	Mass (%)	Density (g/cm^3)	Mass (%)	Density (g/cm^3)	Mass (%)	Density (g/cm^3)
Classifier Underflow	7%	3.20	24.00%	3.68	<1.00%	4.00	<0.2%	4.10
30% Solids Concentrate	5%	3.20	24.90%	3.60	27.00%	3.70	2%	3.90
35 % Solids Concentrate	4%	3.20	22.00%	3.62	26.90%	3.70	<2%	3.94
40% Solids Concentrate	6%	3.14	24.00%	3,62	25.00%	3.70	<2%	3.90
Range (g/ml)	3.10 – 3.26		3.40 – 3.80				3.80 – 4.10	

4.9 Summarised conclusion

At 30% solids in the feed, the recovery of ZrO_2 by Compact Turbo spiral increased from 86.65% to 97.45% when the split to the concentrate increased from 80% to 85%. It then decreased to 93.38% when the split increased further to 90%. For the MG12 and the HG10 spirals, the recoveries of ZrO_2 increased directly with the increasing split. For the MG12 spiral, the ZrO_2 recoveries and the splits were 88.30% recovery at 80% split, 89.46% at 85% split, and 97.06% at 90% split. For the HG10 spiral, the recoveries were 91.36% at 80% split, 92.51% at 85% split, and 94.99% at 90% split. The Compact Turbo spiral was consistently low in Al_2O_3 recovery to the concentrate, followed by the HG10 and then the MG12. The Compact Turbo spiral indicated the best separation of ZrO_2 and Al_2O_3 at 30% solids compared to the MG12 and the HG10 spiral.

At 35% solids in the feed, the Compact Turbo spiral could not achieve the desired splits of 80%, 85% and 90% due to bleaching. The recovery of ZrO_2 by Compact Turbo spiral at 78% maximum split achieved was 93.08% with the lowest Al_2O_3 recovery at 53.71%. For the MG12 and the HG10 spirals, the recoveries of ZrO_2 increased directly with the increasing split. The MG12 spiral achieved the highest recovery of 96.11% of ZrO_2 and 88.50% Al_2O_3 at 90% split. The HG10 spiral achieved the highest recovery of 95.47% of ZrO_2 and 89.29% Al_2O_3 at 90% split.

At 40% solids in the feed, the Compact Turbo spiral could not achieve the desired splits of 80%, 85% and 90% due to bleaching. The recovery of ZrO_2 by Compact Turbo spiral at 68% maximum split achieved was 86.26% with the lowest Al_2O_3 recovery at 42.78%. The HG10 spiral could not achieve the desired splits of 85% and 90% at 40% solids in the feed due to beaching. The MG12 spiral was able to handle all the splits and was characterised by high 97.10% ZrO_2 and 90.76% Al_2O_3 recoveries, indicating poor separation as the solids in the feed increased.

The overall ZrO_2 quality of the concentrate deteriorated when the split to the concentrate increased, in line with the literature. In the Compact Turbo spiral, the Al_2O_3 reported preferentially to the tails while it preferred to go to the middlings for the MG12 and the HG12 spirals.

When combining all the data and observing the operational feed rate, the recoveries of ZrO_2 and Al_2O_3 increased and then decreased for the Compact Turbo and the MG12 spirals. This was in line with the literature. For the HG10 spiral, the recoveries of both the ZrO_2 and Al_2O_3 declined consistently throughout the study.

The Alicoco spiral was not able to handle any of the desired solid's content in the feed and splits to the concentrate. Comparison to the HG10 at lower densities in another test work showed that the Alicoco spiral recovered up to 90% Al_2O_3 at 70% ZrO_2 recovery to the concentrate. The HG10 spiral performed better than the Alicoco spiral.

The d_{50} values from the particle size distribution for the Compact Turbo concentrates were below those of the MG12 spiral. The HG10 spiral had the highest d_{50}s of all the spirals. QEMSCAN explained this observation by showing that large quartz particles in the feed samples were not occurring in the Compact Turbo concentrates. This indicated the ability of the Compact Turbo spiral to separate the particles on size which the MG12 and HG10 spirals could not achieve. QEMSCAN also showed the complexity of the aluminium bearing particles which had different density peaks while the zircon bearing particles were consistent. The particle size, chemical and mineral analyses by QEMSCAN prove the rejection of course particles with the concentrates by the Compact Turbo spiral being finer than the feed.

Chapter 5 Influence of operating conditions on the recovery of zircon and aluminium

5.1 Introduction

The results that were presented in Chapter 4 are discussed in this chapter. A slurry made up of classifier CL003 underflow from the Wet Circuit was separated using different spirals. With the solids content by weight percentage varying from 30%, to 35% and to 40% while the mass pull to the concentrate varied from 80%, to 85% and to 90% per solids content in the feed, the slurry was separated using the Compact Turbo, the MG12 and the HG10 spirals from Mineral Technologies as well as the Alicoco type H Spiral from Mineral Technology Co. Ltd. The assessment in this chapter includes the effects of the operational conditions which mainly are mainly displayed by the variability of the feed rate to the spirals.

The aim of the separation was to establish the ability of the Compact Turbo and Alicoco spirals to separate zircon and aluminium. This could inform usability of this technology in the context of the GCO operation.

5.2 Recovery of zircon and aluminium to the concentrate

The results in Section 4.2 in the previous chapter shows that as the yield to the concentrate increased, the recovery of ZrO_2 and Al_2O_3 to the concentrate increased (refer to Figures 4.2 – 4.4). The quality results in Section 4.3 show that as the yield to the concentrate increased, the quality of the ZrO_2 in the concentrate decreased while the contaminant, which is the Al_2O_3 increased (See Tables 4.1 – 4.3). These results are combined to present operating regimes. Figure 5.1 below indicates that as the quality of the ZrO_2 in the concentrate improved, its recovery decreased with all the MG12, the HG10 and the Compact Turbo spirals.

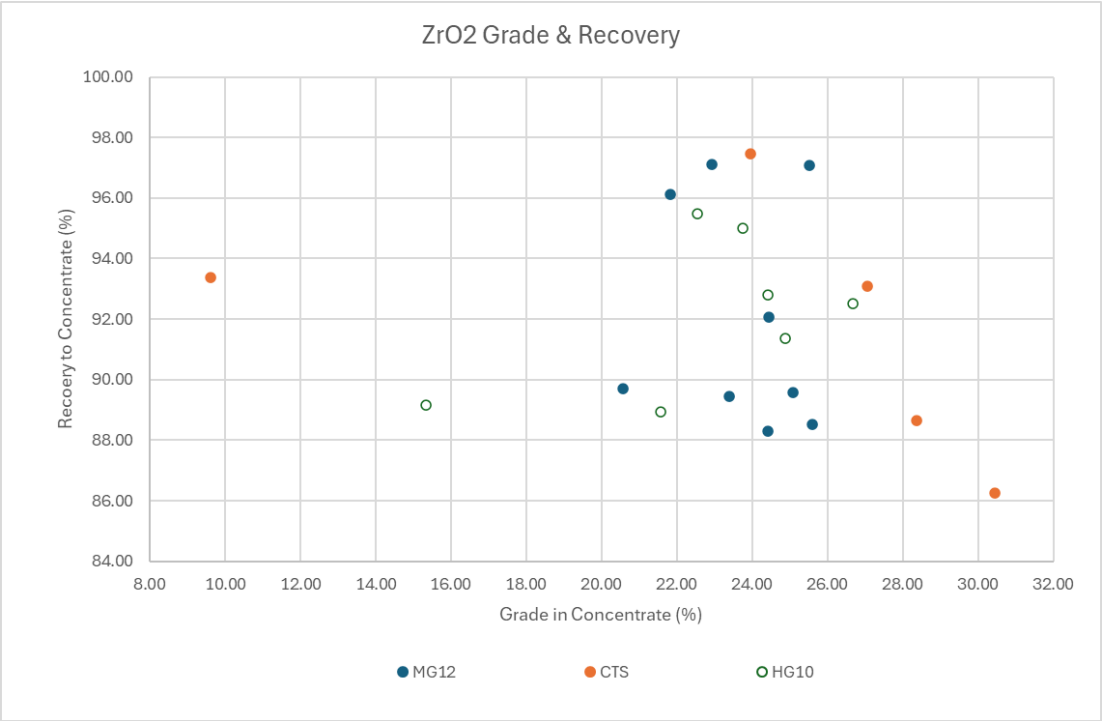

Figure 5.1: The recovery and grade chart for the operating regimes separation of the classifier underflow through the Compact Turbo (CTS), MG12 and HG10 spirals

For each spiral in Figure 5.1, the overall trend shows that the ZrO2 recovery tends to decrease when the grade of ZrO_2 in the concentrate increases. This is in line with Wills and Napier-Munn (2006) who explain the recovery-grade curve which states that the recovery decreases as the grade in the concentrate increases. For the Compact Turbo spiral, the 93.38% recovery at 9.62% ZrO_2 grade seems to be an outlier. However, from 23.95% to 30.45% ZrO_2 in the concentrate, the recovery decrease from 97.45% to 86.26% almost linearly. Figure H2 in Appendix H shows a good relationship between the ZrO_2 concentrate grade and the recovery for the Compact Turbo separation.

For the MG12 spiral, there is no clear relationship between the recovery of the ZrO_2 and its grade to the concentrate. At 22.93% ZrO_2, the recovery was 97.10% while at 23.39% ZrO_2, the recovery was 89.46%. These two grades are very close and should have close recoveries. At 24.43%, the recovery was 92.06% while at 24.42% ZrO_2, the recovery was 88.30%. Another point

showing no correlation is ZrO_2 at 25.41% with recovery of 97.06% and 25.61% ZrO_2 with recovery of 88.51%. Indeed, Figure H1 in Appendix H shows poor relationship between the ZrO_2 grade of the concentrate and the recovery.

For the HG10 spiral, the first two points in Figure 5.1 show flat though decreasing recovery as the ZrO_2 grade increased from 15.35% to 21.56% in the concentrate. The recovery then jumped to 95.47%, eventually decreasing almost linearly to 92.51% while the ZrO_2 grade in the concentrate increased to 26.66% (refer to Figure H3 in Appendix H for the relationship between the ZrO_2 grade in the concentrate and the recovery).

The performance of the Compact Turbo and HG10 spirals is explained by Wills and Napier-Munn (2006) recovery-grade curve as the recovery decreases as the grade in the concentrate increases. This behaviour was also observed by Neethling and Cilliers (2012) in copper froth floatation that as the cumulative recovery increases the cumulative grade decreases. Sivamohan and Forssberg (1985) reported the same relationship between the grade of iron (Fe) and recovery to the concentrate at different solids content in the feed.

5.3 Quality of concentrates with changing operating feed conditions and split

Kari et al. (2006) observed that when the feed rate increased and the concentrate grade increased, the recovery decreased with optimum condition established. Reference can be made to Figures 4.8, 4.9, and 4.18; and Tables 4.4, 4.5 and 4.6 in Chapter 4 as well as Figures 5.2 to 5.4 below.

In Figures 5.2 to 5.4, a split, which is not a response variable, has been indicated on the primary Y-axis for explanation purposes. The ZrO_2 and Al_2O_3 grades are indicated on the secondary Y-axis. To read Figure 5.2 for example: when the feed rate to the MG12 spiral was 3.52 tph at the split 90% to the concentrate the ZrO_2 recovery was 96.11% with the ZrO_2 grade of 21.82%. When the feed rate was high at 4.53 tph the ZrO_2 recovery was 89.57% with

the concentrate grade of 25.08%. The split was set at 80% to achieve this 89.57% recovery.

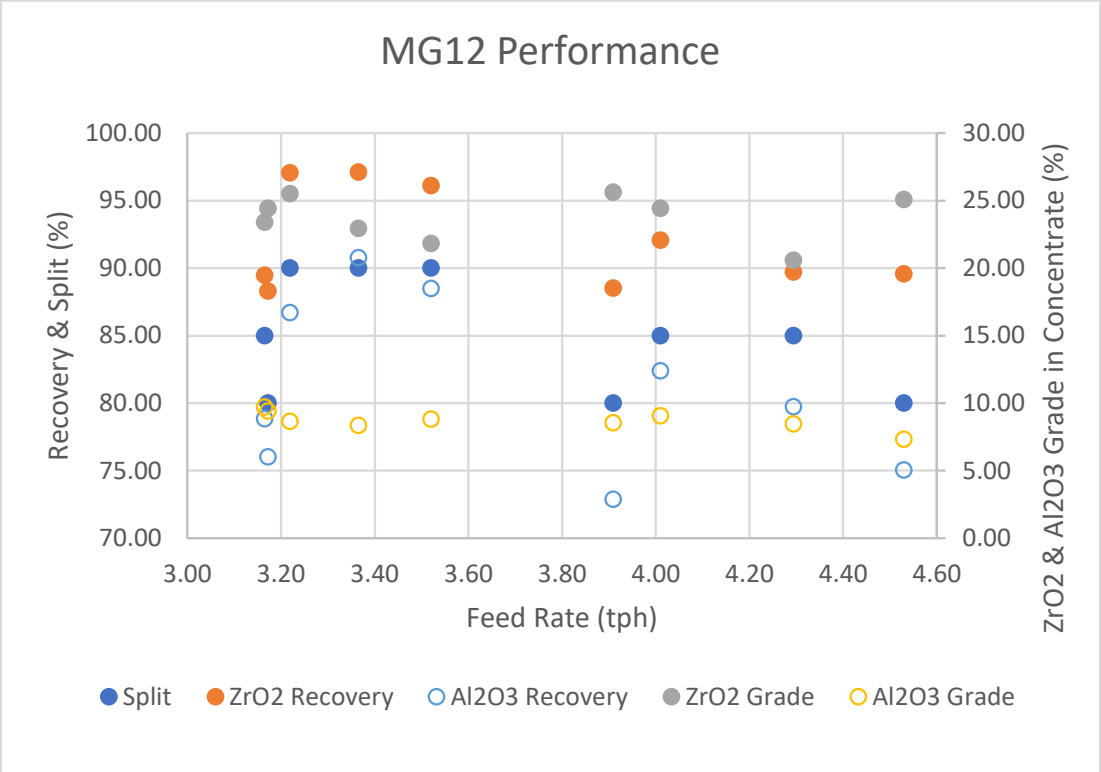

Figure 5.2: The MG12 operating regimes performance as the feed rate increased

When the feed rate increased from 3.17 tph to 4.53 tph the ZrO_2 grade fluctuated between 20.57% and 25.61%. The Al_2O_3 was constant above 8% except at the highest feed rate when it decreased to 7.30%. This is not in line with the observation by Kari et al. (2006). The recoveries of both ZrO_2 and Al_2O_3 however decreased with the increasing feed rate, making this operational pilot scale assessment to be in line with the observation by Kari at al. (2006).

Figure 5.3 below shows the performance of the Compact Turbo spiral as the feed rate increased. The ZrO_2 content in the concentrate initially decreased at then increased from 9.62%. The recovery increased to establish an optimal performance point at 2.75 tph feed rate and 97.45% recovery of the ZrO_2 to the concentrate.

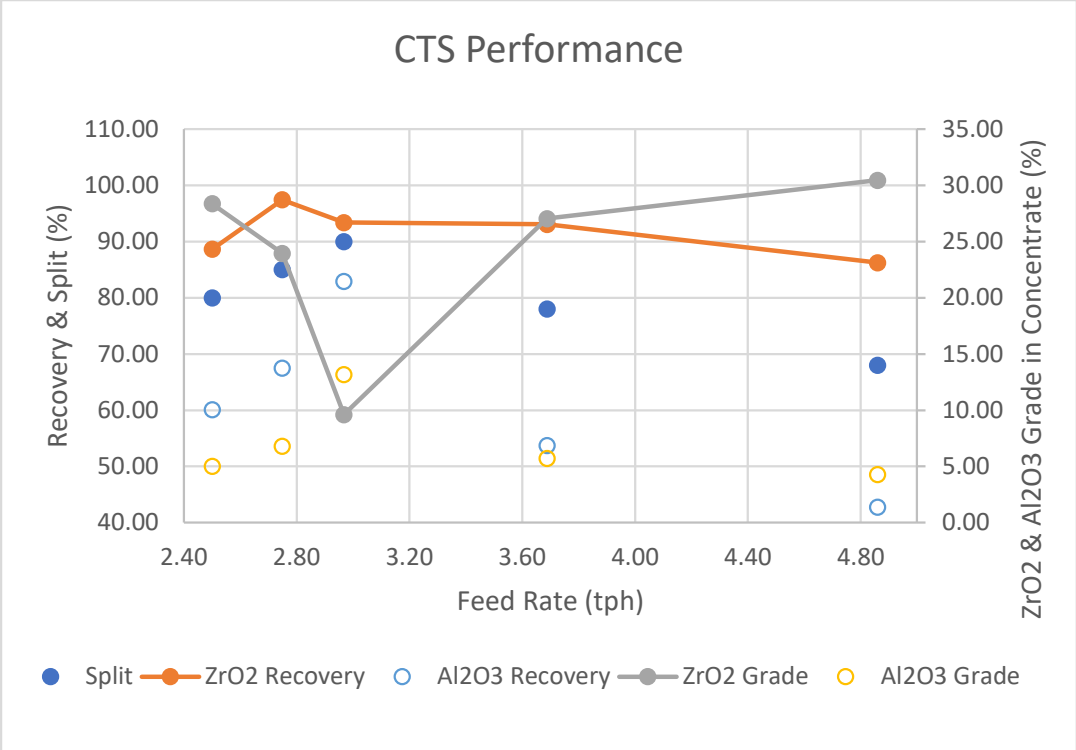

Figure 5.3: Operating regimes performance of the Compact Turbo as feed rate increased

Still in Figure 5.3, the Al_2O_3 grade and recovery increased initially, following the ZrO_2 before they both started to decrease. The performance of the Compact Turbo spiral in this case is much in line with the observation by Kari et al (2006). The ZrO_2 grade in the concentrate remained as high as 30.35% while that of Al_2O_3 remained as low as 4.29% with lowest contaminant reporting to the concentrate at 42.78%.

The performance of the Compact Turbo spiral was in line with the design performance by Mineral Technologies (refer to Figure 5.4 below) as it is expected to yield above 97% recovery of heavy mineral at feed rate of up to 4 tph per column.

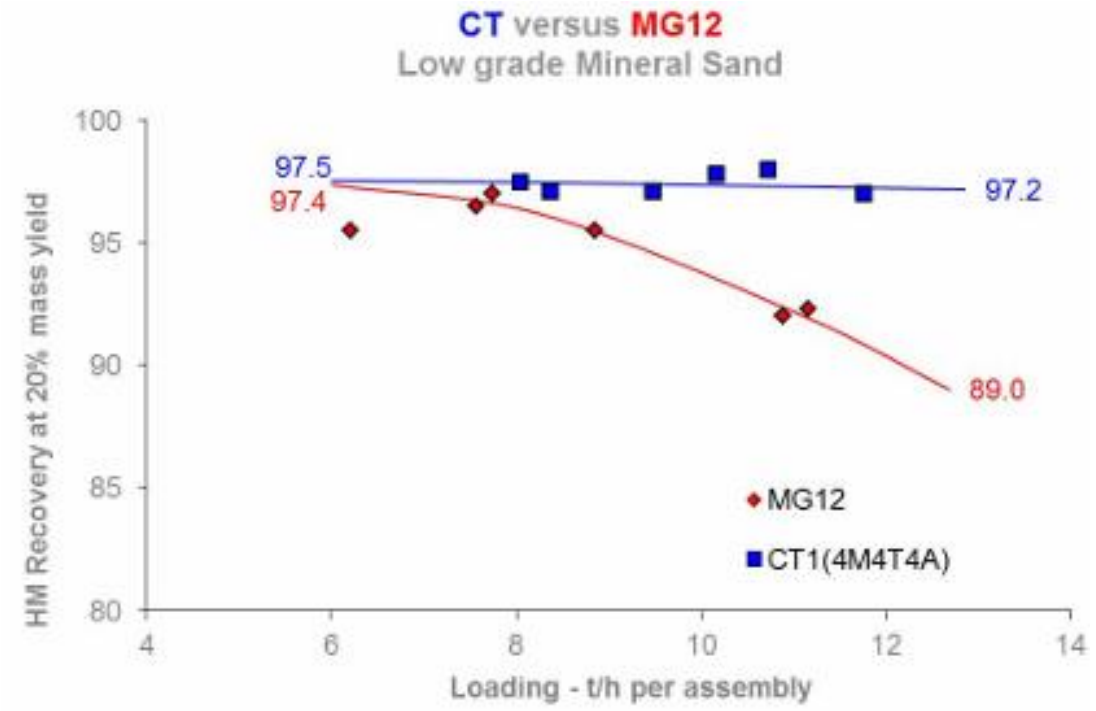

Figure 5.4: Design performance of Compact Turbo and MG12 spirals (Source: Mineral Technologies)

The high split to the concentrate does not favour the quality of the concentrate. Instead, it increased the Al_2O_3 content and decreased the ZrO_2 content when it increased from 68% to 90%.

While treating the classifier CL003 underflow, the HG10 performance shown by Figure 5.5 below does not following the theoretical observations by Kari et al. (2006). As the feed rate increased from 2.64 tph to 3.75 tph, the ZrO_2 grade decreased from 26.66% to 15.35% instead of increasing, while the recovery decreased as per theoretical expectations.

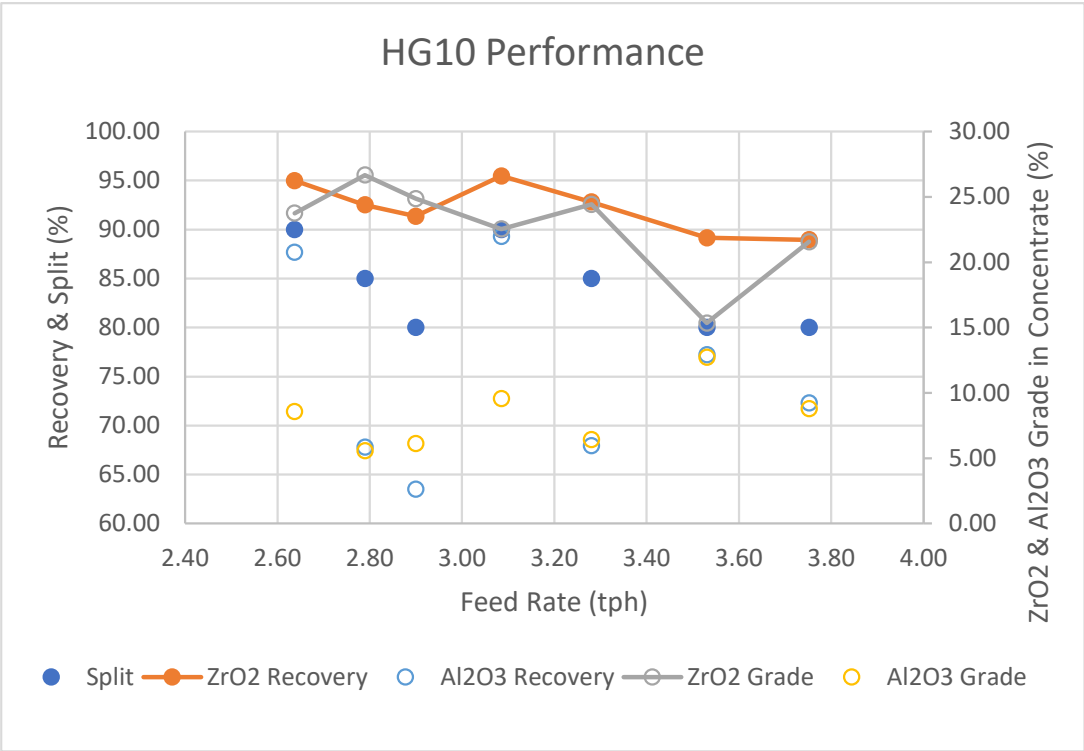

Figure 5.5: The HG10 operating regimes performance as the feed rate increased

As the feed rate increased, the Al_2O_3 in the concentrate increased from 5.57% to 12.71%, with its recovery showing a slight decrease. The HG10 spiral is therefore concentrating the contaminant (Al_2O_3) and rejecting the ZrO_2.

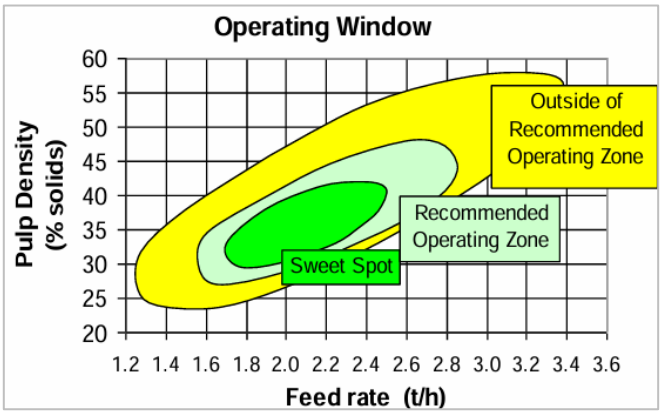

Figure 5.6: The operating window for the HG10 spiral (Source: Mineral Technologies)

The design operating window for the HG10 spiral shows that the spiral operates better below 2.8 tph feed rate. This can explain the good performance in the

first two points in Figure 5.5 where the ZrO_2 increased from 23.8% to 26.7% in the concentrate and the recoveries decreased from 95.0% to 92.5%. The Al_2O_3 content and recovery decreased respectively from 8.6% to 5.6% and from 87.7% to 67.8%. Above the 2.80 tph, the HG10 spiral was operating outside the recommended operating zone with performance that was not in line with Kari et al (2006). The decrease of the ZrO_2 content and increase of Al_2O_3 in the concentrate can be explained by Holland-Batt (1995) that the efficiency of a spiral decreases when the mass pull to the concentrate increases. This can be seen at 90% split to the concentrate.

5.4 Alicoco and HG10 spirals performance at low density feed

Applying the observations by Kari et al (2006), the performance of the Alicoco spiral was compared to that of the HG10 spiral at low solids content in the feed (refer to Tables 4.4 to 4.6 in the previous chapter). The following was noted: Figure 5.7 below shows that when the feed rate increased, the ZrO_2 grade in the concentrate increased marginally from 11.1% at 1.55 tph to 11.3% and 2.87 tph and then it decreased to 11.1% at 3.39 tph. The recovery followed the same trend as the grade, increasing from 63.2% to 74.6% and then decreasing to 67.3%. This is not in line with Kari et al. (2006).

It is however noted that the Al_2O_3 content in the contrate was almost at the same level as the ZrO_2 in Figure 5.7. It exceeded the ZrO_2 at optimum feed rate of 2.87 tph, reaching 11.6% compared to 11.3% ZrO_2. It is also observed that the recovery of the Al_2O_3 to the concentrates was 96.2% compared to 74.6% ZrO_2 at 2.87 tph.

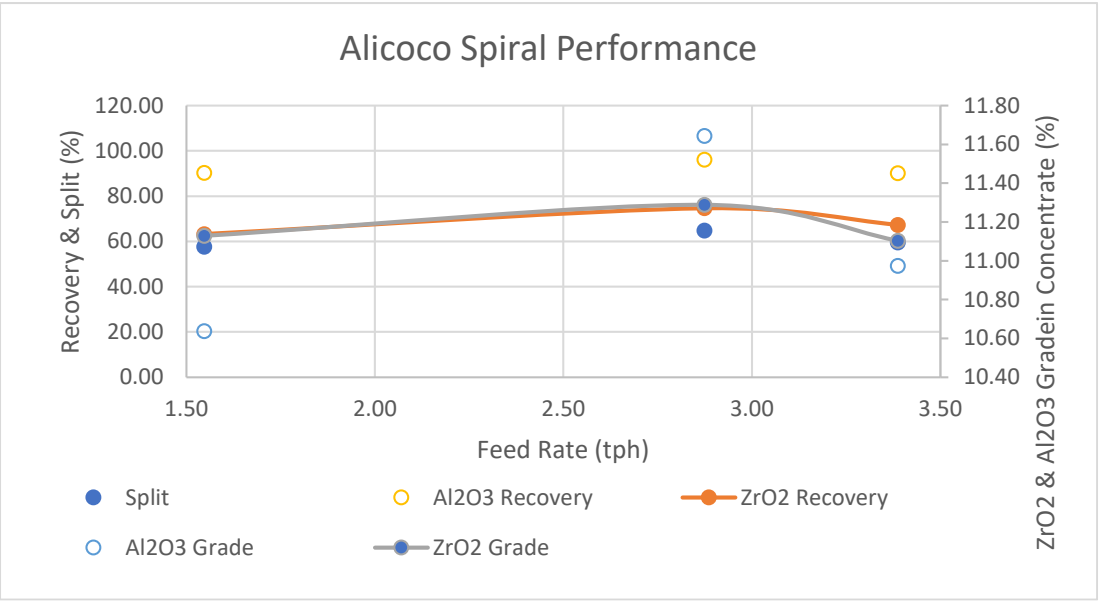

Figure 5.7: Performance of the Alicoco spiral from historical data

The performance of the Alicoco spiral was compared to that of the HG10 (refer to Figure 5.8 below). The feed rate to the HG10 spiral was within the recommended range as per its operating window (refer to Figure 5.6 above). However, it is noted that when the feed rate increased, which coincided with an increase in the split to the concentrate, the concentrate quality of the ZrO_2 decreased from 13.6% to 11.4% as the recovery increased from 86.1% to 91.3%. This is not the same observation as in Figure 5.5 when there was initially as increase in the grade and a decrease in the recovery. It can either indicate the complexity of separating the classifier CL003 underflow stream or the decrease inefficiency of the HG10 spiral at low feed density.

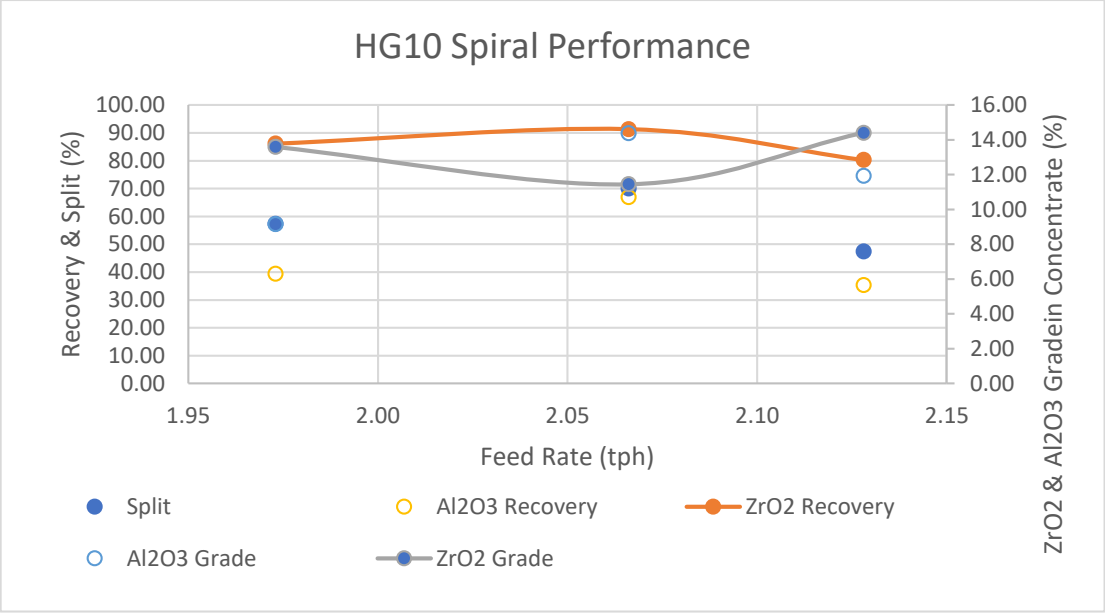

Figure 5.8: Performance of the HG10 spiral from historical data

The Al_2O_3 content of the concentrate is at the same level as that of the ZrO_2, exceeding the ZrO_2 (11.4%) at 14.4% at the feed rate of 2.07 tph. The ZrO_2 recovery to the concentrate was higher than that of the Al_2O_3 (91.3% versus 66.9% at 2.07 tph feed rate).

5.5 Understanding the effects of particle size

Figure 4.12 in Chapter 4 shows the particle size distribution of the concentrates from the Compact Turbo spiral lying to the left of the chart. The Compact Turbo spiral concentrates had the lowest d_{50} of all the spirals, at 116.18 μm maximum compared to 117 μm minimum by MG12 and 120 μm minimum by HG10. The feed to the spirals had a d_{50} of 122 μm. Atasoy and Spottiswood (1995) explain the HG10 similarity of the d_{50} of the concentrate and that of the feed because of even distribution of particles across the spiral surface. This also applies to the MG12 at 35% and 40% solids in the feed. Judging by the low and closer d_{50} values of the concentrates of the Compact Turbo spiral (115.53 μm) and

the MG12 spirals (117 μm) at 30% solids in the feed the finer and heavier particles reported towards the concentrate of the spirals.

This indicates that separation did occur under these conditions especially for the MG12 spiral at 30% solids in the feed while for the Compact Turbo the separation occurred at all solids contents in the feed.

5.6 QEMSCAN for the concentrates from the Compact Turbo spiral

5.6.1 Mineralogy analysis

Table 4.14 in the previous chapter shows that the zircon content in the feed to the Compact Turbo spiral was 32.3% as analysed by QEMSCAN. It marginally increased to 32.4% when the solids content feed was 30% with the concentrate split at 80%. When the solids content in the feed increased to 35% and the split to 78%, the zircon increased to 35.7%. At 40% solids content in the feed and 68% split to the concentrate, the zircon content was 38.8%.

Figure 5.9 below show the QEMSCAN image of (a) the spiral feed, (b) 30% solids concentrate, (c) 35% solids concentrate, and (d) 40% solids concentrate. It explains how the spiral concentrated the zircon. Edahbi et al. (2018) state that the QEMSCAN generates high resolution mineral maps and images and enables quantitative chemical analysis.

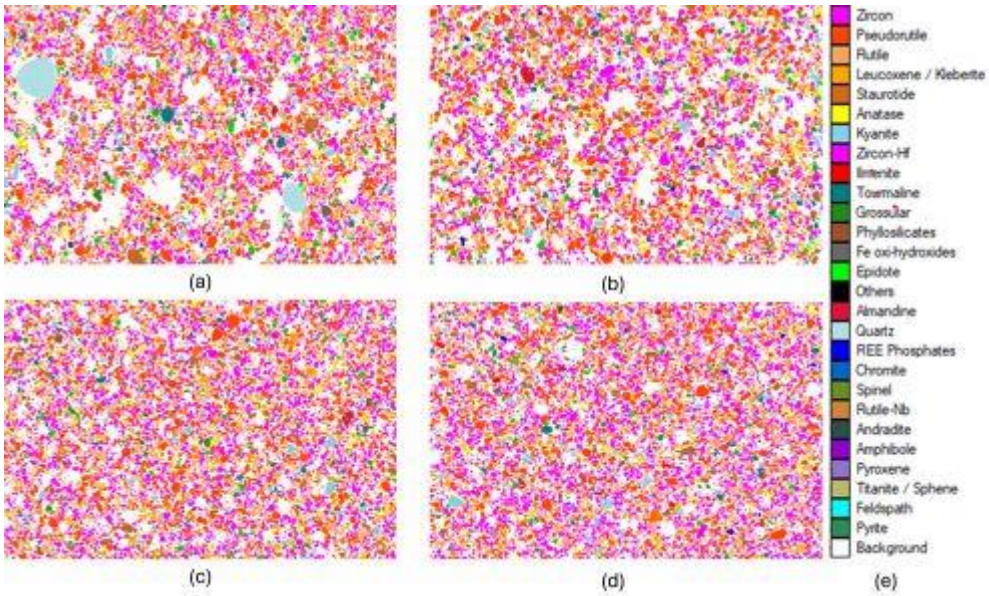

Figure 5.9: QEMSCAN images of (a) tertiary classifier underflow, (b) 30% solid concentrate, (c) 35% solid concentrate, (d) 40% solid concentrate and (e) minerals identification

The chemical analysis in Table 5.1 below shows the aluminium element (Al) decreasing from 4.2% in the spiral feed until it reached 3.2% in the 40% concentrate, a 25% decrease. The zirconium element (Zr) increased from 15.8% until it reached 19.2% in the 40% concentrate, which was 22% increase. These are in line with the results in Tables 4.2 – 4.4 of Chapter 4 analysed by the GCO Laboratory as well as the findings reported by Edahbi et al. (2018).

5.6.2 Analysis of particle size distribution results

Big particles such as quartz in Figure 5.9(a) do not appear in the concentrates. Quantitative data in Table 4.14 shows a quartz content of 2.4% in Figure 5.9(a), 0.4% in Figure 5.9(b), 0.3% in Figure 5.9(c) and 0.3% in Figure 5.9(d). The quartz, which is rich in silica (SiO_2) was rejected by the Compact Turbo spiral, decreasing by 89.9% from the feed to the 40% solids concentrate. This is in line with the particle size distribution in Table 4.11, showing a decrease in d_{80}

and d_{50}, from respectively 186 μm and 132 μm to 169 μm and 125 μm in the feed and the 40% solids.

Table 5.1: QEMSCAN elementary results

	Feed	30% split 80%			35% split 78%			40% split 68%		
Element	**Mass %**	**Mass %**	**Absolute Difference %**	**Relative Difference %**	**Mass %**	**Absolute Difference %**	**Relative Difference %**	**Mass %**	**Absolute Difference %**	**Relative Difference %**
Al	4.23	3.57	3.57	-16%	3.47	-0.76	-18%	3.18	-1.05	-25%
B	0.06	0.03	0.03	-50%	0.03	-0.03	-50%	0.03	-0.03	-50%
Ca	0.49	0.34	0.34	-31%	0.37	-0.12	-24%	0.32	-0.17	-35%
Ce	0.12	0.14	0.14	17%	0.13	0.01	8%	0.15	0.03	25%
Cr	0.17	0.20	0.2	18%	0.18	0.01	6%	0.19	0.02	12%
F	0.04	0.10	0.1	150%	0.09	0.05	125%	0.08	0.04	100%
Fe	7.96	8.81	8.81	11%	8.18	0.22	3%	7.54	-0.42	-5%
H	0.04	0.04	0.04	0%	0.03	-0.01	-25%	0.03	-0.01	-25%
Hf	0.73	0.76	0.76	4%	0.83	0.1	14%	0.91	0.18	25%
K	0.01	0.01	0.01	0%	0.01	0	0%	0.01	0	0%
La	0.01	0.02	0.02	100%	0.01	0	0%	0.01	0	0%
Mg	0.21	0.17	0.17	-19%	0.15	-0.06	-29%	0.15	-0.06	-29%
Mn	0.11	0.12	0.12	9%	0.11	0	0%	0.11	0	0%
Na	0.04	0.02	0.02	-50%	0.02	-0.02	-50%	0.02	-0.02	-50%
Nb	0.06	0.06	0.06	0%	0.06	0	0%	0.05	-0.01	-17%
Nd	0.01	0.01	0.01	0%	0.01	0	0%	0.01	0	0%
O	27.45	25.10	25.1	-9%	25.96	-1.49	-5%	26.79	-0.66	-2%
P	0.04	0.05	0.05	25%	0.05	0.01	25%	0.05	0.01	25%
Si	8.91	7.50	7.5	-16%	8.03	-0.88	-10%	8.34	-0.57	-6%
Ti	21.41	22.95	22.95	7%	21.65	0.24	1%	20.90	-0.51	-2%
Zr	15.77	16.07	16.07	2%	17.72	1.95	12%	19.23	3.46	22%

According to Kursun et al. (2016), particle size analysis is a key requirement in managing a beneficiation process. Particle size determines the behaviour of material. In this case, the behaviour of the bigger quartz particles in Figure 5.9(a) are rejected to the middlings and tails as they do not make their way to the concentrate. This is clear with staurolite as QEMSCAN shows a significant difference between the feed and the concentrate as Figure 5.10 below shows.

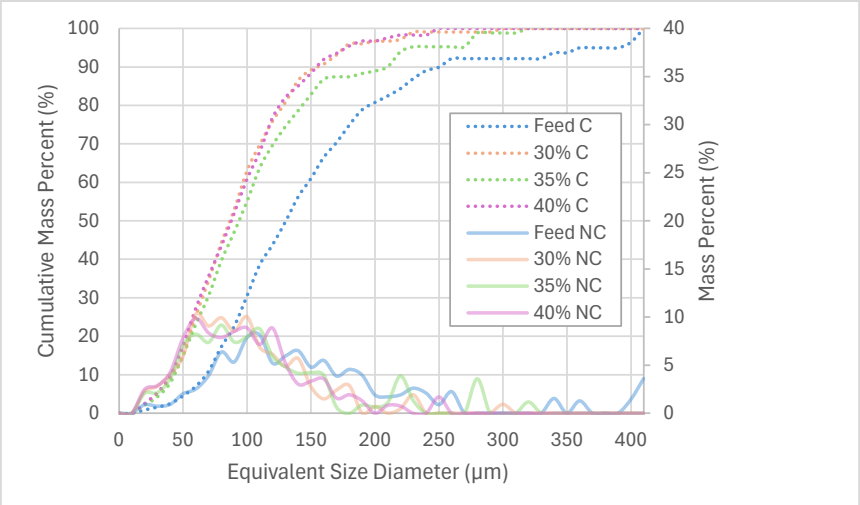

Figure 5.10: QEMSCAN particle size analysis of staurolite for the classifier underflow, 30% solids concentrate, 35% concentrate, and the 40% solids concentrate (C is for cumulative, NC is for non-cumulative)

Figure 5.10 shows a good association between the particle size of the feed with a d_{50} and d_{80} of 130 mm and 195 mm respectively. As the zircon concentration increases in the concentrates, reaching the highest content in the 40% solids concentrate, the d_{50} and d_{80} values of the staurolites particles reached 86 mm and 124 mm respective. The d_{50} value decreased by 34% and the d_{80} value decreased by 35% in line with Kursun et al. (2016).

5.6.3 Analysis of particle density results

A difference in the densities of minerals particles is exploited to bring about gravity concentrations. Through the gravity separation medium particles move apart from each other due to the density differences (Gülsoy and Gülcan,

2019). Figure 4.18 shows the difference in densities of the zircon and aluminium bearing particles.

The zircon particles peaked at 4.70 in the feed and the majority aluminium bearing particles peaked at 3.68 in the feed. Table 4.12 shows that the zircon particles have a density range of 4.20 – 4.75 g/ml.

The ratios of zircon particle (heavy component in Table 4.12) and the aluminium bearing particle (light component in Table 4.13) in the classifier underflow based on Figure 4.18 and Gill (1991) are in Table 5.2 below.

The multi-peaks of the aluminium bearing particles indicate an inconsistent mineral property that can impose a challenge to a separation equipment targeting a density class. In Table 5.2, Peak 1 accounts for 15% of the aluminium-bearing particles. With a separation ratio of 1.68, above 1.50 ratio by Gill (1991), these peaks separate well and are expected to be rejected to the middlings and tailings streams.

Table 5.2: The Gill (1991) separation ratio of the zircon and aluminium-bearing particles in the classifier underflow

Peak	Heavy Component (Zircon)	Light Component (Aluminium)	Fluid (Water)	Ratio
1	4.70	3.20	1.00	1.68
2	4.70	3.68	1.00	1.38
3	4.70	4.00	1.00	1.23
4	4.70	4.10	1.00	1.19

The separation ratio in Peak 2 was 1.38 which is lower than the first peak, falling further in Peak 3 at 1.23 and Peak 4 at 1.19, indicating a decrease in separation as the aluminium-bearing particles density increased. Although the range is clear between the two types of particles, as they get closer, the ratio falls below the theoretical one and the separation between the zircon and the aluminium-bearing particles deteriorates.

The d_{50} and d_{80} values of all the particles are above 75 μm and below 212 μm in Table 4.11. In the classifier underflow sample, the d_{50} value for the zircon particles was 105 μm, lower than those of staurolite at 130 μm and kyanite at 140 μm. The d_{80} values followed the same trend at 137 μm for the zircon particles, 195 μm for staurolite and 193 μm for kyanite particles. This indicates a possible but not so easy separation according to Gill (1991).

At 30% solids in the feed, the d_{50} value for the zircon particles was 105 μm; it was 85 μm for staurolite and 135 μm for kyanite. The same trend is seen at 35% and 40% solids except in the classifier underflow sample in Table 4.11 with both d_{50} and d_{80} of staurolite and kyanite particles straddling those of the zircon particles.

The d_{50} and d_{80} of staurolite particles reduced from 130 μm and 195 μm respectively in the classifier underflow to be below of those of the zircon particles in the 30%, 35% and 40% solids samples.

5.7 Design features of the Compact Turbo spiral

Figure 3.6 shows all the spirals that were tested in the pilot plant. The Compact Turbo spiral in Figure 3.6(a) and Figure 2.28(a) is designed differently compared to the Alicoco (Figure 3.6(a) and Figure 2.29, the MG12 and the HG10 spirals in Figure 3.6(b). Its distinctive modular features is the main physical difference, in addition to the performance difference, when compared to the other spirals.

5.8 Zircon balance and recovery at Wet Circuit without and with Compact Turbo spiral

A balance that was done in the Wet Circuit is presented in Table 5.3 below. The underflow for Classifier 4 is Con 1, for Classifier 2 is Con 2 and for

Classifier 3 in Con 3. The Compact Turbo spiral concentrates are at the bottom of Table 5.2.

Using Equation (2.2) in Chapter 2, substituting the TPH and ZrO_2 % or Al_2O_3 % as in Table 5.3 below results to the recoveries in Tables 5.4 and 5.5 below. In Table 5.3, the feed F to the Wet Circuit is 40.93 tph with a feed grade f of ZrO_2 of 18.03%. The 30% concentrate at 85% split flow rate C was 2.65 tph with a concentrate grade c of 23.39%.

If the Compact Turbo spiral had been fitted to treat the Classifier 3 underflow, the ZrO_2 recovery to Con 3 was going to be a 2.65 tph multiplied by 23.39% divided by 40.93 tph multiplied by 18.03%. The recoveries of ZrO_2 to Con 3 in Table 5.4 are 8.39%, 10.50% and 13.69% for 30% solids and 85% split concentrate, 35% solids and 78% split concentrate and 40% solids and 68% split concentrate respectively for the Compact Turbo spiral.

Table 5.3: Mass balance around the Wet Circuit

		TPH	ZrO_2 %	Al_2O_3 %
Rougher Spirals	**Feed**	40.93	18.03	4.24
	Cons	19.27	33.94	3.72
	Mids	4.40	10.05	8.40
	Tails	17.26	2.30	3.75
Classifier 4	**Feed**	10.81	50.98	1.21
	Underflow	10.12	53.96	0.86
	Overflow	0.69	7.33	6.28
Classifier 2	**Feed**	4.21	32.70	3.39
	Underflow	1.39	46.67	1.22
	Overflow	2.82	25.83	4.46
Classifier 3	**Feed**	4.94	11.42	11.44
	Underflow	4.82	11.69	11.69
	Overflow	0.12	0.59	1.06
Compact Turbo spiral concentrates				
30% 85%	Concentrate	2.65	23.39	9.69
35% 78%	Concentrate	2.87	27.05	5.73
40% 68%	Concentrate	3.32	30.45	4.29

The combining the Con 1, Con 2 and modelled Con 3 recoveries provide what the total Wet Circuit recovery could be if the classifier 3 underflow was treated with a Compact Turbo spiral.

Table 5.4: Recovery of ZrO_2 at the Wet Circuit without and with the Compact Turbo spiral

	Without	30% 85%	35% 78%	40% 68%
Con 1	74.00%	74.00%	74.00%	74.00%
Con 2	8.78%	8.78%	8.78%	8.78%
Con 3	7.63%	8.39%	10.50%	13.69%
TOTAL	90.40%	91.17%	93.27%	96.46%

Table 5.4 shows that the total ZrO_2 recovery from the circuit balance was 90.40%. If the classifier 3 underflow passed through the Compact Turbo spiral,

upgrading the zircon, though decreasing the underflow from 4.82 tph to the flow rates of the Compact Turbo concentrates in Table 5.3, the overall ZrO_2 recovery would increase, reaching 96.46% in Table 5.4. The total ZrO_2 recovery is obtained by adding the Con 1, Con 2 and Con 3 recoveries without the Compact Turbo spirals concentrates (add 74.00%, 8.78% and 7.63% a total of 90.40%). It is also obtained by adding the recoveries of Con 1, Con 2 and of the Compact Turbo spirals concentrates (add 74.00%, 8.78% and 13.69% to a total of 96.46%). The ZrO_2 recovery is expected to increase from 90.40% to 91.17%, 93.27% and ultimately to 96.46%.

Table 5.5 below shows that the Al_2O_3 recovery in the Wet Circuit is expected to decrease from 38.47%, which is the current plant performance without the Compact Turbo spiral, to 20.79%, 15.45% or 14.20% depending on the concentrate of the Compact Turbo spiral.

Table 5.5: Recovery of Al_2O_3 at the Wet Circuit without and with the Compact Turbo spiral

	Without	**30% 85%**	**35% 78%**	**40% 68%**
Con 1	5.02%	5.02%	5.02%	5.02%
Con 2	0.98%	0.98%	0.98%	0.98%
Con 3	32.48%	14.80%	9.46%	8.20%
TOTAL	38.47%	20.79%	15.45%	14.20%

5.9 Concluding remarks

The results of the research study of Compact Turbo, MG12, HGO and Alicoco spiral separators have been presented. The study was conducted by varying the content of solids in the feed from 30% to 35% and to 40% by weight; and by varying the split or yield to the concentrate from 80% to 85% and 90%.

For the Compact Turbo spiral the ZrO_2 recovery increased as the yield to the concentrate increased. When the grade of the ZrO_2 in the concentrate increased, the ZrO_2 recovery to the concentrate decreased as per literature.

This trend was evident in the Compact Turbo spiral separator. The ZrO_2 grade and recovery relationship was not that clear with the MG12 and the HG10 spiral separators. For the MG12 spiral, there was no clear relationship between the recovery and the concentrate grade. For the HG10 spiral, there was a combination of no relationship and then a decreasing recovery with an increasing ZrO_2 grade in the concentrate.

The relationship between the operational conditions feed rate and the recovery of ZrO_2 by the Compact Turbo spiral shows the trend of the ZrO_2 recovery initially increasing, reaching an optimum point and then decreasing as the performance feed rate increased. The recovery also followed the split at is increased. The ZrO_2 grade decreased and as the split increased. The Al_2O_3 was the opposite of the ZrO_2 grade. This further defined the relationship between the two contents that they displace each other in the concentrate, with Al_2O_3 acting like a true contaminant as it kept increasing while the ZrO_2 decreased with an increasing split. The Al_2O_3 recovery decreased as the feed rate trend increased.

An increasing operating condition feed rate to the MG12 spiral resulted to a decreasing ZrO_2 recovery and a fairly constant Al_2O_3 grade and a decreasing Al_2O_3 recovery to the concentrate. The ZrO_2 grade fluctuated with an increasing feed rate.

When the operational feed rate to the HG10 spiral increased the recovery, and the ZrO_2 grade in the concentrate decreased continuously. The Al_2O_3 grade and recovery to the concentrate showed an overall increasing trend. While the HG10 spiral had indicated good grades of Al_2O_3 closer to the grades produced by the Compact Turbo spiral in some tests, the efficiency in separating the sample from the Classifier 3 underflow was low.

The Alicoco spiral could not handle any of the study operating parameters due to beaching. A test conducted at lower pulp densities in the feed showed the recoveries of ZrO_2 and Al_2O_3, their grades and the split behaved the same way.

There was an increase and then a decrease in all the performance indicators with the Al_2O_3 recovery to the concentrate consistently far higher than that of the ZrO_2. As the Alicoco spiral was compared to the HG10 spiral, the HG10 spiral demonstrated a good performance with the ZrO_2 recovery to the concentrate being higher than that of the Al_2O_3.

Mineralogy results by QEMSCAN showed the zircon content increasing from the feed to the Compact Turbo spiral concentrates. This was in line with the chemical analysis. Chemical analysis at element level showed a decreasing trend for aluminium (Al) as the zircon content increased in the concentrate. Similar to the laboratory particle size analysis, QEMSCAN also showed the particle size of the feed to the spiral being courser than the concentrates. The high-resolution particle images from the QEMSCAN show large quartz particles being present in the feed but could not be detected in the concentrates. This is a clear indication of particle size playing a role in Compact Turbo spiral separation of the sample from the Classifier 3 underflow.

Recovery simulation of the Wet Circuit with a Compact Turbo spiral shows the overall increase of zircon recovery. Without the Compact Turbo effects the circuit recovery was 90.40%. With the Compact Turbo the recovery can be expected to increase to above 96% overall.

The Compact Turbo spiral is designed differently compared to the Alicoco, the MG12 and the HG10 spirals which share similar physical features.

Chapter 6 Conclusion and recommendations

6.1 Introduction

The Wet Circuit at the Mineral Separation Plant of the Grande Côte Opérations (GCO) has never been able to achieve the design recovery of zircon since the operation began. Circuit's adjustments have either resulted to contamination of the zircon rich concentrates or to the loss of zircon to tails. The main contaminants are the silicates such as kyanite, staurolite and quartz. The currently installed separation equipment such as the spiral, wet shaking tables and up-flow classifier separators is struggling to yield required zircon recoveries in good qualities. Therefore, the research study was commissioned to investigate the performance and ability of the two new spiral separators in the market, to separate ZrO_2 from Al_2O_3 at the Wet Circuit. The tested new spirals are Compact Turbo spiral by Mineral Technologies (Pty) Ltd (Australia) and Type H spiral by Alicoco Mineral Technology Co. Ltd (China).

One main objective of the research was to test the abilities of the two spirals in rejecting Al_2O_3 while recovering ZrO_2 from a stream making up the tertiary concentrate in the Wet Circuit. The other main objective was to compare the performance of the two new spirals in the market to the MG12 and the HG10 spirals which are already installed in the Wet Circuit. The implication of the study is that GCO will be able to institute improvement and innovation projects if the two new spirals are able to separate the zircon from the silicates at good recoveries and concentrates grades.

Two research questions were as follows:

- Could the Compact Turbo and Alicoco spirals improve the quality of the stream making up the tertiary concentrate through the rejection of aluminium silicates?
- Why it is difficult to separate zircon and aluminium particles?

To answer the questions a sample was collected from a Classifier 3 underflow stream making up the tertiary concentrate. The stream was rich in both ZrO_2 and Al_2O_3. A pilot plant or spiral rig fitted with the Compact Turbo, Alicoco, MG12 and HG10 spirals was then used to recreate a slurry of 30%, 35% and 40% solids by weight in the feed. Splitter positions were used to increase the yield to the concentrate from 80%, to 85% and to 90%. Samples were taken for chemical, mineralogy, QEMSCAN, particle size and particle density analyses. Operation conditions feed rate performance was evaluated.

In this chapter, conclusions and recommendations are provided from the research study.

6.2 Summary of the research findings

The Compact Turbo spiral achieved its best quality of the concentrate when the content of the solids in the feed was 40% by weight. The ZrO_2 in the concentrate was 30.5% and the Al_2O_3 content was 4.3% with the split to the concentrate at 68.0%. The flow rates were 3.32 tph for the concentrate and 4.86 tph for the operational feed rate. The recovery of ZrO_2 was 86.3% at the Al2O3 recovery to the concentrate of 42.8%.

The highest recovery which was achieved by the Compact Turbo spiral was 97.5% at 30% solids in the feed. The ZrO_2 was 24.0% and the Al_2O_3 was 6.8% in the concentrate at 85% split. The flow rates for the concentrate and the operational conditions feed rate were 1.99 tph and 2.75 tph respectively. The Al_2O_3 recovery under these conditions was 67.5%.

The Compact Turbo spiral was able to separate the ZrO_2 and Al_2O_3 along the particle size, with the bigger particles of staurolite in the feed not appearing in the concentrate as they were not detected by the QEMSCAN.

The specific densities of the minerals remain close to the theoretical values in both the feed and the concentrates. Multi-peals of densities of the aluminium-

bearing particles were discovered. Low separation ratios for particles with the specific density of 4.0 showed that it is difficult to separate these from the zircon particles. The quartz was rejected almost completely by the Compact Turbo spiral, with traces remaining in the concentrate in all the splits.

The best quality for the MG12 spiral concentrate was achieved at 30% solids in the feed. The ZrO_2 in the concentrate was 25.5% and the Al_2O_3 was 8.7% with the split to the concentrate at 90%. This was achieved at 2.98 tph concentrate and 3.22 tph operational feed rate. The highest ZrO_2 recovery of 97.1% was achieved together with this best concentrate. The Al_2O_3 recovery was 86.70%. The particle size effects were seen at low solids concentration in the feed as there was some selectivity to a certain extent. However, as the feed pulp density increased, the concentrate became coarser towards the feed particle size distribution.

For the HG 10 spiral, the best concentrate was achieved at 30% solids in the feed. The ZrO_2 in the concentrate was 26.7% and the Al_2O_3 was 5.6% with the split to the concentrate at 85.2%. The concentrate was at 2.38 tph concentrate, the feed rate at 2.79 tph and at the ZrO_2 recovery of 92.5%. The Al_2O_3 recovery was 67.81%.

The HG10 spiral achieved the best ZrO_2 recovery of 95.0% at 30% solids in the feed. The ZrO_2 was 23.8% and the Al_2O_3 was 8.6% in the concentrate at 90% split. The flow rates for the concentrate and the feed rate were 2.41 tph and 2.64 tph respectively. The Al_2O_3 recovery was 87.7%. The particle size distribution does not show any sense of separation between the feed and the concentrates as its d_{50} remained constant around 121 mm throughout.

The Compact Turbo spiral produced superior quality of the concentrate at high capacity compared to all other concentrates produced. Although the yield was low at 40% solids, the quality of the concentrate, the ZrO_2 recovery and the Al_2O_3 rejection made the performance settings favourable with 3.32 tph concentrate. The d_{50} clearly showed that the particle size distribution played a

critical role in achieving the rejection of the silicates by the Compact Turbo spiral.

The Alicoco Type H spiral was not able to handle the operational conditions that were set for the test work due to beaching under all intended settings. The test results at low pulp densities showed that the Alicoco spiral concentrated the Al_2O_3 up to 90% to the concentrate and the ZrO_2 recovery was very low or below 70% when the spiral was tested between 14% (1.13 g/ cm^3 pulp density) and 23% (1.20 g/cm^3 pulp density) solids in the feed. The spiral rejected the zircon to the middlings and the tails. As the majority of the zircon was between the concentrate and the middlings, the Alicoco spiral demonstrated poor separation of zircon and the silicates.

The TiO_2 recovery and SiO_2 rejection were high for the Alicoco spiral but not better than those of the Compact Turbo, the MG12 and the HG10 spirals.

The operating performance trends of the spirals as indicated by the feed rate relationship to the recovery and the grade of the concentrate shows the performance was in line with the literature.

To answer the first research question as to whether the Compact Turbo and the Alicoco spirals can improve the quality of a stream that makes up Con 3 at the Wet Circuit at GCO by rejecting aluminium silicates and retaining zircon:

Compact Turbo spiral: Yes, this spiral can improve the quality of the Con 3 as it has demonstrated that it is able to produce the cleanest concentrate at 3.32 tph which is 68.3% of the feed at the lowest contaminant that could be achieved.

Alicoco spiral: No, this spiral was not able to handle the feed with the solids content of 30% and more. The performance data was limited as a result due to the spiral not being able to handle the targeted operational conditions. Even at low feed pulp density the spiral failed to produce a clean concentrate, instead recovering more silicates than it recovered the zircon.

The second research question was why it is currently difficult to separate the zircon and aluminium particles in the tertiary concentrate.

Currently, GCO is making use of mostly the HG10 and the MG12 spirals together with the MG6 spiral. This research has shown that in terms of particle size there is no separation in the HG10; and there is a little bit of separation in the MG12 spiral at low feed pulp density. And the QEMSCAN agrees with the particle size analysis that the only separation will occur through sizing which is being achieved by the Compact Turbo spiral. For this particular stream, the currently installed spirals are not able to reject the silicates as a result. The Compact Turbo spiral, on the other hand, improved the zircon content by up to 20% from the feed to the concentrate. There is also a decrease of up to 36% of staurolite and 31% of kyanite, with the quartz reduced by up to 90%. There is consistency in the XRF results and the elementary results by QEMSCAN that showed the reduction in aluminium and the increase in zircon occurred at element level as up to 25% alumina (Al) decreased and 22% zirconium (Zr) increased from the feed to the 40% solids concentrate.

Staurolite is one contaminant that shows the most reduction in particle size between the feed and the concentrates with a 70 μm reduction between the classifier underflow and the 40% solids concentrate. The d_{50} value showed a 45 μm reduction between the classifier underflow and the 30% solid concentrate.

The difference in density between the zircon particles and the particles that are bearing aluminium was evident. The classifier underflow had a mixture of density peaks or clusters. The maximum density for the aluminium bearing particles was 4.10 g/cm^3 while the minimum density for the zircon particles is 4.20 g/cm^3. There was no overlapping in particle density between the zircon particles and those that carry aluminium. Low separation ratios between zircon particles and the aluminium-bearing particles with 4.0 specific gravity peaks indicate difficulty in separating such particles.

By installing the Compact Turbo spiral under current conditions at CGO, according to the last Wet Circuit balance, the overall recovery of ZrO_2 in all the three concentrates combined can improve from 90.4% to the range of 91.2% to 96.5%. The Al_2O_3 recovery is can also improve by decreasing from 38.5% to the range of 14.2% to 20.8%.

6.3 Recommendations for future work

The consistency of high-quality concentrate with high zircon and low silicates creates a need to explore the benefit that can come with the Compact Turbo spiral. It is recommended to install and test the Compact Turbo spiral online where adjustments can be made to obtain more results under various operational conditions.

The operational conditions of the MG12 spiral can be visited to ensure that the feed pulp density is low enough not to cause a bottleneck but to reject the silicates.

The duties of the HG10 spirals need to be reviewed so that they are put in areas where they are effective, not to handle streams with elevated contaminants.

To improve the verifiability of the results samples at 30%, 35% and 40% solids contents could be taken in buckets of known volumes and weights, water decanted, solids dried and weighed, solids specific gravity determined, and pulp densities back calculated to confirm the pulp densities.

Further testing to include pulp density isolation, extensive feed flow rate and splitter position investigation, and statistical robustness in the analyses of results. Slurry solids concentration to be verified independently for a robust mass-balance method.

The effects of spiral design on the separation should be investigated to establish physical spiral features that resulted to the observed differences in

spirals performances. Feed-grade variability, scale-up risk, and design of experiment approach to be considered in future test work.

The process modelling and fluid dynamics studies can be conducted to understand spiral separation.

All products from the spirals being compared to be analysed by QEMSCAN to explain the mechanisms behind each technology.

References

Abduriyim, A., Belousova, M., Sutherland, F., 2012. U-Pb age and origin of gem zircon from the New England sapphire fields. Australian Journal of Earth Sciences, vol. 59, no. 7, pp. 1067 – 1081

Alaee, N.H., Sargheyni, J., Pezeshkan, M., Kianoush, P., 2025. Design and optimization of a spiral separator for enhanced chromite recovery and sustainability. Cleaner Engineering and Technology, vol. 24, p. 100880

Alderton, D., 2021. Other Silicates: The Al2SiO5 polymorphs, cordierite, staurolite, epidote, chlorite and serpentine. Royal Holloway, University of London, Egham, United Kingdom

Ali, E., 2001. Understanding the operation of industrial MSF plants Part I: Stability and steady-state analysis. Desalination, vol. 143, no. 1, pp. 53 – 72

Amao, A.O., Al-Ramadan, K., Koeshidayatullah, A., 2016. Automated mineralogical methodology to study carbonate grain microstructure: an example from oncoids. Environmental Earth Sciences, vol. 75, p. 666

AMC, 2010. Grande Cote Project Definitive Feasibility Study. Engineering and Technical. MDL Mineral Sands Group, vol. 1

Anthony, J.W., Bideaux, R.A., Bladh, K.W., Nichols, M.C., 1995. Handbook of mineralogy: Silica, silicates. Vol II. Mineralogical Society of America, Chantilly, VA, USA

Arnold, B.J., Klima, M.S., Bethell, P.J., 2007. Designing the coal preparation plant of the future. Society for Mining, Metallurgy, and Exploration, USA

Atasoy, Y., Spottiswood, D.J., 1995. A study of particle separation in a spiral concentrator. Minerals Engineering, vol. 8, no. 10, pp. 1197 – 1208

AusIMM., 2012. Cost Estimation Handbook – Monograph 27. Chapter 12: Beneficiation – Concentration. The Australian Institute of Mining and Metallurgy, Second Edition

Burt, R.O., Mills, C., 1985. Gravity concentration – 1000 years old and still improving. Canadian Institute of Mining, Metallurgy and Petroleum, pp. 438 – 447

Davies, P.O.J., Goodman, R.H., Deschamps, J.A., 1991. Recent developments in spiral design, construction and application. Minerals Engineering, vol. 4, no. 3/4, pp. 437 – 456

De Klerk, E., 2004. A laboratory experiment to teach closed-loop system identification. IEEE Transactions on Education, vol. 47, no. 2, pp. 276 – 283

Dehaine, Q., Filippov, L.O., 2016. Modelling heavy and gangue mineral size recovery curves using the spiral concentration of heavy minerals from kaolin residues. Powder Technology, vol. 292, pp. 331 – 341

Dehaine, Q., Tijsseling, L.T., Glass, H.J., Tormanen, T., Butcher, A.R., 2021. Geometallurgy of cobalt ores: a review. Minerals Engineering, vol. 160, p. 106656

Dieye, M., Van Lichtervelde, M., Ndiaye, A.A., Gueye, M., Blancher, S.M., 2020. Mineralogical characterization of heavy mineral concentrates from Senegalese Great Cost by using Qemscan and SEM. International Journal of Geosciences, vol. 2020, no. 11, pp. 800 – 817

Dixit, P., Tiwari, R., Mukherjee, A.K., Banerjee, P.K., 2015. Application of response surface methodology for modeling and optimization of spiral separator for processing of iron ore slime. Powder Technology, vol. 275, pp. 105 – 112

Edahbi, M., Benzaazoua, M., Plante, B., Doire, S., Kormos, L., 2018. Mineralogical characterization using QEMSCAN® and leaching potential study of REE within silicate ores: A case study of the Matamec project, Québec, Canada. Journal of Geochemical Exploration, vol. 85, pp. 64 – 73

Galvin, K.P., Zhou, J., Price, A.J., Agrwal, P., Iveson, S.M., 2016. Single-stage recovery and concentration of mineral sands using a REFLUX™ classifier. Minerals Engineering, vol. 93, pp. 32 – 40

Gao, Y., Zhang, G., Wang, M., Liu, D., 2018. The critical role of pulp density on flotation separation of nickel-copper sulfide from fine serpentine. Minerals, vol. 8, no. 8, p. 317

GCO, 2013. WCP & MSP Spiral Concentrator Banks: Operation & Service Manual. Grande Côte Opérations

GCO, 2022. Circuit balances and process flow diagrams. Grande Côte Opérations

GCO, 2024. Reconciliation Report. Grande Côte Opérations

Geneyton, A., Diack, M., 2020. Procedure for spiral separators performance assessment – MG12 and MT10 separators case study. Eramet.

Gill, C.B., 1991. Materials beneficiation: Gravity concentration. Springer-Verlag, New York, USA

Grammatikopoulos, T., Mercer, W., Gunning, C., 2013. Mineralogical characterisation using QEMSCAN of the Nechalacho heavy rare earth metal deposit, Northwest Territories, Canada. Canadian Metallurgical Quarterly, vol. 52, no. 3, pp. 265 – 277

Grobler, J., Zietsman, J., 2017. The influence of trash minerals and agglomerate particles on spiral separation performance. Journal of the Southern African Institute of Mining and Metallurgy, vol 117, no. 5, pp. 435 – 442

Grobler, J.D., Bosman, J.B., 2009. Gravity separator performance evaluation using Qemscan® particle mineral analysis. The 7th International Heavy Minerals Conference ‘What next’, Champagne Sports Resort, Drakensberg, 20

– 23 September 2009, The Southern African Institute of Mining and Metallurgy, pp. 91 – 98

Gülsoy, Ö.Y., Gülcan, E., 2019. A new method for gravity separation: Vibrating table gravity concentrator. Separation and Purification Technology, vol. 211, pp. 124 – 134

Haldar, S.K., 2020. Introduction to mineralogy and petrology. The Mining Geology and Metallurgical Institutes, Kolkata, West Bengal

Hattab, M.M., El-Rabeiy, S., Ghazy, R.A., 2023. Detecting coastal black sand areas using remote sensing and gis in Egypt. International Journal of Environmental Studies and Researches, vol. 1, no. 3, pp. 1 – 8

Hedrick, J.B., Waked, L., 1989. Heavy minerals, including monazite, in Egypt's Black Sands deposits. Journal of the Less-Common Metals, vol. 148, pp. 79 – 84

Holland-Batt, A.B., 1995. Some design considerations for spiral separators. Minerals Engineering, vol. 8, no. 11, pp. 1381 – 1395

Jalloh, A.B., Sasaki, K., Thomas, M.O., Jalloh, Y., 2013. The geology, mineral resources of Sierra Leone and how the resources can be used to develop the nation. Procedia Earth and Planetary Science, vol. 6, pp. 131 – 138

Jones, G., 2009. Mineral sands: An overview of the industry. Unpublished, Iluka Resources Limited, Capel

Jones, G., O'Brien, V., 2014. Aspects of resource estimation for mineral sands deposits. Applied Earth Science (Transactions of the Institute of Mining and Metallurgy: Section B), vol. 123, no. 2, pp. 86 – 94

Kari, C., Kapure, G., Mohan Rao, S., 2006. Effect of operating parameters on the performance of spiral concentrator. Proceedings of the International Seminar on Mineral Processing Technology, Chennai, India, pp. 316 – 319

Kenis, P., Skurzyński, J., Jary, Z., Kubik, R., 2020. A new methodological approach (QEMSCAN®) in the mineralogical study of Polish loess: Guidelines for further research. Open Geosciences, vol. 12, no. 1, pp. 342 – 353

Killian, S.F., Master, S., Viljoen, R.P., Wilson, M.G.C., 2016. The great mineral fields of Africa. Episodes, vol. 39, no. 2, pp. 85 – 103

Krynine, P.D., 1946. The tourmaline group in sediments. Journal of Geology, vol. 54, no. 2, pp. 65 – 87

Kursun, I., Ozkan, S.G., Terzi, M., Tombal, T.D., 2016. Determination of particle size distribution of quartz sands by novel methods: A case study. 6th International Conference on Computer Applications in the Minerals Industries, Istanbul, Turkey, 5 – 7 October 2016, CAMI2016-49, pp. 1 – 6

Lishchuk, V., Koch, P., Ghorbani, Y, Butcher, A.R., 2020. Towards integrated geometallurgical approach: critical review of current practices and future trends. Minerals Engineering, vol. 145, p. 106072

Lund, C., Lamberg, P., 2014. Geometallurgy – A tool for better resource efficiency. European Geologist, vol. 2014, no. 37, pp. 39 – 43

MacHunter, R.M.G., Pax, R.A., 2007. Whole plant process modelling incorporating an estimate on the impact of uncertainties in equipment and orebody composition on separation performance. The 6th International Heavy Minerals Conference 'Back to Basics', The Southern African Institute of Mining and Metallurgy, pp. 15 – 20

Mahran, G.M.A., Doheim, M.A., Ali, M.H.A., Gawad, A.F.A., 2015. CFD simulation of particulate flow in a spiral concentrator. Production-oriented testing/numerical simulation. Materials Testing, vol. 57, no. 9, pp. 811 – 816

Majumder, A.K., Barnwal, J.P., 2003. Development of a new cola washability index. Minerals Engineering, vol. 17, no. 1, pp. 93 – 96

Mineral Technologies, 2021. CT Separator – Cleaning and Maintenance. Downer, Queensland, Australia

Neethling, S.J., Cilliers, J.J., 2012. Grade-recovery curves: A new approach for analysis of and predicting from plant data. Minerals Engineering, vol. 36 – 38, pp. 105 – 110

Pan, X., Li, S., Li, Y., Guo, P., Zhao, X., Cai, Y., 2022. Resource, characteristic, purification and application of quartz: a review. Minerals Engineering, vol. 184, p. 107600

Pascoe, R.D., Power, M.R., Simpson, B., 2007. QEMSCAN analysis as a tool for improved understanding of gravity separator performance. Minerals Engineering, vol. 20, pp. 487 – 495

Perks, C., Mudd, G., 2019. Titanium, zirconium resources and production: A state-of-the-art literature review. Ore Geology Reviews, vol. 107, pp. 629 – 646

Perry, R.H., Green, D.W., Maloney, J.O., 1997. Perry's Chemical Engineer's Handbook. Seventh Edition, McGraw-Hill

Philander, C., Rozendaal, A., 2011. The contributions of geometallurgy to the recovery of lithified heavy mineral resources at the Namakwa Sands mine, West Coast of South Africa. Minerals Engineering, vol. 24, no. 12, pp. 1357 – 1364

Philander, C., Rozendaal, A., 2013. The application of a novel geometallurgical template model to characterise the Namakwa Sands heavy mineral deposit, West Coast of South Africa. Minerals Engineering, vol. 52, pp. 82 – 94

Ramsaywork, P., Vermaak, M.K.G., Viljoen, R., 2010. Case study: high-capacity spiral concentrators. Journal of the Southern African Institute of Mining and Metallurgy, vol. 110, no. 11, pp. 637 – 642

Reyneke, L. Wallmach, T., 2007. Characterization of FeTi-oxide species occurring in the Ranobe heavy mineral deposit, Madagascar. Sixth

International Heavy Minerals Conference ‘Back to Basics’, The Southern African Institute of Mining and Metallurgy

Richards, R.G., MacHunter, D.M., Gates, P.J., Palmer, M.K., 2000. Gravity separation of ultra-fine minerals using spiral separators. Minerals Engineering, vol. 13, no. 1, pp. 65 – 77

Richardson, J.F., Harker, J.H., Backhurst, J.R., 2002. Coulson and Richardson’s Chemical Engineering, vol. 2, Fifth Edition. Butterworth Heinemann

Sadeghi, M., Bazin, C., 2020. The use of process analysis and simulations to identity paths to improve the operation of an iron ore gravity concentration circuit. Advances in Chemical Engineering and Science, vol. 10, no. 3, pp. 149 – 170

Sinott, R.K., 2005. Chemical engineering design. Coulson & Richardson’s Chemical Engineering, vol. 6, Fourth Edition. Elsevier

Sivamohan, R., Forssberg, E., 1985. Principles of spiral concentration. International Journal of Mineral Processing, vol. 15, no. 3, pp. 173 – 181

Sudikondala, P., Mangadoddy, N., Kumar, M., Tripathy, S.K., Yanamandra, R.M., 2022. CFD modelling of spiral concentrator at moderate feed solids content – Prediction of particle segregation. Transactions of the Indian Institute of Metals, vol. 77, no. 12, pp. 4193 – 4203

Tangsathitkulchai, C., Austin, L.G., 1989. Slurry density effects on ball milling in a laboratory ball mill. Powder Technology, vol. 59, no. 4, pp. 285 – 293

Tiu, G., Ghorbani, Y., Jansson, N., Wanhainen, C., Bolin, N., 2023. Quantifying the variability of a complex ore using geometallurgical domains. Minerals Engineering, vol. 203, p. 108323

Tonžetić, I.Z., Butcher, A.R., Cropp, A.F., Pudmenzky, C., 2006. Automated SEM analysis measurement and characterisation of dust using QEMSCAN.

Second Aerosol Workshop, School of Physical and Chemical Sciences, Queensland University of Technology

Tripathy, S.K., Murthy, Y.R., 2012. Modeling and optimization of spiral concentration of ultrafine chromite. Powder Technology, vol. 221, pp. 387 – 394

Van Gosen, B.S., Fey, D.L., Shah, A.K., Verplanch, P.L., Hoefen, T.M., 2013. Deposit model for heavy-mineral sands in coastal environments. Department of the Interior, U.S. Geological Survey Scientific Investigations Report 2010-5070-L, 51 p.

Vigoroso, L., Caffaro, F., Tronci, M., Fargnoli, M., 2025. Ergonomics and design for safety: A scoping review and bibliometric analysis in the industrial engineering literature. Safety Science, vol. 185, p. 106799

Walker, S., 2016. Going with gravity: A roundup of current technologies that use the force of gravity for heavy mineral recovery. Engineering and Mining Journal, November 2016, pp. 28 – 32

Walklate, J.R., Fourie, P.J., 2006. A history of gravity separation at Richards Bay Minerals. Journal of the Southern African Institute of Mining and Metallurgy, vol. 106, no. 11, pp. 741 – 748

Wallmach, T., Duhamel-Achin, E., Blancher, S., 2012. Mineralogical characterisation of premium and intermediate zircon concentrates from Grande Cote, Senegal with special reference to Fe-Impurities texturally associated with zircon particles. Eramet Research, France

Wills, B.A., Finch, J.A., 2016. Mineral processing technology: An introduction to the practical aspects of ore treatment and mineral recovery. Eighth Edition, Elsevier Science & Technology Books

Wills, B.A., Napier-Munn, T., 2006. Mineral processing technology: An introduction to the practical aspects of ore treatment and mineral recovery. Seventh Edition, Elsevier Science & Technology Books

Appendices

Appendix A: Spirals Performance at 30% Solids in the Feed (1.30 g/cm^3 pulp density)

Table A1: Flow rates, at 80% split to concentrate, chemical analysis and recovery at 30% solids in the feed (1.30 g/cm^3 pulp density).

MG 12														
Split 80 %		Split	LABORATORY ASSAYS						RECOVERY					
Streams	tph	%	TiO2 %	ZrO2 %	Fe2O3 %	Al2O3 %	SiO2 %	Free SIO2	TiO2 %	ZrO2 %	Fe2O3 %	Al2O3 %	SiO2 %	Free SIO2
Con	2.59	81.81	34.13	24.42	12.14	9.41	18.82	1.90	81.35	88.30	80.69	76.01	79.51	52.14
Mids	0.51	16.17	37.85	15.61	13.95	13.87	16.82	2.08	17.83	11.15	18.32	22.14	14.05	11.27
Tails	0.06	2.02	13.99	6.14	6.04	9.29	61.83	54.12	0.82	0.55	0.99	1.85	6.44	36.59
TOTAL	3.17	100.00	34.33	22.63	12.31	10.13	19.36	2.98	100	100	100	100	100	100

HG 10														
Split 80 %		Split	LABORATORY ASSAYS						RECOVERY					
Streams	tph	%	TiO2 %	ZrO2 %	Fe2O3 %	Al2O3 %	SiO2 %	Free SIO2	TiO2 %	ZrO2 %	Fe2O3 %	Al2O3 %	SiO2 %	Free SIO2
Con	2.40	82.89	35.76	24.87	12.92	6.12	17.15	1.65	84.23	91.36	83.70	63.49	78.11	46.91
Mids	0.20	7.07	29.77	5.82	15.07	24.98	20.35	4.95	5.98	1.82	8.32	22.09	7.90	11.96
Tails	0.29	10.04	34.31	15.31	10.17	11.47	25.36	11.97	9.79	6.81	7.98	14.42	14.00	41.13
TOTAL	2.90	100.00	35.19	22.56	12.80	7.99	18.20	2.92	100	100	100	100	100	100

CTS														
Split 80 %		Split	LABORATORY ASSAYS						RECOVERY					
Streams	tph	%	TiO2 %	ZrO2 %	Fe2O3 %	Al2O3 %	SiO2 %	Free SIO2	TiO2 %	ZrO2 %	Fe2O3 %	Al2O3 %	SiO2 %	Free SIO2
Con	1.99	79.51	34.03	28.37	11.04	5.02	17.95	1.25	80.73	88.65	75.95	60.09	74.95	33.27
Mids	0.32	12.91	37.70	21.35	13.72	7.60	16.13	1.65	14.52	10.83	15.33	14.77	10.94	7.13
Tails	0.19	7.58	21.01	1.74	13.31	22.04	35.46	23.57	4.75	0.52	8.73	25.14	14.11	59.61
TOTAL	2.50	100.00	33.52	25.45	11.56	6.64	19.04	3.00	100.00	100.00	100.00	100.00	100.00	100.00

Table A2: Flow rates, at 85% split to concentrate, chemical analysis and recovery at 30% solids in the feed (1.30 g/cm^3 pulp density).

MG 12														
Split 85 %		Split	LABORATORY ASSAYS						RECOVERY					
Streams	tph	%	TiO2 %	ZrO2 %	Fe2O3 %	Al2O3 %	SiO2 %	Free SIO2	TiO2 %	ZrO2 %	Fe2O3 %	Al2O3 %	SiO2 %	Free SIO2
Con	2.65	83.68	34.90	23.39	12.37	9.69	18.54	2.00	83.58	89.46	82.81	78.84	81.49	56.55
Mids	0.46	14.44	37.78	15.23	14.12	13.85	16.31	1.77	15.62	10.05	16.31	19.44	12.38	8.68
Tails	0.06	1.88	14.85	5.63	5.87	9.40	62.24	54.72	0.80	0.48	0.88	1.72	6.14	34.77
TOTAL	3.17	100.00	34.94	21.88	12.50	10.29	19.03	2.95	100	100	100	100	100	100

HG 10														
Split 85 %		Split	LABORATORY ASSAYS						RECOVERY					
Streams	tph	%	TiO2 %	ZrO2 %	Fe2O3 %	Al2O3 %	SiO2 %	Free SIO2	TiO2 %	ZrO2 %	Fe2O3 %	Al2O3 %	SiO2 %	Free SIO2
Con	2.38	85.17	34.46	26.66	12.03	5.57	17.74	1.63	86.18	92.51	86.41	67.81	79.92	44.14
Mids	0.15	5.32	27.31	6.84	12.52	22.58	25.38	10.67	4.27	1.48	5.62	17.18	7.15	18.11
Tails	0.27	9.51	34.19	15.50	9.94	11.04	25.72	12.45	9.55	6.01	7.97	15.01	12.94	37.75
TOTAL	2.79	100.00	34.05	24.55	11.86	6.99	18.91	3.14	100	100	100	100	100	100

ALICOCO														
Split 85 %		Split	LABORATORY ASSAYS						RECOVERY					
Streams	tph	%	TiO2 %	ZrO2 %	Fe2O3 %	Al2O3 %	SiO2 %	Free SIO2	TiO2 %	ZrO2 %	Fe2O3 %	Al2O3 %	SiO2 %	Free SIO2
Con 1	0.046	66.67							0	0	0	0	0	0
Con 2	0.011	16.67							0	0	0	0	0	0
Mids	0.006	8.33							0	0	0	0	0	0
Tails	0.006	8.33							0	0	0	0	0	0
TOTAL	0.07	100.00	0	0	0	0	0	0	0	0	0	0	0	0

CTS														
Split 85 %		Split	LABORATORY ASSAYS						RECOVERY					
Streams	tph	%	TiO2 %	ZrO2 %	Fe2O3 %	Al2O3 %	SiO2 %	Free SIO2	TiO2 %	ZrO2 %	Fe2O3 %	Al2O3 %	SiO2 %	Free SIO2
Con	2.35	85.49	36.21	23.95	12.60	6.79	16.99	1.62	88.90	97.45	84.84	67.51	76.40	32.96
Mids	0.25	9.02	35.53	5.20	15.18	18.53	19.06	7.19	9.20	2.23	10.79	19.45	9.04	15.39
Tails	0.15	5.49	12.07	1.20	10.11	20.40	50.42	39.62	1.90	0.31	4.37	13.03	14.56	51.64
TOTAL	2.75	100.00	34.83	21.01	12.69	8.59	19.01	4.21	100	100	100	100	100	100

Table A3: Flow rates, at 90% split to concentrate, chemical analysis and recovery at 30% solids in the feed (1.30 g/cm^3 pulp density).

MG 12														
Split 90 %		Split	LABORATORY ASSAYS						RECOVERY					
Streams	tph	%	TiO2 %	ZrO2 %	Fe2O3 %	Al2O3 %	SiO2 %	Free SIO2	TiO2 %	ZrO2 %	Fe2O3 %	Al2O3 %	SiO2 %	Free SIO2
Con	2.98	92.44	32.90	25.51	11.51	8.65	17.94	0.86	92.25	97.06	91.61	86.70	89.65	45.80
Mids	0.20	6.37	38.44	10.52	14.42	17.68	16.98	2.88	7.42	2.76	7.91	12.21	5.84	10.49
Tails	0.04	1.19	8.93	3.66	4.71	8.45	70.21	64.15	0.32	0.18	0.48	1.09	4.51	43.71
TOTAL	3.22	100.00	32.97	24.30	11.61	9.22	18.50	1.75	100	100	100	100	100	100

HG 10														
Split 90 %		Split	LABORATORY ASSAYS						RECOVERY					
Streams	tph	%	TiO2 %	ZrO2 %	Fe2O3 %	Al2O3 %	SiO2 %	Free SIO2	TiO2 %	ZrO2 %	Fe2O3 %	Al2O3 %	SiO2 %	Free SIO2
Con	2.41	91.27	35.15	23.75	12.71	8.56	17.74	1.5795	91.63	94.99	93.02	87.66	87.36	54.17
Mids	0.06	2.17	30.75	8.33	9.79	17.87	30.06	16.97	1.91	0.79	1.71	4.36	3.53	13.86
Tails	0.17	6.56	34.49	14.67	10.03	10.84	25.72	12.97	6.46	4.22	5.28	7.98	9.11	31.97
TOTAL	2.64	100.00	35.01	22.82	12.47	8.91	18.53	2.66	100	100	100	100	100	100

CTS														
Split 90 %		Split	LABORATORY ASSAYS						RECOVERY					
Streams	tph	%	TiO2 %	ZrO2 %	Fe2O3 %	Al2O3 %	SiO2 %	Free SIO2	TiO2 %	ZrO2 %	Fe2O3 %	Al2O3 %	SiO2 %	Free SIO2
Con	2.60	87.69	40.67	9.62	15.02	13.16	15.45	4.0655	90.13	93.38	88.06	82.94	82.64	72.37
Mids	0.08	2.64	41.18	11.09	14.46	12.69	15.87	3.979	2.74	3.24	2.55	2.41	2.55	2.13
Tails	0.29	9.67	29.15	3.16	14.53	21.08	25.11	12.987	7.12	3.38	9.39	14.65	14.81	25.50
TOTAL	2.97	100.00	39.57	9.03	14.95	13.91	16.40	4.93	100	100	100	100	100	100

Appendix B: Spirals Performance at 35% Solids in the Feed (1.36 g/cm3 pulp density)

Table B1: Flow rates, at 80% split to concentrate, chemical analysis and recovery at 35% solids in the feed (1.36 g/cm^3 pulp density).

MG 12												
Split 80 %		**Split**	**LABORATORY ASSAYS**					**RECOVERY**				
Streams	tph	%	TiO2 %	ZrO2 %	Al2O3 %	SiO2 %	Free SIO2	TiO2 %	ZrO2 %	Al2O3 %	SiO2 %	Free SIO2
Con	3.12	79.72	33.36	25.61	8.53	18.37	1.31	78.47	88.51	72.87	77.45	38.36
Mids	0.68	17.30	38.16	13.53	13.10	16.94	3.62	19.48	10.15	24.30	15.50	23.07
Tails	0.12	2.98	23.33	10.37	8.86	44.79	35.17	2.05	1.34	2.83	7.05	38.57
TOTAL	3.91	100.00	33.89	23.06	9.33	18.91	2.72	100	100	100	100	100

HG 10												
Split 80 %		**Split**	**LABORATORY ASSAYS**					**RECOVERY**				
Streams	tph	%	TiO2 %	ZrO2 %	Al2O3 %	SiO2 %	Free SIO2	TiO2 %	ZrO2 %	Al2O3 %	SiO2 %	Free SIO2
Con	3.12	83.05	36.54	21.56	8.80	15.93	0.75	83.13	88.94	72.32	74.74	24.12
Mids	0.16	4.24	25.88	3.57	26.39	23.84	8.86	3.35	0.84	12.35	6.37	16.23
Tails	0.48	12.71	34.77	14.50	10.92	23.56	10.86	13.52	10.22	15.33	18.89	59.65
TOTAL	3.75	100.00	35.80	19.74	9.91	17.36	2.53	100	100	100	100	100

CTS												
Split 78 %		**Split**	**LABORATORY ASSAYS**					**RECOVERY**				
Streams	tph	%	TiO2 %	ZrO2 %	Al2O3 %	SiO2 %	Free SIO2	TiO2 %	ZrO2 %	Al2O3 %	SiO2 %	Free SIO2
Con	2.87	77.70	36.21	27.05	5.73	17.33	0.94	77.51	93.08	53.71	75.66	30.92
Mids	0.22	6.03	43.16	12.46	11.38	14.70	2.78	7.17	3.33	8.29	4.98	7.09
Tails	0.60	16.27	34.18	4.99	19.35	21.17	9.00	15.32	3.60	38.01	19.36	61.98
TOTAL	3.69	100.00	36.30	22.58	8.28	17.79	2.36	100	100	100	100	100

Table B2: Flow rates, at 85% split to concentrate, chemical analysis and recovery at 35% solids in the feed (1.36 g/cm^3 pulp density).

MG 12												
Split 85 %		**Split**	**LABORATORY ASSAYS**					**RECOVERY**				
Streams	tph	%	TiO2 %	ZrO2 %	Al2O3 %	SiO2 %	Free SIO2	TiO2 %	ZrO2 %	Al2O3 %	SiO2 %	Free SIO2
Con	3.45	86.09	34.86	24.43	9.06	17.84	1.10	86.05	92.06	82.38	83.95	44.17
Mids	0.47	11.62	37.28	13.62	12.39	16.83	3.83	12.42	6.93	15.20	10.69	20.77
Tails	0.09	2.29	23.28	10.07	10.03	42.82	32.77	1.53	1.01	2.43	5.36	35.06
TOTAL	4.01	100.00	34.88	22.85	9.47	18.30	2.14	100	100	100	100	100

HG 10												
Split 85 %		**Split**	**LABORATORY ASSAYS**					**RECOVERY**				
Streams	tph	%	TiO2 %	ZrO2 %	Al2O3 %	SiO2 %	Free SIO2	TiO2 %	ZrO2 %	Al2O3 %	SiO2 %	Free SIO2
Con	2.79	84.93	36.88	24.42	6.43	17.39	1.96	86.18	92.80	67.95	80.89	54.42
Mids	0.17	5.05	29.28	5.47	25.64	21.95	6.39	4.07	1.24	16.12	6.07	10.53
Tails	0.33	10.02	35.35	13.31	12.78	23.76	10.72	9.75	5.97	15.94	13.04	35.04
TOTAL	3.28	100.00	36.34	22.35	8.03	18.26	3.06	100	100	100	100	100

Table B3: Flow rates, at 90% split to concentrate, chemical analysis and recovery at 35% solids in the feed (1.36 g/cm^3 pulp density).

MG 12												
Split 90 %		**Split**	**LABORATORY ASSAYS**					**RECOVERY**				
Streams	tph	%	TiO2 %	ZrO2 %	Al2O3 %	SiO2 %	Free SIO2	TiO2 %	ZrO2 %	Al2O3 %	SiO2 %	Free SIO2
Con	3.24	92.16	35.48	21.82	8.80	17.39	2.08	93.15	96.11	88.50	86.80	56.04
Mids	0.21	5.98	37.36	12.70	15.65	17.34	3.16	6.36	3.63	10.22	5.62	5.53
Tails	0.07	1.86	9.09	2.96	6.32	75.27	70.63	0.48	0.26	1.29	7.59	38.44
TOTAL	3.52	100.00	34.33	22.63	10.13	19.36	2.98	100	100	100	100	100

HG 10												
Split 90 %		**Split**	**LABORATORY ASSAYS**					**RECOVERY**				
Streams	tph	%	TiO2 %	ZrO2 %	Al2O3 %	SiO2 %	Free SIO2	TiO2 %	ZrO2 %	Al2O3 %	SiO2 %	Free SIO2
Con	2.83	91.82	35.70	22.53	9.55	17.21	1.166	92.40	95.47	89.29	87.54	46.49
Mids	0.03	1.03	28.83	6.34	20.50	30.28	16.86	0.84	0.30	2.15	1.73	7.53
Tails	0.22	7.15	33.58	12.82	11.76	27.10	14.81	6.77	4.23	8.56	10.73	45.98
TOTAL	3.09	100.00	35.48	21.67	9.82	18.05	2.30	100	100	100	100	100

Appendix C: Spirals Performance at 40% Solids in the Feed (1.44 g/cm3 pulp density)

Table C1: Flow rates, at 80% split to concentrate, chemical analysis and recovery at 40% solids in the feed (1.44 g/cm^3 pulp density).

MG 12												
Split 80 %		Split	LABORATORY ASSAYS					RECOVERY				
Streams	tph	%	TiO2 %	ZrO2 %	Al2O3 %	SiO2 %	Free SIO2	TiO2 %	ZrO2 %	Al2O3 %	SiO2 %	Free SIO2
Con	3.75	82.69	33.48	25.08	7.30	18.15	1.95	81.70	89.57	75.04	81.08	55.63
Mids	0.64	14.16	37.47	14.18	12.17	16.73	3.56	15.66	8.67	21.41	12.80	17.34
Tails	0.14	3.14	28.43	12.99	9.08	36.01	24.97	2.64	1.76	3.55	6.12	27.03
TOTAL	4.53	100.00	33.89	23.16	8.05	18.51	2.90	100	100	100	100	100

HG 10												
Split 80 %		Split	ESSAY					RECOVERY				
Streams	tph	%	TiO2 %	ZrO2 %	Al2O3 %	SiO2 %	Free SIO2	TiO2 %	ZrO2 %	Al2O3 %	SiO2 %	Free SIO2
Con	2.84	80.45	26.05	15.35	12.71	23.62	9.60	76.77	89.15	77.22	78.60	72.60
Mids	0.17	4.78	34.91	7.33	18.78	16.82	3.77	6.12	2.53	6.78	3.33	1.70
Tails	0.52	14.77	31.64	7.81	14.35	29.58	18.51	17.12	8.32	16.00	18.07	25.70
TOTAL	3.53	100.00	27.30	13.85	13.24	24.18	10.63	100	100	100	100	100

CTS												
Split 68 %		Split	ESSAY					RECOVERY				
Streams	tph	%	TiO2 %	ZrO2 %	Al2O3 %	SiO2 %	Free SIO2	TiO2 %	ZrO2 %	Al2O3 %	SiO2 %	Free SIO2
Con	3.32	68.27	31.86	30.45	4.29	18.05	0.68	64.41	86.26	42.78	71.10	24.90
Mids	0.31	6.31	41.56	19.96	7.77	15.38	1.51	7.77	5.23	7.17	5.60	5.15
Tails	1.23	25.42	36.98	8.08	13.48	15.88	5.11	27.83	8.52	50.05	23.30	69.96
TOTAL	4.86	100.00	33.77	24.10	6.84	17.33	1.86	100	100	100	100	100

Table C2: Flow rates, at 85% split to concentrate, chemical analysis and recovery at 40% solids in the feed (1.44 g/cm^3 pulp density).

MG 12												
Split 85 %		Split	LABORATORY ASSAYS					RECOVERY				
Streams	tph	%	TiO2 %	ZrO2 %	Al2O3 %	SiO2 %	Free SIO2	TiO2 %	ZrO2 %	Al2O3 %	SiO2 %	Free SIO2
Con	3.65	84.96	35.39	20.57	8.44	16.39	1.88	85.39	89.70	79.72	80.56	52.54
Mids	0.52	12.13	37.51	14.66	12.53	16.72	3.12	12.92	9.13	16.90	11.73	12.44
Tails	0.13	2.91	20.46	7.87	10.45	45.77	36.61	1.69	1.18	3.38	7.71	35.02
TOTAL	4.29	100.00	35.22	19.48	8.99	17.28	3.04	100	100	100	100	100

Table C3: Flow rates, at 90% split to concentrate, chemical analysis and recovery at 40% solids in the feed (1.44 g/cm^3 pulp density).

MG 12												
Split 90 %		Split	LABORATORY ASSAYS					RECOVERY				
Streams	tph	%	TiO2 %	ZrO2 %	Al2O3 %	SiO2 %	Free SIO2	TiO2 %	ZrO2 %	Al2O3 %	SiO2 %	Free SIO2
Con	3.14	93.27	34.76	22.93	8.35	17.64	2.00	94.21	97.10	90.76	88.58	57.08
Mids	0.18	5.33	36.92	12.00	13.74	16.84	3.96	5.72	2.90	8.53	4.83	6.46
Tails	0.05	1.40	1.94	0.00	4.33	87.26	85.09	0.08	0.00	0.71	6.59	36.47
TOTAL	3.36	100.00	34.42	22.03	8.58	18.58	3.27	100	100	100	100	100

Appendix D: Mineral Assemblage

Table D1: Compact Turbo spiral mineral assemblage for the concentrate (by GCO Laboratory)

MINERAL	T1 30% SPLIT 80% CON	T2 30% SPLIT 85% CON	T3 30% SPLIT 90% CON	T2 35% SPLIT 78% CON	T2 40% SPLIT 68% CON
%THM	99.36%	99.49%	99.52%	99.78%	98.68%
%HS	0.14%	0.27%	0.61%	0.32%	0.12%
%Mags	35.45%	33.15%	40.31%	36.92%	34.06%
%NMags	64.42%	66.58%	59.08%	62.76%	65.82%
%VHM	81.40%	83.70%	83.05%	82.40%	78.40%
%Trash	17.77%	15.79%	16.47%	17.38%	20.28%
%Ilmenite	20.21%	18.74%	18.77%	21.25%	17.80%
%Rutile	17.26%	13.81%	15.62%	13.42%	12.44%
%Leucoxene	7.40%	7.59%	12.07%	7.21%	7.71%
%Zircon	36.53%	43.55%	36.58%	40.51%	40.45%
%Kyanite	5.16%	3.68%	4.57%	3.26%	4.07%
% Staurolite	3.77%	3.06%	3.93%	3.40%	4.25%
%Monazite	0.12%	0.10%	0.11%	0.09%	0.01%
%Chromite	0.17%	0.17%	0.23%	0.17%	0.14%
%Silicates	4.63%	2.70%	4.51%	2.76%	3.85%
%Quartz	0.64%	0.51%	0.48%	0.22%	1.32%
%Others	3.92%	6.08%	3.11%	7.70%	7.96%
Sum of Minerals	99.81%	100.00%	100.00%	100.00%	100.00%

Table D2: MG12 spiral mineral assemblage for the concentrate (by GCO Laboratory)

MINERAL	T1 30% SPLIT 80% CON	T2 30% SPLIT 85% CON	T3 30% SPLIT 90% CON	T1 35% SPLIT 80% CON1	T2 35% SPLIT 85% CON1	T3 35% SPLIT 90% CON1	T1 40% SPLIT 80% CON1	T2 40% SPLIT 85% CON1	T3 40% SPLIT 90% CON1
%THM	99.42%	99.37%	99.27%	99.77%	99.71%	99.70%	99.27%	99.67%	99.86%
%HS	0.30%	0.44%	0.25%	0.40%	0.25%	0.25%	0.34%	0.41%	0.36%
%Mags	33.86%	44.54%	45.98%	46.09%	46.35%	46.57%	47.35%	45.26%	46.35%
%NMags	65.84%	55.02%	53.77%	53.51%	53.40%	53.17%	52.30%	54.32%	53.29%
%VHM	74.17%	80.76%	83.93%	79.83%	81.41%	81.12%	80.13%	80.89%	83.33%
%Trash	25.25%	18.61%	15.33%	19.94%	18.30%	18.59%	19.14%	18.78%	16.53%
%Ilmenite	19.70%	20.46%	18.62%	21.14%	22.11%	22.16%	21.06%	21.71%	24.09%
%Rutile	11.44%	11.78%	11.26%	11.75%	12.69%	12.64%	11.89%	10.44%	11.49%
%Leucoxene	6.81%	10.57%	11.11%	10.68%	10.42%	10.46%	11.14%	10.42%	9.80%
%Zircon	36.22%	37.95%	42.95%	36.26%	36.19%	35.86%	36.03%	38.32%	37.94%
%Kyanite	5.62%	0.36%	0.35%	0.35%	0.36%	0.36%	4.09%	0.36%	0.67%
% Staurolite	3.32%	7.28%	6.15%	6.73%	7.65%	7.72%	10.56%	6.84%	6.16%
%Monazite	0.01%	0.01%	0.01%	0.02%	0.01%	0.01%	0.02%	0.01%	0.01%
%Chromite	0.13%	0.22%	0.21%	0.24%	0.24%	0.24%	0.24%	0.24%	0.24%
%Silicates	2.64%	4.67%	2.75%	4.96%	2.29%	2.32%	2.61%	2.16%	2.10%
%Quartz	0.58%	0.63%	0.73%	0.23%	0.29%	0.30%	0.73%	0.33%	0.14%
%Others	13.52%	6.07%	5.87%	7.64%	7.74%	7.93%	1.62%	9.18%	7.35%
Sum of Minerals	100.00%	100.00%	100.00%	100.00%	100.00%	100.00%	100.00%	100.00%	100.00%

Table D3: HG10 spiral mineral assemblage for the concentrate (by GCO Laboratory)

MINERAL	T2 30% SPLIT 80 CON	T1 30% SPLIT 85%	T3 30% CON HG10 90%	T1 35% CON HG10 80%	T2 35% CON HG10 85%	T3 35% CON HG10 90%	T2 40% CON HG10 80%
%THM	99.49%	99.47%	99.76%	99.78%	99.23%	99.46%	99.35%
%HS	0.27%	0.26%	0.31%	0.25%	0.24%	0.41%	0.42%
%Mags	33.15%	30.87%	46.92%	46.49%	45.67%	46.41%	47.33%
%NMags	66.58%	68.87%	52.77%	53.26%	54.10%	53.19%	52.25%
%VHM	83.53%	73.23%	82.24%	83.86%	83.09%	79.67%	84.03%
%Trash	15.96%	26.24%	17.52%	15.92%	16.14%	19.79%	15.32%
%Ilmenite	18.76%	19.06%	25.83%	24.66%	25.13%	24.33%	23.78%
%Rutile	13.63%	11.41%	12.39%	13.66%	12.64%	13.08%	11.81%
%Leucoxene	7.58%	5.93%	8.90%	10.37%	9.04%	8.92%	10.41%
%Zircon	43.55%	36.83%	35.12%	35.17%	36.29%	33.35%	38.02%
%Kyanite	3.91%	6.64%	4.39%	4.49%	4.16%	5.32%	3.34%
% Staurolite	3.04%	2.56%	6.37%	5.84%	5.78%	6.47%	6.10%
%Monazite	0.03%	0.01%	0.03%	0.09%	0.03%	0.03%	0.03%
%Chromite	0.17%	0.10%	0.23%	0.25%	0.22%	0.23%	0.24%
%Silicates	2.61%	2.17%	3.69%	3.61%	3.84%	3.87%	3.51%
%Quartz	0.51%	0.53%	0.24%	0.22%	0.77%	0.54%	0.65%
%Others	6.21%	14.75%	2.81%	1.63%	2.10%	3.86%	2.10%
Sum of Minerals	100.00%	100.00%	100.00%	100.00%	100.00%	100.0%	100.00%

Appendix E: Particle Size Distributions

Figure E1: PSD for the Compact Turbo Spiral

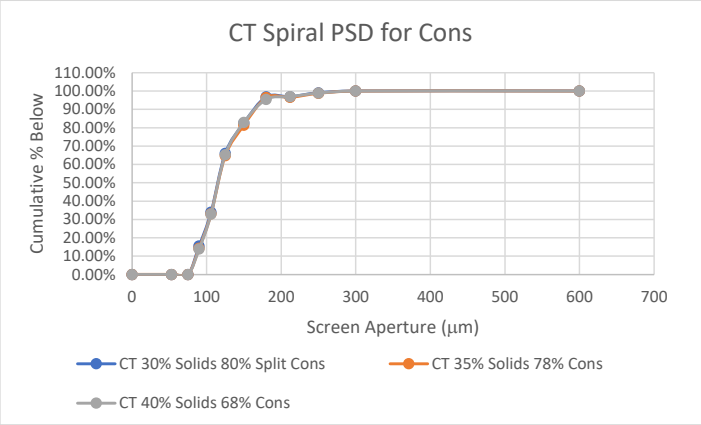

Table E1: d_{50} for the Compact Turbo Spiral

	Split to the Concentrate		
Feed Solids	**80%**	**78%**	**68%**
	d_{50} (µm)	**d_{50} (µm)**	**d_{50} (µm)**
30%	115.53		
35%		116.18	
40%			116.04

Figure E2: PSD for the MG12 Spiral

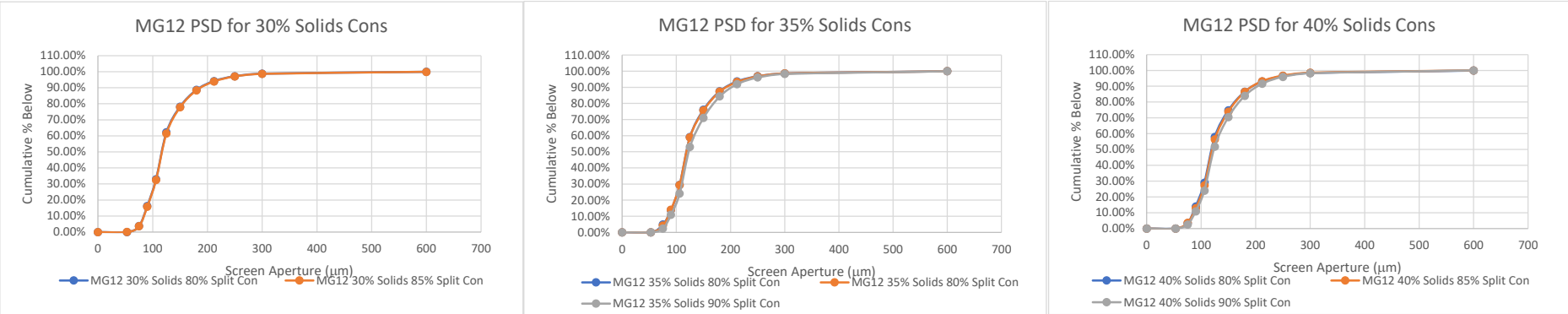

Table E2: d_{50} for MG12 Spiral

	Split to the Concentrate		
Feed Solids	**80%**	**85%**	**90%**
	d_{50} (µm)	**d_{50} (µm)**	**d_{50} (µm)**
30%	117	117	
35%	119	119	123
40%	120	121	124

Figure E3: PSD for the HG10 Spiral

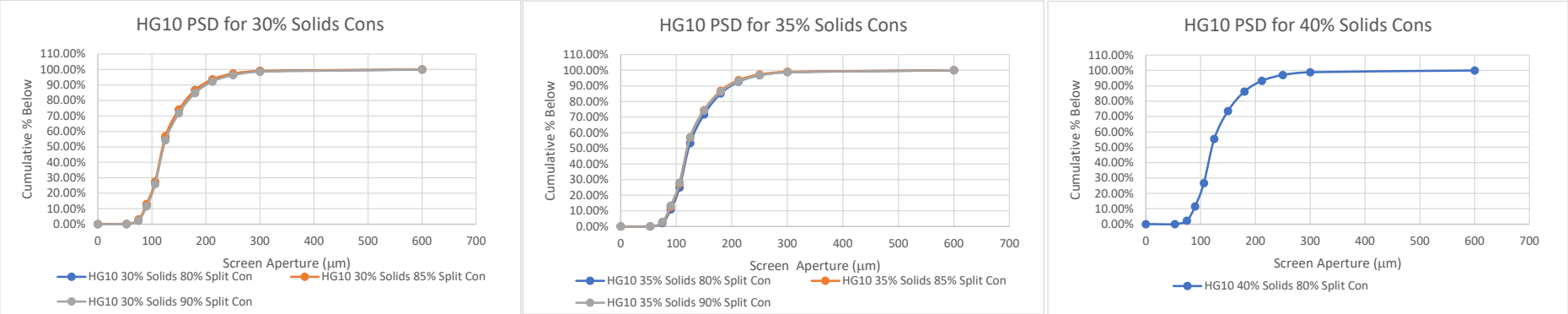

Table E3: d_{50} for HG10 Spiral

	Split to the Concentrate		
Feed Solids	**80%**	**85%**	**90%**
	d_{50} (µm)	**d_{50} (µm)**	**d_{50} (µm)**
30%	121	121	122
35%	123	121	120
40%	121		

Figure E4: PSD for the Classifier Underflow

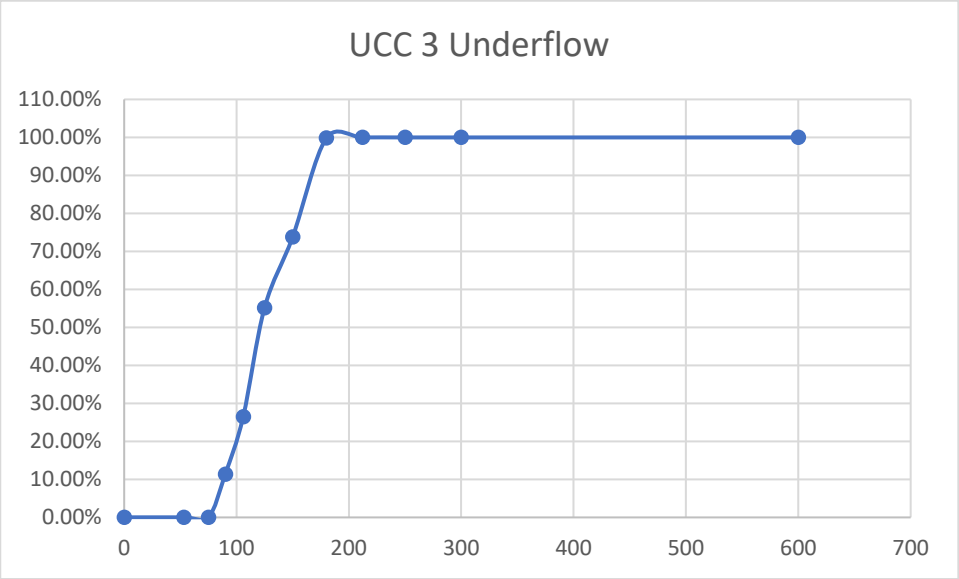

d_{50}: 121.60 μm

Appendix F: Comparison of Alicoco and HG10 spirals in 2022

Table F1: Alicoco spiral treating classifier underflow in 2022

			LABORATORY ASSAYS						RECOVERY					
Test1	**TPH**	**YIELD %**	**TiO2 %**	**ZrO2 %**	**Fe2O3 %**	**Al2O3 %**	**SiO2 %**	**free SiO2**	**TiO2 %**	**ZrO2 %**	**Fe2O3 %**	**Al2O3 %**	**SiO2 %**	**free SiO2**
Con	1.00	57.62	40.38	11.13	9.03	10.64	20.28	10.45	72.36	63.23	46.47	90.29	38.66	28.35
Mid	0.20	17.81	29.90	11.76	15.99	2.85	27.00	17.58	16.56	20.65	25.43	7.49	15.90	14.74
Tails	0.34	24.58	14.50	6.65	12.80	0.61	55.88	49.18	11.08	16.12	28.10	2.22	45.43	56.91
Feed (calc)	1.55	100.00	32.15	10.14	11.19	6.79	30.23	21.24	100.00	100.00	100.00	100.00	100.00	100.00

			LABORATORY ASSAYS						RECOVERY					
Test2	**TPH**	**YIELD %**	**TiO2 %**	**ZrO2 %**	**Fe2O3 %**	**Al2O3 %**	**SiO2 %**	**free SiO2**	**TiO2 %**	**ZrO2 %**	**Fe2O3 %**	**Al2O3 %**	**SiO2 %**	**free SiO2**
Con	2.02	59.58	35.98	11.10	9.41	10.97	22.73	12.54	72.57	67.34	51.19	90.20	42.68	33.01
Mid	0.51	15.05	28.34	10.86	15.98	2.50	29.80	20.56	14.44	16.63	21.96	5.20	14.14	13.67
Tails	0.86	25.37	15.13	6.21	11.59	1.31	54.02	47.56	12.99	16.03	26.85	4.60	43.19	53.32
Feed (calc)	3.39	100.00	29.54	9.82	10.95	7.25	31.73	22.63	100.00	100.00	100.00	100.00	100.00	100.00

			LABORATORY ASSAYS						RECOVERY					
Test2	**TPH**	**YIELD %**	**TiO2 %**	**ZrO2 %**	**Fe2O3 %**	**Al2O3 %**	**SiO2 %**	**free SiO2**	**TiO2 %**	**ZrO2 %**	**Fe2O3 %**	**Al2O3 %**	**SiO2 %**	**free SiO2**
Con	1.66	64.82	36.44	11.29	9.94	11.64	21.95	11.16	80.45	74.63	58.55	96.19	43.98	31.54
Mid	0.51	13.16	24.53	10.72	18.20	1.63	31.11	21.19	10.99	14.39	21.77	2.73	12.65	12.16
Tails	0.71	22.02	11.42	4.89	9.83	0.39	63.72	58.61	8.56	10.98	19.68	1.08	43.37	56.29
Feed (calc)	2.87	100.00	29.36	9.80	11.00	7.85	32.35	22.93	100.00	100.00	100.00	100.00	100.00	100.00

Table F2: HG10 spiral treating classifier underflow in 2022

			LABORATORY ASSAYS						RECOVERY					
Test 1	**TPH**	**YIELD %**	**TiO2 %**	**ZrO2 %**	**Fe2O3 %**	**Al2O3 %**	**SiO2 %**	**free SiO2**	**TiO2 %**	**ZrO2 %**	**Fe2O3 %**	**Al2O3 %**	**SiO2 %**	**free SiO2**
Con	1.01	47.45	39.28	14.40	9.98	11.93	19.00	5.84	54.77	80.29	50.25	35.30	34.45	19.92
Mids	0.29	13.67	38.08	5.05	10.84	19.54	21.31	9.01	15.30	8.12	15.74	16.65	11.13	8.86
Tails	0.83	38.87	26.21	2.54	8.24	19.82	36.65	25.47	29.94	11.60	34.02	48.04	54.43	71.22
Feed (calc)	2.13	100.00	34.04	8.51	9.42	16.04	26.18	13.90	100.00	100.00	100.00	100.00	100.00	100.00

			LABORATORY ASSAYS						RECOVERY					
Test 2	**TPH**	**YIELD %**	**TiO2 %**	**ZrO2 %**	**Fe2O3 %**	**Al2O3 %**	**SiO2 %**	**free SiO2**	**TiO2 %**	**ZrO2 %**	**Fe2O3 %**	**Al2O3 %**	**SiO2 %**	**free SiO2**
Con	1.13	57.39	37.36	13.59	11.90	9.16	18.40	7.03	64.84	86.13	64.28	39.39	41.25	28.00
Mids	0.16	8.23	34.67	5.11	12.91	14.71	20.60	10.68	8.63	4.65	10.00	9.08	6.62	6.11
Tails	0.68	34.37	25.53	2.43	7.95	20.01	38.83	27.62	26.53	9.22	25.71	51.54	52.13	65.89
Feed (calc)	1.97	100.00	33.07	9.06	10.63	13.34	25.61	14.41	100.00	100.00	100.00	100.00	100.00	100.00

			LABORATORY ASSAYS						RECOVERY					
Test 3	**TPH**	**YIELD %**	**TiO2 %**	**ZrO2 %**	**Fe2O3 %**	**Al2O3 %**	**SiO2 %**	**free SiO2**	**TiO2 %**	**ZrO2 %**	**Fe2O3 %**	**Al2O3 %**	**SiO2 %**	**free SiO2**
Con	1.45	70.08	37.19	11.44	9.97	14.38	21.52	8.61	79.17	91.33	79.21	66.90	51.74	35.02
Mids	0.05	2.36	24.58	1.95	8.77	25.28	32.95	19.34	1.76	0.52	2.35	3.97	2.67	2.65
Tails	0.57	27.55	22.78	2.60	5.90	15.93	48.23	38.97	19.07	8.15	18.44	29.13	45.59	62.33
Feed (calc)	2.07	100.00	32.92	8.78	8.82	15.06	29.15	17.23	100.00	100.00	100.00	100.00	100.00	100.00

Appendix G: QEMSCAN Results

Table G1: QEMSCAN mineralogy results

	Feed	30% split 80%			35% split 78%			40% split 68%		
Mineral Name	Mass Fraction %	Mass Fraction %	Absolute Difference %	Relative Difference %	Mass Fraction %	Absolute Difference %	Relative Difference %	Mass Fraction %	Absolute Difference %	Relative Difference %
Zircon	**32.32**	**32.38**	**0.06%**	**0%**	**35.74**	**3.42%**	**11%**	**38.78**	**6.46%**	**20%**
Pseudorutile	19.97	22.85	2.88%	**14%**	20.78	0.81%	**4%**	19.14	-0.83%	**-4%**
Rutile	17.37	17.13	-0.24%	**-1%**	16.53	-0.84%	**-5%**	17.02	-0.35%	**-2%**
Leucoxene / Kleberite	6.84	7.79	0.95%	**14%**	7.36	0.52%	**8%**	6.55	-0.29%	**-4%**
Staurotide	**5.71**	**4.12**	**-1.59%**	**-28%**	**4.36**	**-1.35%**	**-24%**	**3.68**	**-2.03%**	**-36%**
Kyanite	**3.34**	**2.80**	**-0.54%**	**-16%**	**2.46**	**-0.88%**	**-26%**	**2.32**	**-1.02%**	**-31%**
Anatase	3.29	3.65	0.36%	**11%**	3.60	0.31%	**9%**	3.36	0.07%	**2%**
Quartz	2.41	0.35	-2.06%	**-85%**	0.31	-2.10%	**-87%**	0.25	-2.16%	**-90%**
Tourmaline	1.88	0.98	-0.90%	**-48%**	0.93	-0.95%	**-51%**	1.04	-0.84%	**-45%**
Epidote	**1.46**	**0.84**	**-0.62%**	**-42%**	**0.87**	**-0.59%**	**-40%**	**0.84**	**-0.62%**	**-42%**
Grossular	1.41	1.07	-0.34%	**-24%**	1.17	-0.24%	**-17%**	0.99	-0.42%	**-30%**
Ilmenite	0.80	1.25	0.45%	**56%**	1.09	0.29%	**36%**	1.07	0.27%	**34%**
Phyllosilicates	0.71	1.02	0.31%	**44%**	0.93	0.22%	**31%**	0.99	0.28%	**39%**
Fe oxi-hydroxides	0.59	1.02	0.43%	**73%**	1.06	0.47%	**80%**	0.96	0.37%	**63%**
Spinel	0.23	0.19	0.04%	**-17%**	0.14	-0.09%	**-39%**	0.09	-0.14%	**-61%**
Almandine	0.12	0.23	0.11%	**92%**	0.21	0.09%	**75%**	0.25	0.13%	**108%**
Rutile-Nb	0.12	0.10	-0.02%	**-17%**	0.09	-0.03%	**-25%**	0.08	-0.04%	**-33%**
REE Phosphates	0.11	0.19	0.08%	**73%**	0.15	0.04%	**36%**	0.18	0.07%	**64%**
Chromite	0.10	0.13	0.03%	**30%**	0.08	-0.02%	**-20%**	0.13	0.03%	**30%**
Others	0.09	0.23	0.14%	**156%**	0.25	0.16%	**178%**	0.26	0.17%	**189%**
Pyroxene	0.06	0.01	-0.05%	**-83%**	0.02	-0.04%	**-67%**	0.04	-0.02%	**-33%**
Amphibole	0.05	0.04	-0.01%	**-20%**	0.08	0.03%	**60%**	0.05	0.00%	**0%**
Titanite / Sphene	0.04	0.04	0.00%	**0%**	0.04	0.00%	**0%**	0.03	-0.01%	**-25%**
Andradite	0.03	0.02	-0.01%	**-33%**	0.02	-0.01%	**-33%**	0.05	0.02%	**67%**
Feldspath	0.01	0.01	0.00%	**0%**	0.01	0.00%	**0%**	0.01	0.00%	**0%**
Background	0.00	0.00	0.00%	**0%**	0.00	0.00%	**0%**	0.00	0.00%	**0%**
Pyrite	0.00	0.00	0.00%	**0%**	0.00	0.00%	**0%**	0.00	0.00%	**0%**

Figure G1: The QEMSCAN mineralogy analysis, showing the quality of the Compact Turbo spiral feed and the concentrates

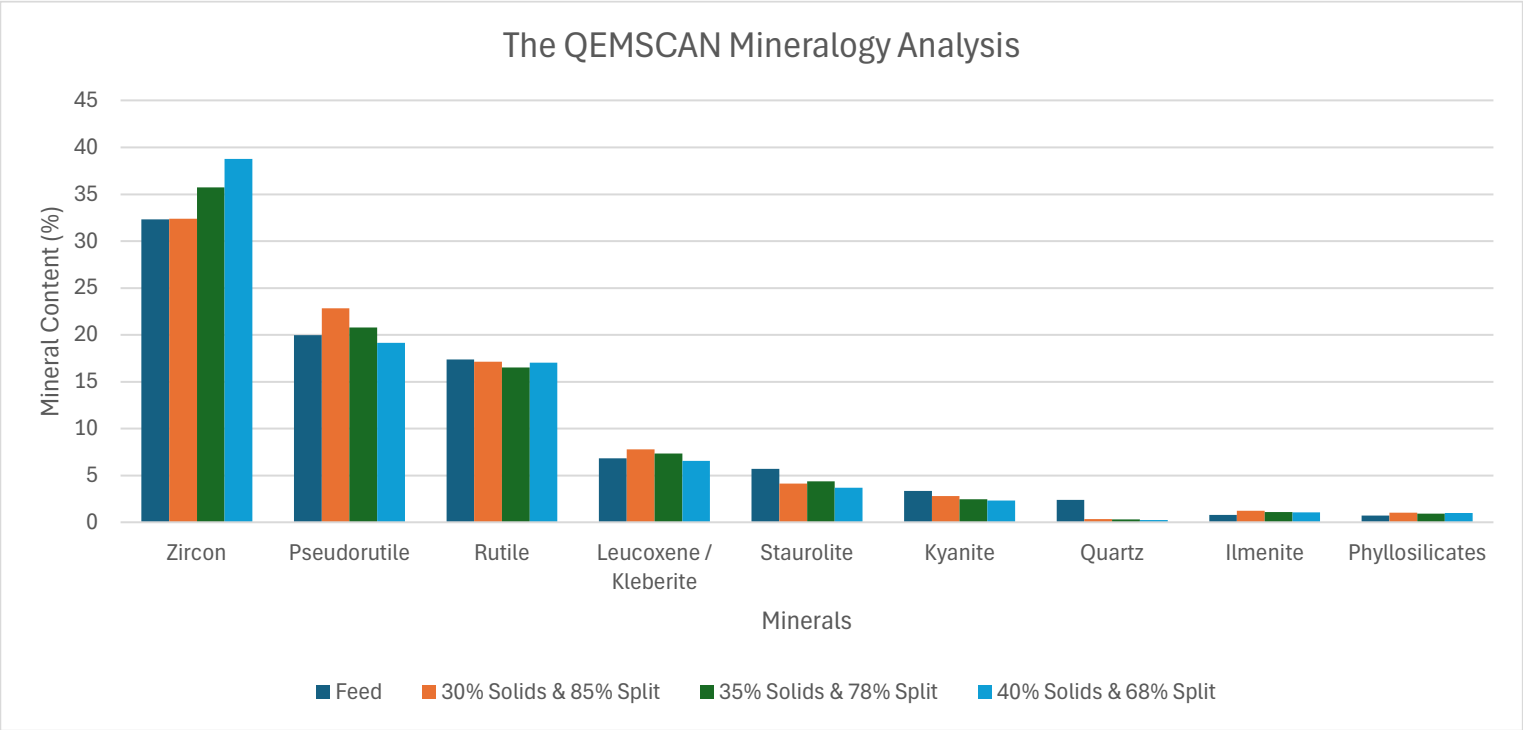

Appendix H: Recovery and grade curves

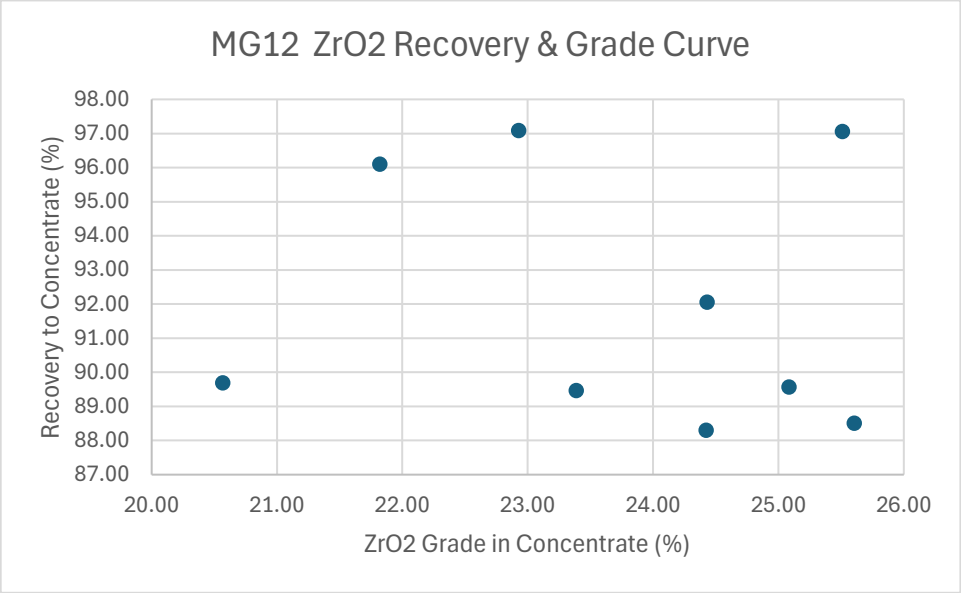

Figure H1: The MG12 recovery and grade curves for the ZrO_2

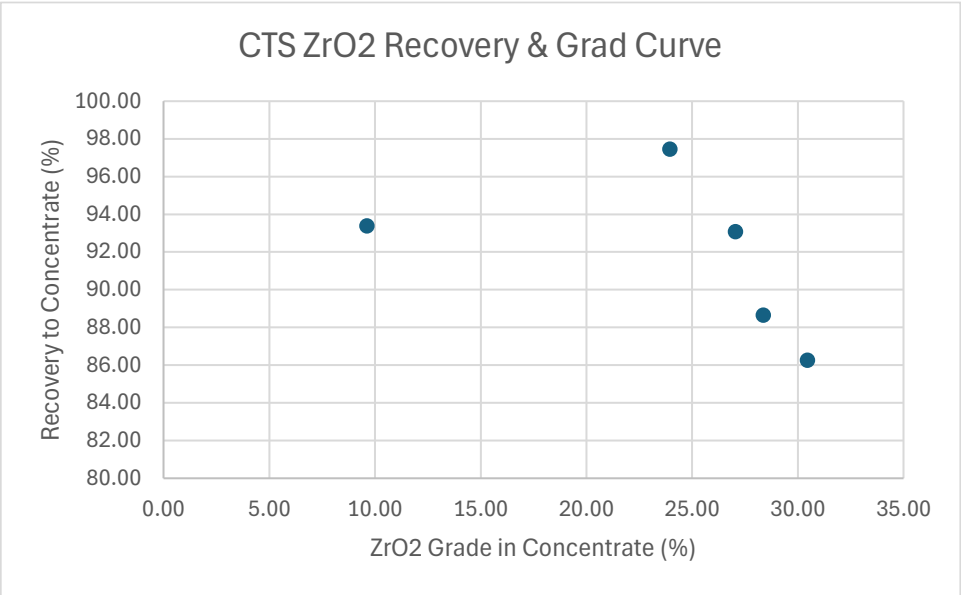

Figure H2: The Compact Turbo recovery and grade curve for the ZrO_2

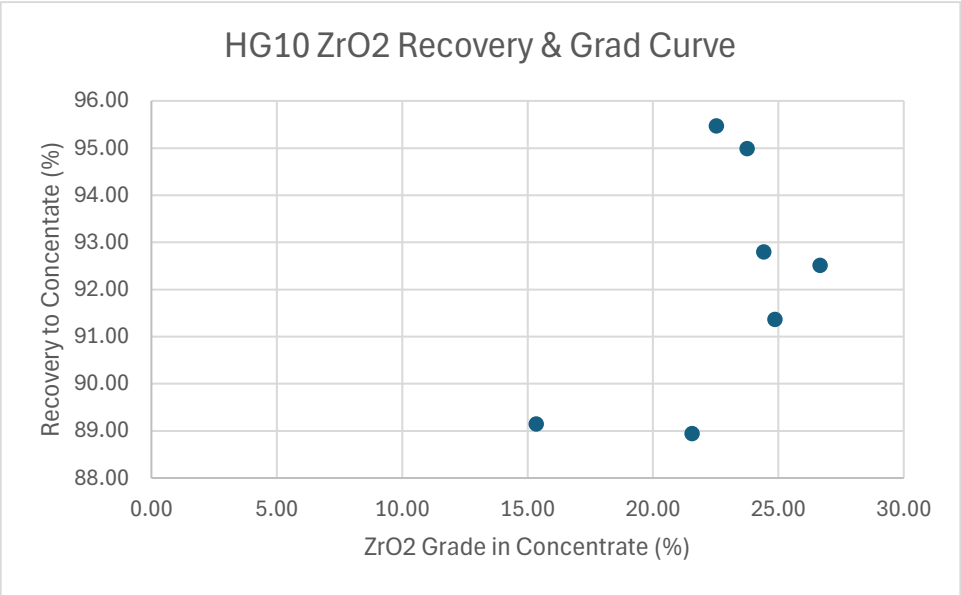

Figure H3: The HG10 recovery and grade curve for the ZrO_2

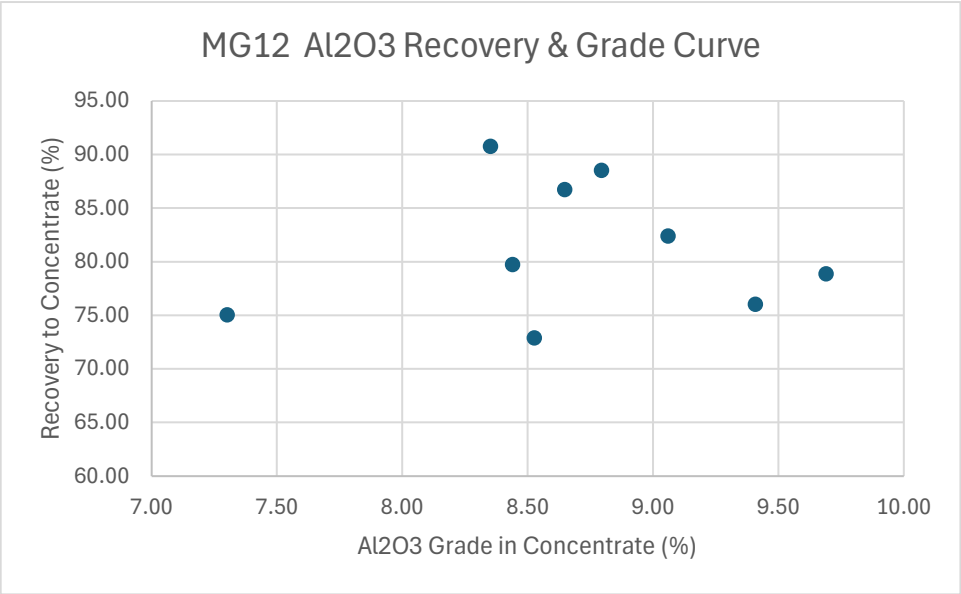

Figure H4: The MG12 recovery and grade curve for the Al_2O_3

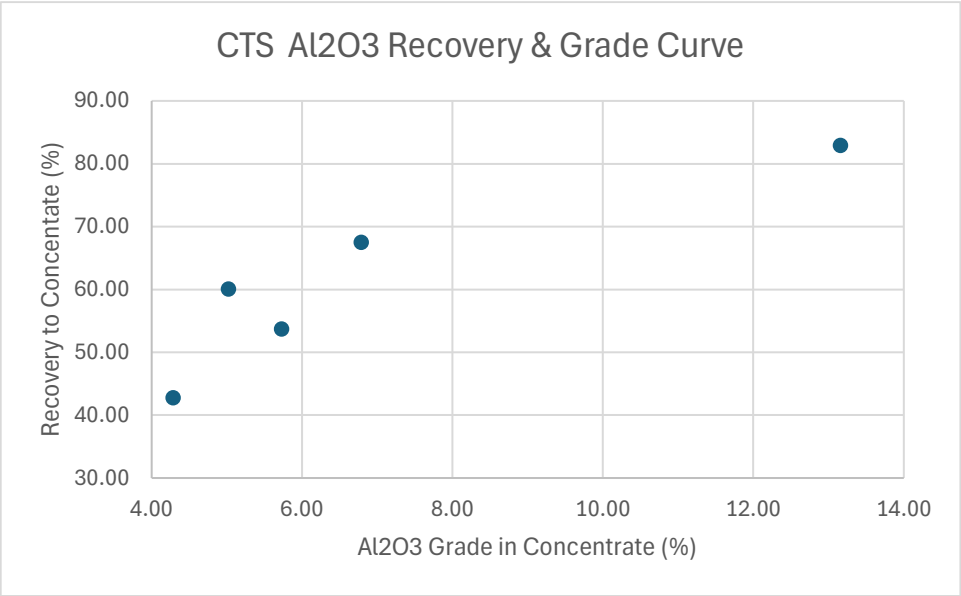

Figure H5: The Compact Turbo recovery and grade curve for the Al_2O_3

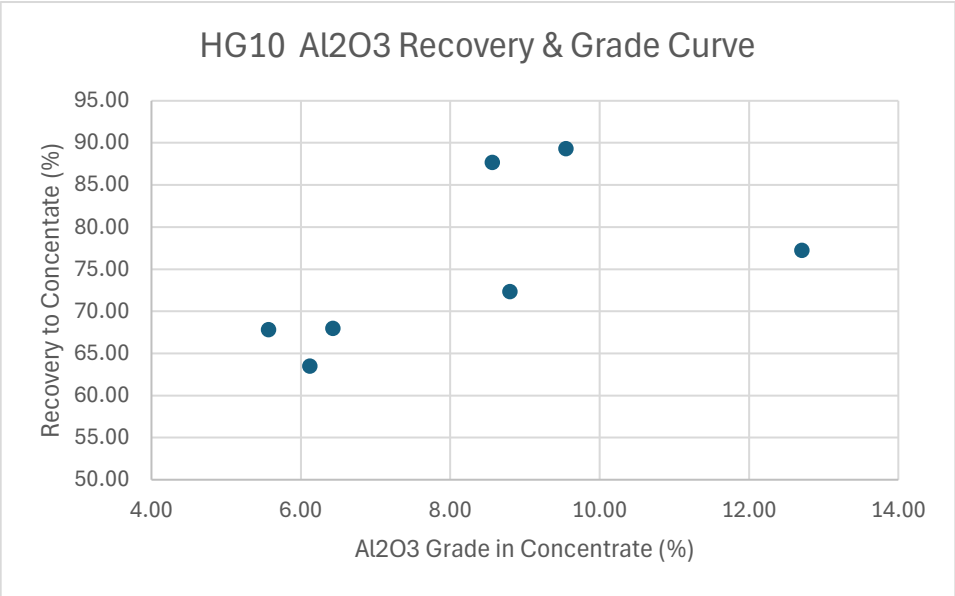

Figure H6: The HG10 recovery and grade curve for the Al_2O_3

APPENDIX I: Splitter Positions

Table I1: Splitter positions for the MG12, HG10 and the Compact Turbo spirals at 30%, 35% and 40% feed pulp densities.

MG 12

Feed Solids	30%		
Split	80%	85%	90%
Stage 1	17	8	8
Stage 2	15.5	6.5	6.5
Stage 3	5	5	5
Bottom	5	5	5

Feed Solids	35%		
Split	80%	85%	90%
Stage 1	7	8	10
Stage 2	5.5	6.5	8.5
Stage 3	5	5	5
Bottom	5.3	5	4

Feed Solids	40%		
Split	80%	85%	90%
Stage 1	17	19	18
Stage 2	15.5	18	16.5
Stage 3	15		15
Bottom	5.5	4.2	4.5

HG 10

Feed Solids	30%		
Split	80%	85%	90%
Stage 1	0	0	0
Stage 2	3	3	3
Stage 3	4.5	3	2.5
Bottom	C 15 - M 1	C 15 - M 1	C 15 - M 1

Feed Solids	35%		
Split	80%	85%	90%
Stage 1	0	0	0
Stage 2	3	3	3
Stage 3	2.5	2.5	2
Bottom	C 15 - M 1	C 15 - M 1	C 13,5 - M 1

Feed Solids	40%		
Split	80%	85%	90%
Stage 1			
Stage 2			
Stage 3			
Bottom			

Compact Turbo

Feed Solids	30%		
Split	80%	85%	90%
Stage 1	140	140	140
Stage 2	110	115	140
Stage 3	90	115	140
Stage 4	90	115	140
Stage 5	140	140	140

Feed Solids	35%		
Split	80%	85%	90%
Stage 1	140		
Stage 2	140		
Stage 3	140		
Stage 4	140		
Stage 5	140		

Feed Solids	40%		
Split	80%	85%	90%
Stage 1	140		
Stage 2	140		
Stage 3	140		
Stage 4	140		
Stage 5	140		

Table I2: Splitter positions for the Alicoco and the HG10spirals at low feed pulp densities.

Alicoco

	Test1	Test2	Test3
Top splitter	0	0	0
Middle splitter	1	1	1
Bottom splitter	2	2	2

HG10

	Test1	Test2	Test3
Top splitter	0	0	0
Middle splitter	2	2	2
Bottom splitter	3.5	3	3